

CHANGES IN THE DEGREE OF SUBSTITUTION  
OF PAC FROM PYROLYSIS OF A HIGH VOLATILE BITUMINOUS COAL

Mary J. Wornat, Adel F. Sarofim, and John P. Longwell

Department of Chemical Engineering, Massachusetts Institute of Technology  
77 Massachusetts Avenue, Cambridge, Massachusetts 02139

INTRODUCTION

When pyrolyzed, coal forms a complex mixture of polycyclic aromatic compounds (PAC), many of which carry functional groups as substitutes for ring hydrogen. Further subsection of PAC to pyrolytic conditions causes changes in their composition--manifested partly by changes in the degree of substitution. The presence or absence of substituent groups is of importance to environmental issues concerning both the sources of environmental PAC and their health effects. Researchers (22,26,36,45) studying PAC in the air, water, and soil have tried to deduce information about the PAC source fuels and their process temperatures from relative abundances of certain alkylated and unalkylated PAC.

Focussing particularly on alkyl and amino substituents, several researchers (14,18,30,31,32,54) have attempted to establish a link between biological activity (i.e., carcinogenicity or mutagenicity) and the presence or absence of substituent groups. Results to date indicate that biological activity is a complex function of the identity of the parent PAC, the nature of the functional group, the size of the functional group (18,32), and the position of the substitution (2,3,21,33,34,47)--all factors that influence the electron distribution within the compound. It is logical that these factors should also be the ones that govern PAC reactivity under pyrolytic conditions, but a thorough investigation of all of these influences lies beyond the scope of any single work. It is our objective to determine how the degree of substitution and the nature of the substituent groups influence the pyrolysis behavior of coal-derived PAC.

Previous work has already revealed some information about pyrolysis-induced changes in substitution of PAC from coal pyrolysis. Serio (46) has used nuclear magnetic resonance spectroscopy (NMR) to show that increasing pyrolysis severity by either temperature or time effects an increase in aromaticity and a decrease in the presence of functional groups. Employing Fourier transform infrared spectroscopy (FT-IR), Solomon, et al. (50) and Freihaut and Seery (13) report that high temperature coal tar exhibits a considerable reduction (as compared to lower temperature tar) of IR absorption in the regions associated with functional group attachment to aromatic rings. Other researchers (5,25,53) have used gas chromatography-mass spectrometry (GC-MS) to identify some specific alkylated PAC produced in coal pyrolysis experiments. We are unaware of any work to date that reports total mass yields of substituted and unsubstituted PAC from coal pyrolysis.

EXPERIMENTAL EQUIPMENT AND PROCEDURES

To produce the PAC of this study, 44-53  $\mu\text{m}$  particles of PSOC 997, a Pittsburgh Seam high volatile bituminous coal, are fluidized in argon and fed at a rate of 2.5 g/hour into the laminar flow, drop-tube pyrolysis furnace of Figure 1. Details of the furnace appear elsewhere (41). An optical pyrometer is used to measure furnace

temperature, which can be set to values of 1000 K to 2000 K by adjustment of the electrical power input. Particle residence time, or "drop distance," is controlled by adjusting the vertical position of the water-cooled collection probe. As pyrolysis products exit the reaction zone at 5.3 std l/min, they encounter 17.1 std l/min of argon quench gas at the top of the collection probe and another 4.8 std l/min through the walls of the probe inner tube as they travel the length of the collection probe. Leaving the probe, they enter an impactor for size-separation of the solid pyrolysis products. Char particles, the larger of these, deposit on the first stages; aerosols (i.e., PAC-coated soot) end up on the lowest impactor stages and the Millipore teflon filter (hole size, .2  $\mu\text{m}$ ) following the impactor. After passing through the filter, the gases are channeled to infrared detectors for measurement of CO and CO<sub>2</sub>, and to a flame ionization detector for measurement of hydrocarbon volatiles. A small portion of gas is diverted to a 750 ml glass bulb for subsequent GC-MS analysis.

After all products are weighed, the aerosols are placed in teflon-capped, 30-ml amber glass bottles of Caledon distilled-in-glass HPLC grade dichloromethane (DCM) and sonicated for five minutes. Syringe-fulls of the particle/liquid suspension are passed through a Millipore teflon filter (hole size .2  $\mu\text{m}$ ) to remove the soot particles from the PAC/DCM solution. The mass of the residue soot is taken and subtracted from that before sonication to give the mass of the PAC. Triplicate 100- $\mu\text{l}$  aliquots of the PAC/DCM solution are removed, evaporated, and weighed according to the procedure of Lafleur, *et al.* (27) to verify the PAC yields. This latter procedure gives  $\geq$  90% recovery for naphthalene and 100% recovery for species of  $\geq$  three rings, so negligible PAC mass is lost during evaporation since, in our experiments, one-ring aromatics and lighter hydrocarbons stay in the gas phase; only aromatics of  $\geq$  two rings condense onto the soot.

The PAC/DCM solutions undergo analysis by GC-MS, HPLC, and FT-IR. The GC component of the GC-MS system is a Hewlett-Packard Model 5890, equipped with a Quadrex Super Cap Series, methyl silicone (film thickness .10  $\mu\text{m}$ ) high temperature, aluminum clad capillary column (15 m x .2 mm i.d.). Sample volumes of .1  $\mu\text{l}$  are introduced into the splitless injector, maintained at 300°C. The detector is kept at 320°C, and the column temperature is programmed from 40°C to 320°C at 10°C/min. The mass spectrometer, Hewlett-Packard Model 5970, operates in electron impact mode at an ionizing voltage of 70 eV. Mass spectra are taken at a frequency of .77 scans/second, over a mass to charge ratio range of 41 to 600.

The HPLC system, fully described elsewhere (28), consists of a Perkin-Elmer Series 4 quaternary solvent delivery system coupled to a Model LC-85B variable wavelength ultraviolet (UV) detector. 1.5 ml/min of DCM (same grade as above) flows through the steric exclusion column (50 cm long x 10 mm i.d.), which is packed with 500 Å Jordi-Gel poly(divinylbenzene). Samples are injected through either a 6- $\mu\text{l}$  or a 100- $\mu\text{l}$  Rheodyne injection loop, and a microswitch on the injector actuates the data system to insure reproducible starting times. As demonstrated in another publication (28), substituted PAC elute in the first 23.9 ml; unsubstituted, afterward. The proportions of the UV response areas before and after 23.9 ml are taken to represent respectively the proportions of substituted and unsubstituted PAC. (To alleviate uncertainty about the relative UV response factors for the two classes of PAC, we have collected the eluates before and after 23.9 ml for one sample, concentrated them under nitrogen, and subjected them to the microbalance weighing procedure (27) mentioned above. Because the UV area technique gives good agreement with the weighing procedure, this latter, more time-consuming procedure is unnecessary.)

For FT-IR analysis, drops of the PAC/DCM solutions are placed on KBr discs (20 mm x 2 mm), and the solvent is allowed to evaporate. The discs are placed in an IBM Model IR/32 Fourier Transform Infrared Spectrometer, equipped with a Globar source and a mercury-cadmium telluride detector. The resulting absorbance spectra represent 64 scans, taken at a resolution of  $8 \text{ cm}^{-1}$ . To insure that the PAC composition is uniform over the surface of the disc, each disc is rotated slightly two times for additional determinations.

## RESULTS AND DISCUSSION

Figure 2 displays the yields of soot and PAC collected on the aerosol filter for the two sets of experiments: Set 1, constant drop distance (6 in) and variable temperature, and Set 2, constant temperature (1375 K) and variable drop distance. First, it should be noted that our maximum PAC yield of ~9% lies significantly below the 24-26% primary tar yields obtained from experiments conducted under less severe conditions (7,46). Our maximum PAC yield or "zero point" thus corresponds to a significant degree of primary tar conversion (~65%). Evident from Figure 2 are the drop in PAC yield and the compensating rise in soot yield as pyrolysis conditions increase in severity--by an increase in either temperature or distance. The constancy of the sum of PAC and soot yields ( $21.34\% \pm 0.97\%$  for Set 1;  $19.86\% \pm 1.09\%$  for Set 2) supports the previously reported notion that PAC serve as precursors to soot (9,17,24,42,52). It should be borne in mind, however, that our experiments and ones done prior to them (41) also show small temperature- and time-induced decreases in the yields of char,  $\text{CO}_2$ , and hydrocarbons and an increase in that of  $\text{CO}$ .

To better understand this apparent transformation of PAC to soot, it is necessary to investigate the compositional changes in the PAC that accompany their conversion. We have chosen to describe compositional changes of the PAC in terms of their aromatic ring number distribution and their degree of functional group substitution. A discussion of changes in the ring number distributions of coal-derived PAC will appear elsewhere (55); this paper focusses on pyrolysis-induced changes in the degree of substitution.

The question of how the degree of substitution changes can be partially answered by the GC-MS total ion chromatograms in Figure 3, featuring PAC from three Set 1 experiments. Since PAC elute in the order of decreasing volatility or of increasing molecular weight, addition of a functional group brings about a small increase in retention time; addition of an aromatic ring, a large increase. Readily apparent from Figure 3 is the loss of compositional complexity as temperature is raised. The lowest temperature sample is comprised of a multitude of peaks, many unresolved, which correspond to unsubstituted PAC and their substituted homologs. As temperature increases, the number of peaks diminishes drastically. Large gaps emerge between clusters of unsubstituted PAC isomers--indicating a marked depletion in the substituted species.

Even though GC-MS can easily give a qualitative picture of substitutional differences in PAC from coal, it is extremely difficult to use GC-MS quantitatively due to the unresolvability of some peaks, the uncertainty of response factors, the limited number of species included in available mass spectra libraries, and the virtual indistinguishability of mass spectra of some isomeric PAC (at least for mass spectra from systems with electron impact ionization sources (6,19,23)). Even if all of these difficulties are surmounted, the usefulness of GC-MS still extends only to the portion of the PAC sample that is gas chromatographable, *i.e.*, to the

vaporizable components. (It should be noted that this vaporization limitation of GC-MS systems promises to soon be eliminated by the introduction of new supercritical fluid chromatography-MS systems (35).)

Unlike GC, HPLC is limited in applicability only by component solubility in the mobile phase; but, except for microcolumn HPLC techniques (43), the price for the wider range of component applicability is the loss of separation efficiency as evident in peak resolution. This "drawback" can be an advantage in analyzing mixtures as complex as fossil fuel products, however, because HPLC methods can be tailored to make bulk separations according to one or two structural parameters. We have recently developed a method with a steric exclusion HPLC column that takes advantage of a nonexclusion effect to separate substituted from unsubstituted PAC (28). Non-nitrogen-containing PAC with alkyl, phenyl, hydroxyl, carbonyl, carboxyl, etheric, esteric, cyano, or nitro functional groups elute as size-excluded species. Unsubstituted PAC are adsorbed onto the column and elute later (28). Nitrogen-containing PAC are also delayed by adsorption unless they have a substituent group that sterically blocks the N atom from the adsorption site (29).

Figure 4 presents the results of applying this technique to the PAC from the two sets of experiments. Yields of substituted PAC fall monotonically with either increasing temperature or drop distance. Over the temperature interval investigated in Set 1, the drop is by two orders of magnitude; over the distance interval in Set 2, the drop is by almost an order of magnitude. Yields of unsubstituted PAC, on the other hand, exhibit a dual behavior. They appear to be insensitive to pyrolysis conditions at temperatures  $\leq 1312$  K for Set 1 and at distances  $\leq 4$  inches for Set 2. Beyond these "critical values," however, they too decay with an increase in either temperature or distance. Again the decline is more dramatic for the experiments in Set 1.

The qualitative similarity of the curves in Figure 4a to those in 4b suggests that the data of the two sets of experiments be compared as plots versus a parameter of pyrolysis severity--such as total PAC yield--that accounts for both temperature and time effects. The result of combining Figures 2 and 4 appears in Figure 5, which contains data from Sets 1 and 2 as well as experiments conducted at combinations of temperature and distance not covered by these Sets.

The fact that all the data (to a first approximation) lie on the same lines suggests the following for the ranges of temperature (1125 to 1473 K) and time (approximately .050 to .325 sec particle residence times, corresponding to drop distances of 2 to 6 in) investigated:

- 1) The split between substituted and unsubstituted PAC is solely a function of PAC yield (or conversion) and depends on temperature or time only as much as these variables affect PAC yield (or conversion).
- 2) Since pyrolysis at long time and low temperature can give the same results as at short time and high temperature, the PAC conversion reactions have a narrow distribution of activation energies.
- 3) It is more practical to relate substituted and unsubstituted PAC yields to total yield than to temperature and residence time, quantities whose measurements tend to be more system- and method-dependent.

It is convenient to approximate the S (substituted PAC) and the U (unsubstituted PAC) curves in Figure 5 as two line segments of different slope, intersecting

at a critical PAC yield  $Y_c$ , the point after which there is net loss of unsubstituted PAC. The value of  $Y_c$  is 4.5 mass% of coal--corresponding to 48% PAC conversion if the point of maximum PAC yield is taken as 0% conversion. Since both S and U must be 0 at  $Y = 0$ , the equations for the lines can be obtained easily in terms of Y, the total PAC yield:

$$\begin{array}{lll} \text{Regime 1:} & Y > Y_c & U = U_0 \quad S = Y - U_0 \\ \text{Regime 2:} & Y < Y_c & U = (U_0/Y_c)Y \quad S = (1 - U_0/Y_c)Y \end{array}$$

Thus for these experiments, once the critical yield  $Y_c$  and the initial yield of unsubstituted PAC  $U_0$  have been experimentally determined, the yields of substituted and unsubstituted PAC can be calculated solely from measurement of Y. The equations imply a ratio of S to U that, in Regime 1, decreases with decreasing Y and, in Regime 2, stays constant. The data match these approximations much better at large Y than at small Y, however, because the relative error of the straight line approximations for S and U becomes greater as Y decreases. Since secondary pyrolytic reactions depend much less on the parent coal than do the primary pyrolytic reactions, one might expect PAC from other coals (especially other bituminous coals) to exhibit the same "two line" behavior of U and S yields (albeit with different values of  $Y_c$  and  $U_0$ ).

The transition from Regime 1 to Regime 2 in Figure 5 suggests a change in the nature of the functional groups associated with the substituted PAC. Figure 6 displays the FT-IR spectra of samples from three Set 1 experiments--each labeled with the functional groups conventionally assigned (4,48) to peaks at particular bands. These spectra appear unretouched, i.e., their baselines have not been "corrected" to screen out the drift allegedly due to scatter (44,49,51). The prominent functional group absorbances occur at 2850-2980  $\text{cm}^{-1}$  and 1370-1460  $\text{cm}^{-1}$  for alkyl groups; at 3150-3550  $\text{cm}^{-1}$  for OH or the NH of amides or amines; at 1260-1280  $\text{cm}^{-1}$  for etheric C-O; and at 1690-1730  $\text{cm}^{-1}$  for carbonyl groups. The three oxygen-containing groups--hydroxyl, ether, and carbonyl--are the same as those reportedly found in coals of  $\geq 80\%$  carbon (1).

Socrates (48) cautions against comparing changes in relative intensities of functional groups' bands to get changes in their relative amounts because signals associated with particular functional groups can be augmented (and sometimes shifted) by certain adjacent atoms or functional groups (e.g., the intensity of the C-H aromatic stretch band at 1600  $\text{cm}^{-1}$  can be enhanced by either ring nitrogen or hydroxyl groups (51)). Nevertheless, we can make some qualitative observations from the spectra in Figure 6. Most noticeable is that the OH or NH groups responsible for the 3150-3550  $\text{cm}^{-1}$  band in Figure 6a disappear by 1312 K (6c) and remain absent from the spectra of samples produced at higher temperatures. This observation is consistent with the  $^1\text{H}$  NMR determination of a temperature-induced drop in hydroxyl content of the bituminous coal tars of Collin, *et al.* (8). If, as recommended (50), aromatic H is represented by the 700-900  $\text{cm}^{-1}$  band and aliphatic, by the 2800-3000  $\text{cm}^{-1}$  band, then Figure 6 also reveals a reduction in aliphatic (or hydroaromatic) hydrogen relative to aromatic hydrogen--a reduction consistent with the results of Solomon, *et al.* (50) for tars of another Pittsburgh Seam bituminous coal. Figure 6 also implies a relative decrease in etheric functionalities and a relative increase in carbonyl functionalities as temperature increases. PAC thus appears to adhere to the following order of reactivity:

hydroxyl- and/or amino-substituted PAC > alkyl- and ether-substituted PAC > unsubstituted PAC and PAC with carbonyl groups.

It is instructive to compare this experimentally observed order of reactivities with what might be predicted from frontier orbital theory. According to this theory (11), the bonding between two reactants participating in any of a number of kinds of reactions (e.g., concerted, free radical, ionic) occurs by overlap of the highest energy occupied molecular orbital (HOMO) of one species with the lowest energy unoccupied orbital (LUMO) of the other. Reactions are most energetically favored for high HOMO energies and low LUMO energies. If the reactant providing the LUMO is fixed, then the reactivities of compounds reacting with this species will follow the order of the compounds' HOMO energies. Except for a minus sign, ionization potentials are "roughly the energies of the HOMOs" (11), so lower ionization potentials denote higher energy HOMOs and higher reactivities. Figure 7 displays the values of ionization potentials, measured by photoionization mass spectrometry, as reported by Franklin, *et al.* (12) for a variety of one- and two-ring PAC. Figures 7a, b, and e show that the reactivity of an aromatic species is increased by an increase in either the number of alkyl substituents or the number of carbons within an alkyl substituent. Figure 7c reveals the strongly activating effect (relative to benzene) of an amino N attached directly to the aromatic ring. Figure 7d shows the activating effect of etheric or hydroxyl groups and the slightly deactivating effect of the carbonyl group. Thus PAC reactivity, as inferred from ionization potentials, follows the order:

aromatic amines > aromatic ethers  $\approx$  multialkylated PAC  $\approx$  phenols >  
 monoalkylated PAC > unsubstituted PAC > carbonyl-substituted PAC,

consistent with our experimental observations.

The above order helps to explain the behavior of the S curve in Figure 5. In Regime 1, the substituted PAC are composed of a significant portion of very reactive compounds with hydroxyl and/or NH, etheric, and alkyl functional groups. The S curve falls steeply as these very reactive substituted PAC disappear. By the end of Regime 1, the total mass of substituted species--especially that of the most reactive ones--is severely reduced. The slope of the S curve thus becomes less steep.

Interpretation of the U curve in Figure 5 is less clear-cut. In addition to the values in Figure 7, Franklin, *et al.* (12) provide ionization potentials for some PAC of  $\geq$  two rings (e.g., anthracene, 7.55 eV; benzo[*c*]phenanthrene, 8.12 eV; and acenaphthylene, 8.73 eV), which indicate a variation in reactivity among the unsubstituted PAC as well. Two alternatives emerge to account for the behavior of the U curve.

Alternative 1 holds that there is a significant difference between the reactivities of the unsubstituted PAC and the substituted PAC with the more activating functional groups (amino, hydroxyl, ether, multialkyl). While these highly reactive substituted PAC are present (Regime 1), soot formation is dominated by the conversion of these species. There may be conversion reactions within the unsubstituted PAC class to accommodate differences in individual species' reactivities, but there is negligible transfer into the class from conversion of substituted PAC or out of the class from conversion of unsubstituted PAC to soot in Regime 1. At the end of Regime 1, however, the remaining substituted species are much less reactive than those initially present, and there is no longer a large disparity between the reactivities of the substituted and unsubstituted PAC. The unsubstituted PAC begin to convert to soot too, and the U curve declines in Regime 2.

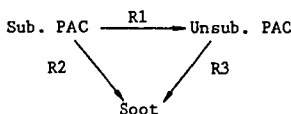
Alternative 2 suggests that, although the substituted PAC are more reactive as a class than the unsubstituted PAC, there are certain unsubstituted PAC with reactivities comparable to those of the more reactive substituted PAC. These more reactive unsubstituted PAC convert to soot in Regime 1, where their loss is offset by a gain in unsubstituted PAC produced by reactions of substituted PAC. As pyrolytic conditions become more severe (Regime 2), conversion of unsubstituted PAC to soot prevails over production of unsubstituted PAC. The balance is upset, and the U curve declines.

The two Alternatives represent fairly extreme cases. It is certainly likely that the true interpretation lies somewhere between these extremes, but our data do not permit us to be any more exact at this time.

The three pronounced peaks between 700 and 900  $\text{cm}^{-1}$  in the spectra of Figure 6 arise from aromatic C-H out-of-plane deformation. The position of each peak denotes the number of adjacent ring hydrogen atoms; 830-900  $\text{cm}^{-1}$ , one lone H atom; 800-860  $\text{cm}^{-1}$ , two adjacent H atoms; 735-820  $\text{cm}^{-1}$ , three to five adjacent H atoms (40,48). Figure 8 portrays the variation in distribution of aromatic hydrogen for the six samples analyzed. Although selective removal of PAC with substituents at certain positions would have some influence on the distribution of aromatic H atoms, one might expect the overall loss of substituted PAC to cause a general shift toward a higher number of adjacent H atoms. Figure 8 displays a slight decrease in the fraction of lone H--more pronounced in Regime 1 ( $8.7 > Y > 4.5$ )--that could be considered consistent with the loss of substituted PAC. Less amenable to explanation, however, is the increase in two adjacent H at the expense of the three adjacent H in Regime 2 ( $Y < 4.5$ )--a sign, perhaps, that other factors are also at work, e.g., destruction of heterocyclic structures and ring build-up processes that can form PAC of larger ring number and a higher degree of peri-condensation. Figure 8 allows no conclusions to be drawn about the relative reactivities of different positional isomers of substituted PAC.

#### EXTENSION: IMPLICATIONS FOR SOOT FORMATION

The conversion of PAC to soot can be approximated by the following scheme:



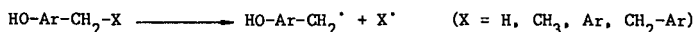
where the three reactions are depicted as irreversible since our experiments never show a net production of substituted PAC or a net destruction of soot. Although many uncertainties remain about the relative dominance of the three reactions, the data imply the following about this network:

- 1) In both Regimes, at least one of either R2 or R1-R3 must occur.
- 2) R3 must occur in Regime 2. It occurs in Regime 1 only if  $R1 = R3$ .
- 3) If soot forms via the combination R1-R3, then  $R1 = R3$  in Regime 1 and  $R1 < R3$  in Regime 2.
- 4) If soot cannot form via the combination R1-R3, then R2 must occur throughout Regimes 1 and 2; and R3 must occur only in Regime 2.

It would appear that if conversion of substituted PAC to soot does first entail conversion to unsubstituted PAC, then it does not merely involve removal of the substituent group: Lewis and Edstrom (38) report 7,12-dimethylbenz[a]-anthracene to form significantly more soot than benz[a]anthracene. Davis and Scully (10) and Glassman (16) report the alkylated naphthalenes and benzenes to have higher sooting tendencies than their unalkylated homologs. If benzene, naphthalene, and benz[a]anthracene are less likely to form soot than their alkylated derivatives, then it is unlikely that conversion of an alkylated PAC to soot proceeds via the removal of the alkyl group to form the unalkylated homolog.

If, as asserted by others (20,24,37), the conversion of PAC to soot involves the formation of a reactive free radical, then PAC reactivity should correlate with the ease of radical formation. The formation of a  $\sigma$ -type radical (e.g., phenyl, naphthyl) by abstraction of a ring-attached H atom or methyl group requires approximately 100 kcal/mole (37)--a high bond dissociation energy due to the localization of the resulting free electron. To form  $\pi$ -type radicals like benzyl, however, requires only about 77 kcal/mole because the resulting unpaired electron is resonance-stabilized (37). Alkyl-substituted PAC would then be expected to be more reactive than unalkylated PAC.

Substituted PAC with hydroxyl groups can evidently form radicals even more easily. Gavalas (15) reports the profound activating effect of a hydroxyl group substituted in the *ortho* or *para* position of an aromatic unit (Ar) linked by a methylene bridge. Because of keto-enol tautomerism, dissociations of the type



are very highly energetically favored over the type



Activation energies for the dissociation of aryl and aryl/alkyl ethers lie in the same range as those of aromatics with alkyl substituents or methylene bridges (15). Thus our experimentally observed order of depletion of PAC parallels that suggested by ease of radical formation: hydroxyl-substituted PAC > alkyl- and ether- substituted PAC > unsubstituted PAC.

#### CONCLUSIONS

1. As observed in previous studies in our laboratory (42), there is a constancy of summed PAC and soot yields that indicates a conversion of PAC to soot.
2. The ability to separate substituted PAC from unsubstituted PAC reveals differences in their pyrolysis behaviors: At low temperatures (< 1312 K at 6 in) or short times (drop distances < 4 in at 1375 K), yields of substituted PAC fall markedly with an increase in either temperature or time; yields of unsubstituted PAC remain constant. Both classes of PAC react away, however, at higher temperatures or longer times.
3. Plotting substituted and unsubstituted PAC yields versus total PAC yield  $Y$  reconciles data taken at constant distance and variable temperature with those taken at constant temperature and variable distance. Because substituted and unsubstituted PAC yields prove to be solely functions of  $Y$ ,  $Y$  aptly serves as a single parameter for pyrolysis severity since it accounts for variations in composition due to either temperature or time.

4. For the bituminous coal investigated, the yields of substituted and unsubstituted PAC suggest two PAC conversion regimes. Although reactivities may vary from species to species within a class, at low PAC conversions, substituted PAC as a class clearly display a much higher decay than the unsubstituted PAC: Substituted PAC yields fall by a factor of ~3.5; whereas the unsubstituted PAC show no net change. Though still evident at high PAC conversion, differences in the two classes' decays are much less pronounced. Unsubstituted PAC yields remain appreciably above those of the substituted PAC, but both classes undergo significant conversion to soot.
5. Conversion of PAC corresponds to differences in the kinds of functional groups present. At high values of Y, FT-IR shows that there are significant amounts of PAC with alkyl, ether, carbonyl, and hydroxyl and/or amino groups. Further pyrolysis, however, effects selective removal of the hydroxyl- and/or amino-substituted PAC. As the unsubstituted PAC become more prevalent, relative contributions from alkyl and ether functionalities go down and carbonyl substitution becomes slightly more significant.
6. Without specifying the kind of reaction mechanism, we can apply frontier orbital theory to PAC conversion reactions. This theory, along with values of ionization potentials found in the literature (12), suggests that PAC reactivity follows the order:
 

aromatic amines > aromatic ethers  $\approx$  multialkylated PAC  $\approx$  phenols >  
 monoalkylated PAC > unsubstituted PAC > carbonyl-substituted PAC,

 which is consistent with our experimental results.
7. If we restrict the PAC conversion reactions to involve free radical formation, then we again see agreement between theory and experiment. Less energy is needed to form free radicals from PAC with hydroxyl, alkyl, and ether substituents than from unsubstituted PAC.

#### ACKNOWLEDGEMENTS

The authors gratefully acknowledge the National Institute of Environmental Health Sciences (Grant NIH 5 P30 ES02109) for support of this research. They also wish to express their appreciation to Professor Preetinder S. Virk and Dr. Arthur L. Lafleur for their helpful discussions and to Ms. Elaine F. Plummer for the GC-MS analyses.

#### REFERENCES

1. A. Attar and G. G. Hendrickson, "Functional Groups and Heteroatoms in Coal," Chapter 5 in Coal Structure, ed. by R. A. Meyers. New York: Academic Press (1982).
2. G. M. Badger, "Carcinogenic Hydrocarbons," Chapter 1 in The Chemical Basis of Carcinogenic Activity. Springfield, Illinois: Charles C. Thomas (1962).
3. T. R. Barfknecht, B. M. Andon, W. G. Thilly, and R. A. Hites, "Soot and Mutation in Bacteria and Human Cells," pp. 231-242 in Chemical Analysis and Biological Fate: Polynuclear Aromatic Hydrocarbons, ed. by M. Cooke and A. J. Dennis. Columbus, Ohio: Battelle Press (1981).
4. N. Berkowitz, "The Methods of Coal Chemistry," Chapter 3 in Coal Science and Technology 7: The Chemistry of Coal. New York: Elsevier (1985).

5. H. Borwitzky and G. Schomburg, "Separation and Identification of Polynuclear Aromatic Compounds in Coal Tar by Using Glass Capillary Chromatography Including Combined Gas Chromatography-Mass Spectrometry," Journal of Chromatography **170**: 99-124 (1979).
6. M. V. Buchanan and M. B. Wise, "Negative Ion Processes for the Unambiguous Identification of Polycyclic Aromatics," Preprints of Papers, American Chemical Society, Division of Fuel Chemistry **31**(1): 191-197 (1986).
7. C. C.-S. Chang, "Thermal Reactions of Freshly Generated Coal Tar Over Calcium Oxide," Ph.D. Thesis, Massachusetts Institute of Technology, Department of Chemical Engineering (1986).
8. P. J. Collin, R. J. Tyler, and M. A. Wilson, "Influence of Pyrolysis Temperature on the Aromatic Fraction of Flash Pyrolysis Tars," Fuel **59**: 819-820 (1980).
9. A. D'Alessio, A. DiLorenzo, A. F. Sarofim, F. Beretta, S. Masi, and C. Venitozzi, "Soot Formation in Methane-Oxygen Flames," pp. 1427-1438 in Proceedings of the Fifteenth Symposium (International) on Combustion (1974).
10. R. A. Davies and D. B. Scully, "Carbon Formation from Aromatic Hydrocarbons II," Combustion and Flame **10**: 165-170 (1966).
11. I. Fleming, Frontier Orbitals and Organic Chemical Reactions. London: John Wiley and Sons (1976).
12. J. L. Franklin, J. G. Dillard, H. M. Rosenstock, J. T. Henson, K. Draxl, and F. H. Field, Ionization Potentials, Appearance Potentials, and Heats of Formation of Gaseous Positive Ions. Washington: National Bureau of Standards (1969).
13. J. D. Freihaut and D. J. Seery, "An Investigation of Yields and Characteristics of Tars Released During the Thermal Decomposition of Coal," Preprints of Papers, American Chemical Society, Division of Fuel Chemistry **26**(2): 133-148 (1981).
14. R. C. Garner and C. N. Martin, "Carcinogenic Aromatic Amines and Related Compounds," Chapter 4 in Chemical Carcinogens, Volume 1. Second Edition, ed. by C. E. Searle. ACS Monograph 182. Washington: American Chemical Society (1984).
15. G. R. Gavalas, "Thermal Reactions of Coal," Chapter 3 in Coal Science and Technology, Volume 4: Coal Pyrolysis. New York: Elsevier (1982).
16. I. Glassman, "Environmental Combustion Considerations," Chapter 8 in Combustion, Second Edition. Orlando, Florida: Academic Press (1987).
17. S. C. Graham, J. B. Homer, and J. L. J. Rosenfeld, "The Formation and Coagulation of Soot Aerosols Generated by the Pyrolysis of Aromatic Hydrocarbons," Proceedings of the Royal Society of London A **344**: 259-285 (1975).
18. W. H. Griest, B. A. Tomkins, J. L. Epler, and T. K. Rao, "Characterization of Multialkylated Polycyclic Aromatic Hydrocarbons in Energy-Related Materials," pp. 395-409 in Polynuclear Aromatic Hydrocarbons, ed. by P. W. Jones and P. Leber. Ann Arbor, Michigan: Ann Arbor Science Publishers (1979).
19. A. Hase, P. H. Lin, and R. A. Hites, "Analysis of Complex Polycyclic Aromatic Hydrocarbon Mixtures by Computerized GC-MS," pp. 435-442 in Carcinogenesis--A Comprehensive Survey Volume 1. Polynuclear Aromatic Hydrocarbons: Chemistry, Metabolism, and Carcinogenesis, ed. by R. I. Freudenthal and P. W. Jones. New York: Raven Press (1976).
20. B. S. Haynes and H. Gg. Wagner, "Soot Formation," Progress in Energy and Combustion Science **7**: 229-273 (1981).
21. S. S. Hecht, M. Loy, and D. Hoffmann, "On the Structure and Carcinogenicity of the Methyl Chrysenes," pp. 325-340 in Carcinogenesis--A Comprehensive Survey Volume 1. Polynuclear Aromatic Hydrocarbons: Chemistry, Metabolism, and Carcinogenesis, ed. by R. I. Freudenthal and P. W. Jones. New York: Raven Press (1976).

22. R. A. Hites, "Sources and Fates of Atmospheric Polycyclic Aromatic Hydrocarbons," Chapter 10 in Atmospheric Aerosol: Source/Air Quality Relationships. ACS Symposium Series 167: 187-196 (1981).
23. R. A. Hites and G. R. Dubay, "Charge-Exchange-Chemical Ionization Mass Spectrometry of Polycyclic Aromatic Compounds," pp. 85-87 in Carcinogenesis--A Comprehensive Survey Volume 3. Polynuclear Aromatic Hydrocarbons, ed. by P. W. Jones and R. I. Freudenthal. New York: Raven Press (1978).
24. J. B. Howard and W. J. Kausch, Jr., "Soot Control by Fuel Additives," Progress in Energy and Combustion Science 6: 263-276 (1980).
25. B. M. Hughes, J. Troost, and R. Liotta, "Pyrolysis/(GC)<sup>2</sup>/MS as a Coal Characterization Technique," Preprints of Papers, American Chemical Society, Division of Fuel Chemistry 26(2): 107-120 (1981).
26. R. E. Laflamme and R. A. Hites, "The Global Distribution of Polycyclic Aromatic Hydrocarbons in Recent Sediments," Geochimica et Cosmochimica Acta 42: 289-303 (1978).
27. A. L. Lafleur, P. A. Monchamp, E. F. Plummer, and E. L. Kruzel, "Evaluation of Gravimetric Methods for Dissoluble Matter in Extracts of Environmental Samples," Analytical Letters 19: 2103-2119 (1986).
28. A. L. Lafleur and M. J. Wornat, "Multimode Retention in High-Performance Size Exclusion Chromatography with Polydivinylbenzene: I. Polycyclic Aromatic Hydrocarbons" (submitted to Analytical Chemistry).
29. A. L. Lafleur and M. J. Wornat, "Multimode Retention in High-Performance Size Exclusion Chromatography with Polydivinylbenzene: II. Heterocyclic Aromatic Compounds" (in progress).
30. R. C. Lao, R. S. Thomas, H. Oja, and L. Dubois, "Application of a Gas Chromatograph-Mass Spectrometer-Data Processor Combination to the Analysis of the Polycyclic Aromatic Hydrocarbon Content of Airborne Pollutants," Analytical Chemistry 45: 908-915 (1973).
31. D. W. Later, T. G. Andros, and M. L. Lee, "Isolation and Identification of Amino Polycyclic Aromatic Hydrocarbons from Coal-Derived Products," Analytical Chemistry 55: 2126-2132 (1983).
32. D. W. Later, E. K. Chess, C. W. Wright, R. B. Lucke, D. D. Mahlum, and B. W. Wilson, "Mass Spectrometric and Chromatographic Methods Applied to the Isolation and Identification of Tumorigenic Polycyclic Aromatic Hydrocarbons in Coal Liquefaction," presented at the Thirty-Second Annual Conference on Mass Spectrometry and Allied Topics, San Antonio, Texas (1984).
33. D. W. Later and B. W. Wright, "Capillary Column Gas Chromatographic Separation of Amino Polycyclic Aromatic Hydrocarbon Isomers," Journal of Chromatography 289: 183-193 (1984).
34. E. J. Lavoie, D. T. Coleman, N. G. Geddie, and J. E. Rice, "Studies of the Mutagenicity and Tumor-Initiating Activity of Methylated Fluorenes," Chemico-Biological Interactions 52: 301-309 (1985).
35. M. L. Lee, personal communication (1987).
36. M. L. Lee, G. P. Prado, J. B. Howard, and R. A. Hites, "Source Identification of Urban Airborne Polycyclic Aromatic Hydrocarbons by Gas Chromatographic Mass Spectrometry and High Resolution Mass Spectrometry," Biomedical Mass Spectrometry 4(3): 182-186 (1977).
37. I. C. Lewis, "Chemistry of Carbonization," Carbon 20: 519-529 (1982).
38. I. C. Lewis and T. Edstrom, "Studies of the Thermal Behavior of Some Polynuclear Aromatics," Proceedings of the Fifth Conference on Carbon. New York: Pergamon Press, 413-430 (1963).
39. D. McNeil, "High Temperature Coal Tar," Chapter 17 in Second Supplementary Volume of Chemistry of Coal Utilization, ed. by M. A. Elliott. New York: John Wiley and Sons (1981).
40. K. Nakanishi, Infrared Absorption Spectroscopy--Practical. San Francisco:

- Holden-Day (1962).
41. R. D. Nenniger, "Aerosols Produced from Coal Pyrolysis," Sc.D. Thesis, Massachusetts Institute of Technology, Department of Chemical Engineering (1986).
  42. R. D. Nenniger, J. B. Howard, and A. F. Sarofim, "Sooting Potential of Coals," pp. 521-524 in Proceedings of the International Conference on Coal Science. Pittsburgh: Pittsburgh Energy Technology Center (1983).
  43. M. Novotny, A. Hirose, and D. Wiesler, "Separation and Characterization of Very Large Neutral Polycyclic Molecules in Fossil Fuels by Microcolumn Liquid Chromatography," Analytical Chemistry 56: 1243-1248 (1984).
  44. P. C. Painter, R. W. Snyder, M. Starsinic, M. M. Coleman, D. W. Kuehn, and A. Davis, "Fourier Transform IR Spectroscopy: Application to the Quantitative Determination of Functional Groups in Coal," Chapter 3 in Coal and Coal Products: Analytical Characterization Techniques, ACS Symposium Series 205, ed. by E. L. Fuller. Washington: American Chemical Society (1982).
  45. E. C. Prahl, E. Crecellus, and R. Carpenter, "Polycyclic Aromatic Hydrocarbons in Washington Coastal Sediments: An Evaluation of Atmospheric and Riverine Routes of Introduction," Environmental Science and Technology 18: 687-693 (1984).
  46. M. A. Serio, "Secondary Reactions of Tar in Coal Pyrolysis," Ph.D. Thesis, Massachusetts Institute of Technology, Department of Chemical Engineering (1984).
  47. B. D. Silverman and J. P. Lowe, "Diol-Epoxy Reactivity of Methylated Polycyclic Aromatic Hydrocarbons (PAH): Ranking the Reactivity of the Positional Monomethyl Isomers," pp. 743-753 in Polynuclear Aromatic Hydrocarbons, Proceedings of the Sixth International Symposium, ed. by M. Cook, A. J. Dennis, and G. L. Fisher. Columbus, Ohio: Battelle Press (1982).
  48. G. Socrates, Infrared Characteristic Group Frequencies. New York: John Wiley and Sons (1980).
  49. P. R. Solomon, R. M. Carangelo, P. E. Best, J. R. Markham, and D. G. Hamblen, "Analysis of Particle Composition, Size, and Temperature by FT-IR Emission/Transmission Spectroscopy," Preprints of Papers, American Chemical Society, Division of Fuel Chemistry 31(1): 141-151 (1986).
  50. P. R. Solomon, D. G. Hamblen, and R. M. Carangelo, "Applications of Fourier-Transform IR Spectroscopy in Fuel Science," Chapter 4 in Coal and Coal Products: Analytical Characterization Techniques, ACS Symposium Series 205, ed. by E. L. Fuller, Jr. Washington: American Chemical Society (1982).
  51. P. R. Solomon, D. G. Hamblen, R. M. Carangelo, J. R. Markham, and M. R. Chaffee, "Application of FT-IR Spectroscopy to Study Hydrocarbon Reaction Chemistry," Preprints of Papers, American Chemical Society, Division of Fuel Chemistry 30(1): 1-12 (1985).
  52. E. E. Tompkins and R. Long, "The Flux of Polycyclic Aromatic Hydrocarbons and of Insoluble Material in Pre-Mixed Acetylene-Oxygen Flames," Proceedings of the Twelfth Symposium (International) on Combustion: 625-633 (1969).
  53. F. J. Vastola and L. J. McGahan, "The Development of Laser Micropyrolysis of Coal Macerals," Preprints of Papers, American Chemical Society, Division of Fuel Chemistry 31(1): 53-59 (1986).
  54. B. W. Wilson, R. Pelroy, and J. T. Cresto, "Identification of Primary Aromatic Amines in Mutagenically Active Sub-Fractions from Coal Liquefaction Materials," Mutation Research 79: 193-202 (1980).
  55. M. J. Wornat, A. F. Sarofim, and J. P. Longwell, "Changes in the Aromatic Ring Number Distribution of PAC from Pyrolysis of a High Volatile Bituminous Coal" (in progress).

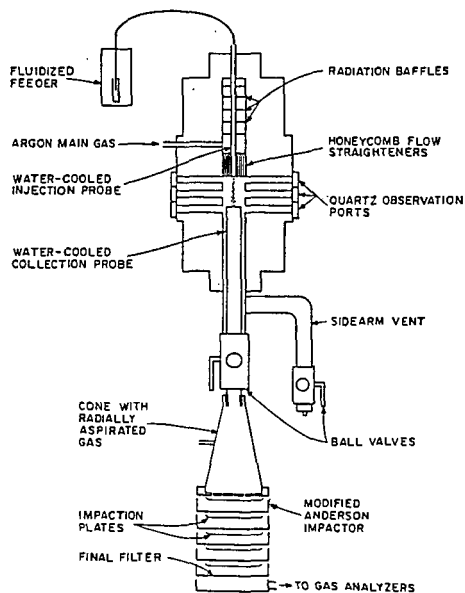


FIGURE 1: THE PYROLYSIS FURNACE AND COLLECTION SYSTEM

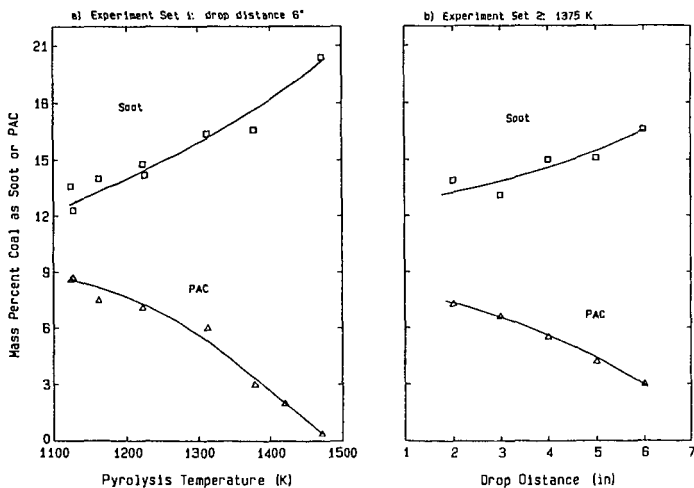


FIGURE 2: SOOT AND PAC YIELDS AT VARIOUS PYROLYSIS CONDITIONS



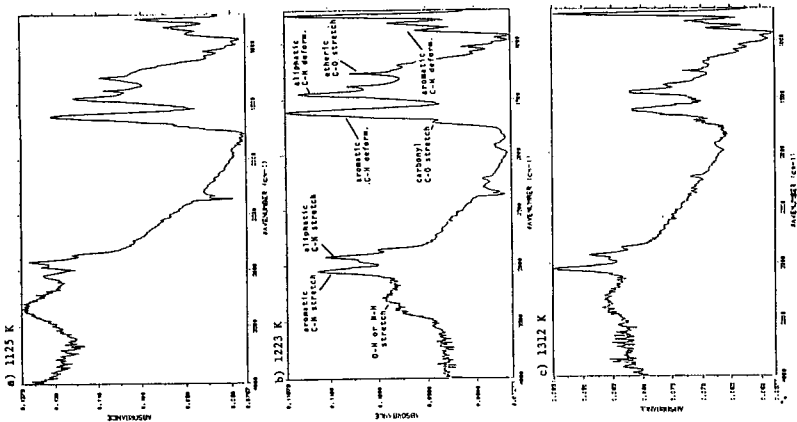


FIGURE 6: FT-IR SPECTRA OF PAC FOR THREE PYROLYSIS TEMPERATURES

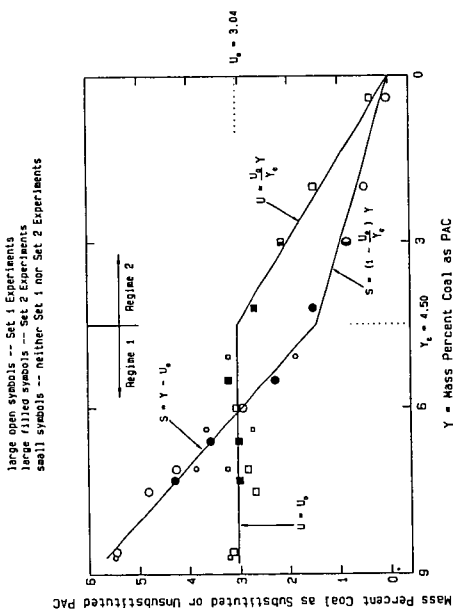


FIGURE 5: SUBSTITUTED AND UNSUBSTITUTED PAC YIELDS VERSUS TOTAL PAC YIELD

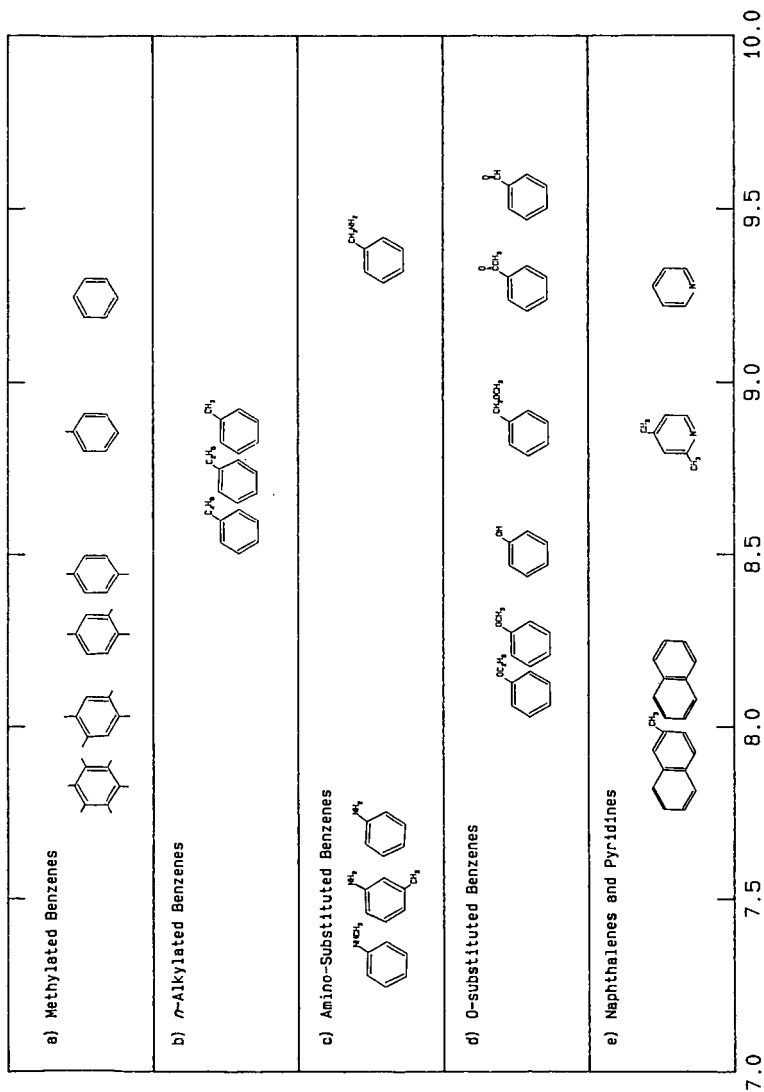


FIGURE 7: IONIZATION POTENTIALS (eV) OF AROMATICS  
from Franklin, *et al.* (12)

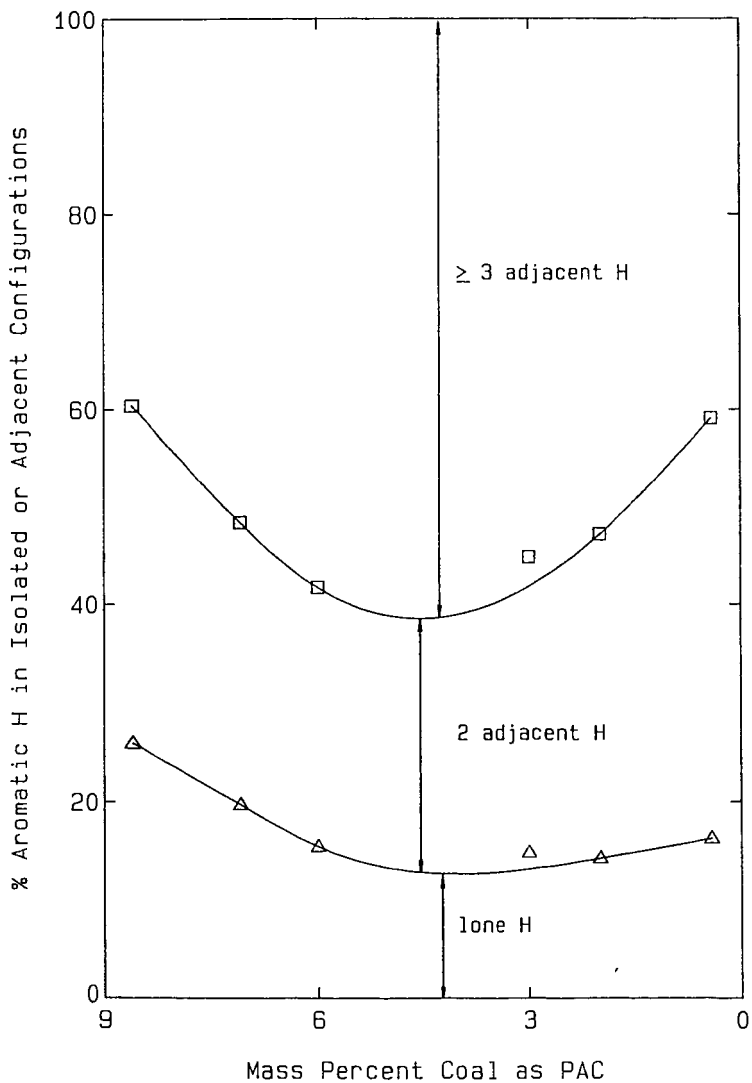


FIGURE 8: VARIATION IN AROMATIC H ADJACENCY FROM FT-IR

# THERMOLYSIS OF SURFACE-ATTACHED 1,3-DIPHENYLPROPANE: IMPACT OF SURFACE IMMOBILIZATION ON THERMAL REACTION MECHANISMS

A. C. Buchanan, III and C. A. Biggs

Chemistry Division  
Oak Ridge National Laboratory  
P. O. Box X  
Oak Ridge, Tennessee 37831-6197

## INTRODUCTION

Attempts to understand the thermal chemistry of coal at the molecular level are severely complicated by its inherent properties: a diverse array of structural units (e.g., aromatic, hydroaromatic, and heterocyclic aromatic clusters connected by short aliphatic and ether links) and functional groups (e.g., phenolic hydroxyls, carboxyls, and basic nitrogens) in a cross-linked macromolecular framework with no repeating units (1,2). One simplifying experimental approach has been the study of individual model compounds that highlight structural features in coal. A complicating feature in the interpretive extrapolation of model compound behavior to coal is the possible modifications in free-radical reactivity patterns resulting from restricted translational mobility in the coal where breaking one bond in the macromolecular structure will result in radical centers that are still attached to the residual framework. We are modeling this phenomenon by studying the thermolysis of model compounds that are immobilized by covalent attachment to an inert surface. Previous studies of surface-immobilized bibenzyl (1,2-diphenylethane) showed that immobilization can profoundly alter free-radical reaction pathways compared with the corresponding fluid phase behavior (3). In particular, free-radical chain pathways became dominant decay routes leading to rearrangement, cyclization, and hydrogenolysis of the bibenzyl groups. In this paper we describe preliminary results on the effects of surface immobilization on the thermolysis of 1,3-diphenylpropane, whose fluid phase behavior has been extensively investigated (4-8).

## EXPERIMENTAL

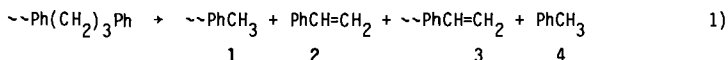
Surface-immobilized 1,3-diphenylpropane ( $\sim$ -DPP) was prepared at saturation coverage by the condensation at 225 °C of excess  $p$ -HOPh(CH<sub>2</sub>)<sub>3</sub>Ph with the surface hydroxyl groups of a fumed silica (Cabosil M-5, Cabot Corp., 200 m<sup>2</sup>/g) according to the procedure described previously for surface-immobilized bibenzyl (3). Excess phenol was removed by heating at 300 (Batch A) or 270 °C (Batch B) for 0.5 h under a dynamic vacuum. The lower temperature used for Batch B appears to minimize a trace amount of reaction (ca. 0.02%) that occurs during this purification stage. GC analysis following a base hydrolysis assay procedure (3) gave coverages of 0.586 (Batch A) and 0.566 (Batch B) mmol  $\sim$ -DPP per gram of final product. The starting phenol was prepared by the acid catalyzed condensation of cinnamyl alcohol (PhCH=CHCH<sub>2</sub>OH) and phenol (9) followed by catalytic hydrogenation (10% Pd/carbon) of the olefinic intermediate.

Thermolysis (in sealed, evacuated tubes) and product analysis procedures have been thoroughly described elsewhere (3). Typically 0.3-0.4 g of surface-attached material (0.17-0.23 mmol  $\sim$ -DPP) are employed, and volatile products are collected in a cold trap and then analyzed by GC and GC-MS. In a separate procedure surface-attached products are liberated as phenols following digestion of the silica in 1 N NaOH, silylated to the corresponding trimethylsilyl ethers, and analyzed as above.

## RESULTS AND DISCUSSION

Thermolyses have been performed at 345 and 375 °C, and the product distributions for the four major primary products and the major secondary products are shown as a function of ~DPP conversion in Figure 1a. The two lowest conversion runs (1.50 and 1.94%) were obtained at 345 °C, while the remainder of the data was obtained at 375 °C. Results from the two different high coverage batches of ~DPP were consistent in terms of products detected and their relative yields. The only difference observed was a slightly slower reaction rate for batch B (ca. 30%) perhaps reflecting a slightly higher purity as a result of purification at the lower temperature (see experimental section).

We find that at low conversions (<3%) ~DPP cracks to form four major products in essentially equal amounts as shown below.

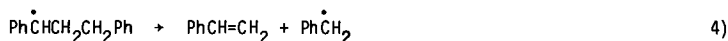
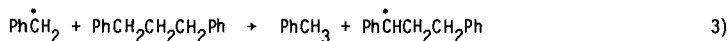


Thermolysis of liquid DPP at very low conversions also gave a correspondingly simple product distribution as shown in Eq. 2 (4).

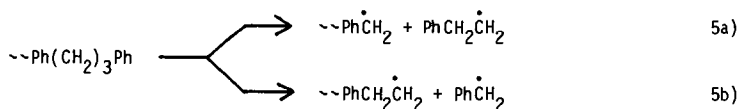


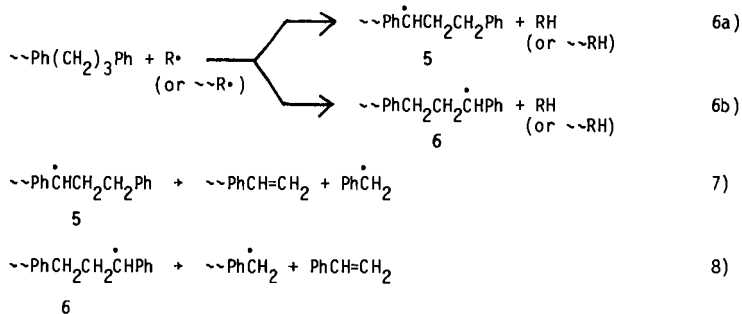
Hence at low conversions, the surface-immobilized DPP is reacting in an analogous fashion to liquid DPP. The additional product pair observed in the thermolysis of ~DPP results from the fact that the two ends of the DPP molecule are no longer equivalent upon covalent surface attachment. The initial rate of the ~DPP reaction is 15-20% h<sup>-1</sup> at 375 °C for the two batches (based on a 2.3-3.0% conversion after a 9 min reaction period), and this decomposition rate is comparable to that measured for liquid DPP (ca. 19% h<sup>-1</sup>) (4). This further indicates that surface immobilization at high coverage is not perturbing the initial reaction behavior of the DPP moiety.

The facile decomposition of liquid DPP was demonstrated to arise from a radical chain route whose chain propagation steps are shown in Eqs. 3 and 4 (4). In the case



of ~DPP, two distinct benzylic radicals can be formed by hydrogen abstraction (Eq. 6) following a small amount of initial homolysis (Eq. 5). Each radical can then undergo a rapid β-scission process (Eqs. 7 and 8) to produce the surface bound and free styrene products (3 and 2 respectively) analogous to Eq. 4. The free and surface-immobilized benzyl radicals propagate the chain by reacting with ~DPP (Eq. 6; R = PhCH<sub>2</sub>) to form the free and surface bound toluene products (4 and 1 respectively) while regenerating 5 and 6.





No selectivity is observed for the two possible decay routes that form the product pairs 1 and 2 or 3 and 4. This suggests that at low conversions, radicals 5 and 6 are formed with equal probability and that their  $\beta$ -scission reactions (Eqs. 7 and 8) occur at equal rates. Trace quantities of other primary products (each <0.05 mol% of the products) including free and surface bound  $\text{PhC}_2\text{H}_5$  (Eq. 6;  $\text{R} = \text{PhC}_2\text{H}_4$ ) and free bibenzyl (from benzyl radical coupling) are also detected.

As the conversion of  $\sim\text{DPP}$  increases, there is a divergence in the yields of the four main products (Fig. 1a), and several secondary products are formed in small but increasing yields. The most significant of these (reaching about 2.8 mol % of the products at 23% conversion) is  $\sim\text{Ph}(\text{CH}_2)_3\text{Ph}\cdot$ , 7 (identified by GC-MS as the corresponding bistrimethylsilyl ether after workup). The formation of this doubly attached product arises from a secondary reaction that consumes 3, perhaps via addition of surface-attached benzyl radical (which would normally have reacted to form 1) to the surface-attached styrene. Additional secondary products observed at higher conversion include several unidentified isomers of composition corresponding to  $\sim\text{C}_{23}\text{H}_{22}\cdot$ . These products also involve the consumption of surface bound styrene (and a  $\sim\text{DPP}$ ) and have a formal analog, 1,3,5-triphenylpentane, amongst the secondary products detected in the thermolysis of liquid DPP (4). However even at the highest conversion studied (23%), the secondary products sum to only 5 mol % of the total products. The radical chain decomposition of surface-immobilized DPP is a very efficient process with an estimated kinetic chain length ( $c.l. \equiv (\text{PhVi} + \sim\text{PhVi})/4\text{PhEt}$ ) of 200 at 345 °C. This calculation assumes that there is no selectivity in the initial homolysis (Eq. 5) and that all  $\text{PhC}_2\text{H}_4\cdot$  start chains.

One of the most interesting features to emerge from this study is an observed selectivity for the radical chain reaction path that forms 1 and 2 relative to that which forms 3 and 4 as the conversion increases. This is most clearly seen in Fig. 1b where the styrene to toluene yield ratio (these products are not consumed in secondary reactions) is used as an indicator of this selectivity. The ratio increases monotonically from a value of 1.00 ( $\pm 0.02$ ) indicating no selectivity at conversions <4% to a value of 1.41 ( $\pm 0.04$ ) at 23% conversion. We previously observed in the case of surface-immobilized bibenzyl that reaction rates of radical chain pathways are very sensitive to changes in surface coverage (3). These studies also indicated that unimolecular steps such as Eqs. 7 and 8 should be unaffected by such surface coverage changes. The observed regioselectivity in the reaction of  $\sim\text{DPP}$  at higher conversions may indicate that, as the molecules of  $\sim\text{DPP}$  become spread apart on the surface, hydrogen abstraction at the benzylic carbon that is farthest from the surface is becoming favored, i.e., selectivity for formation of 6 (Eq. 6b) relative to 5 (Eq. 6a). However the complication resulting from the formation of secondary products, which likely involve the reaction of 5 and 6, does not allow a firm

conclusion to be reached at this time. Additional insights into the cause of this regioselectivity should be gained from current studies being performed at lower initial surface coverages.

#### CONCLUSIONS

Covalent attachment of organic compounds onto an inert silica surface has proven to be a successful methodology for exploring the thermal reaction chemistry of coal model compounds under surface-immobilized conditions at temperatures relevant for coal thermolysis. Previous studies of surface-attached bibenzyl showed that restrictions on free-radical mobility can have a significant impact on reaction rates and on the nature and composition of the reaction products when compared with fluid phase behavior. The current investigation of the thermolysis of surface-immobilized 1,3-diphenylpropane has shown that facile decomposition of the trimethylene link by means of a radical chain process can still occur under surface-immobilized conditions. For  $\sim$ -DPP no selectivity is observed at low conversions for the two competing radical chain decay pathways that cycle through benzylic radicals 5 and 6. However at higher conversions, a selectivity is observed favoring the radical chain route cycling through 6. Experiments are in progress to determine if this selectivity is a result of regioselective hydrogen transfer on the surface at lower surface coverages.

#### ACKNOWLEDGMENTS

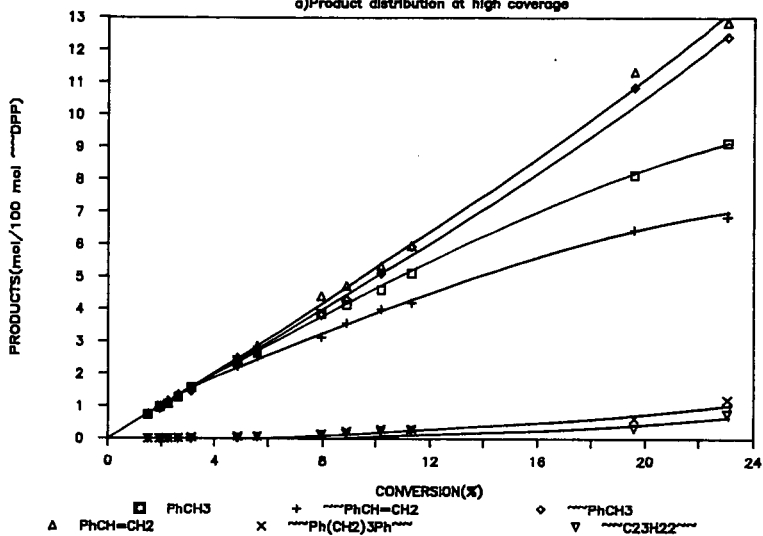
This research was sponsored by the Division of Chemical Sciences, Office of Basic Energy Sciences, U.S. Department of Energy under contract DE-AC05-84OR21400 with Martin Marietta Energy Systems, Inc.

#### REFERENCES

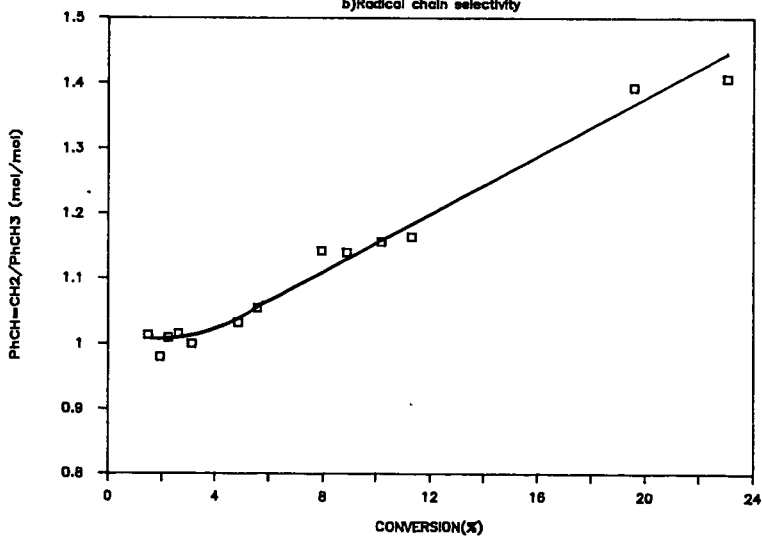
1. Davidson, R. M. In Coal Science; Gorbaty, M. L. Larsen, J. W., Wender, I., Eds.; Academic Press: New York, 1982; Vol 1.
2. Green T.; Kovac, J.; Brenner, D.; Larsen, J. W. In Coal Structure; Meyers, R. A., Ed.; Academic Press: New York, 1982; Chapter 6.
3. (a) Buchanan, III, A. C.; Dunstan, T. D. J.; Douglas, E. C.; Poutsma, M. L. J. Am. Chem. Soc. 1986, 108, 7703. (b) Poutsma, M. L.; Douglas, E. C.; Leach, J. E. Ibid. 1984, 106, 1136.
4. Poutsma, M. L.; Dyer, C. W. J. Org. Chem. 1982, 47, 4903.
5. (a) Gilbert, K. E.; Gajewski, J. J. J. Org. Chem. 1982, 47, 4899. (b) Gilbert, K. E., Ibid. 1984, 49, 6.
6. Sweeting, J. W.; Wilshire, J. F. K. Aust. J. Chem. 1962, 15, 89.
7. (a) Benjamin, B. M.; Raaen, V. F.; Maupin, P. H.; Brown, L. L.; Collins, C. J. Fuel 1978, 57, 269. (b) Collins, C. J.; Raaen, V. F.; Benjamin, B. M.; Maupin P. H.; Roark, W. H. J. Am. Chem. Soc. 1979, 101, 5009.
8. King, H.-H.; Stock, L. M. Fuel 1984, 63, 810.
9. Jurd, L. Tetrahedron Lett. 1969, 33, 2863.

Figure 1. Thermolysis of  $\sim\text{Ph}(\text{CH}_2)_3\text{Ph}$

a) Product distribution at high coverage



b) Radical chain selectivity



## THE CASE FOR INDUCED BOND SCISSION DURING COAL PYROLYSIS

Donald F. McMillen, Ripudaman Malhotra, and S. Esther Nigenda

Department of Chemical Kinetics, SRI International  
333 Ravenswood Ave., Menlo Park, CA, 94025

### INTRODUCTION

Most coal pyrolysis models invoke spontaneous thermal scission of inherently weak bonds as the sole pyrolytic reaction leading to depolymerization of coal structures (1).<sup>\*</sup> In this view, bond scission is dependent only on temperature; the only additional chemical factors that impact the "net" cleavage are scavenging and crosslinking of thermally generated radicals, which can be affected primarily by varying heating rates and other factors that affect heat and mass transport. In contrast to this traditional picture, data obtained by various researchers (partly in the context of coal liquefaction), when taken together, provide a strong argument that induced scission of strong bonds plays a significant role during coal pyrolysis. In this paper we attempt to summarize this argument.

The types of bond cleavage occurring during pyrolysis have been obscured in part because of the inherent difficulty of obtaining mechanistically significant pyrolysis activation energies. It is now well appreciated (3,4) that the apparent activation energy for a mixture that decomposes by a sequence of parallel first order reactions can, under conditions of rising temperature, lie below that of any member of the sequence. This factor is evidently responsible for reported activation energies as low, or lower than, 15 kcal/mole. Thus, when coupled with plausible unimolecular scission A-factors ( $10^{14.5}$  to  $10^{15.5}$ ) and a 5 to 15 kcal distribution of activation energies, rates measured under non-isothermal conditions have been shown to correspond to mean activation energies of 50 to 65 kcal/mol (5). This result has quite naturally been taken as evidence supporting the original presumption of weak bond thermolysis. However, 50 to 65 kcal/mol activation energies in no way exclude bond scission that is chemically induced by other components in the pyrolyzing substrate. In the following paragraphs, we outline some of the evidence that such induced bond scission can take place under pyrolysis conditions, and show how including them helps explain certain coal conversion phenomena.

### EVIDENCE FOR THE OCCURENCE OF INDUCED BOND SCISSION DURING PYROLYSIS

Analogy with Coal Liquefaction. Since the acceptance of the weak-bond-scission/radical-capping model in coal pyrolysis has followed in large part on the acceptance of a similar model in coal liquefaction, and it has now been shown that such a model is inadequate (6-9) for liquefaction, it should also be considered whether the model is inadequate for pyrolysis. The traditional model relegates the liquefaction solvent to a role of merely scavenging thermally generated radicals. However, liquefaction effectiveness of various polycyclic aromatic hydrocarbons (PAH) has been shown very distinctly not to correlate with scavenging, or radical-capping, effectiveness (6,9). For instance, 9,10-dihydroanthracene and its parent hydrocarbon are generally seen to be

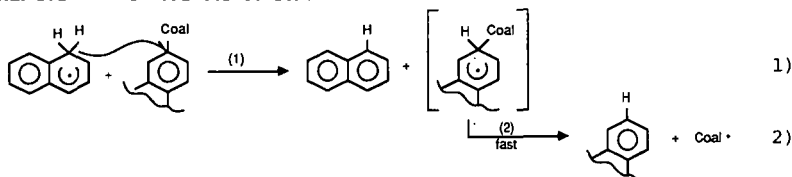
---

\*In the most mechanistically complete model of coal pyrolysis presented to date, Gavalas and co-workers have included bond scission induced by ipso attack of H-atoms on linkages to aromatic rings (2). Their suggestion seems to have been either largely ignored, or considered to be a minor side reaction in the production of volatiles.

substantially inferior to dihydrophenanthrene and dihydropyrene, even though dihydroanthracene is a markedly better scavenger. The inferiority of anthracene is most pronounced in the case where the solvent has no hydroaromatic hydrogen to transfer to the coal, but can only assist in shuttling hydrogen from one part of the coal structure to another (10-12). Under these conditions, the traditional mechanism requires in-situ formation of hydroaromatic, which then acts as the capping agent. Dihydroanthracene is not only the most effective scavenger (13) but because of thermochemical and kinetic considerations, is the hydroaromatic most readily formed by hydrogen transfer from coal structures. Nonetheless, it is typically much less effective than either of the other two PCAH.

Since it is clear that the hydrogen being "shuttled" is not serving merely to scavenge fragments of bonds that have already been broken, it is very likely that this hydrogen shuttling is actually inducing bond scission. It is interesting to note that liquefaction under shuttling conditions not only provides the most striking examples of the inadequacy of the traditional liquefaction mechanism, but also resembles coal pyrolysis, in that all of the hydrogen demand must be supplied by the coal itself.

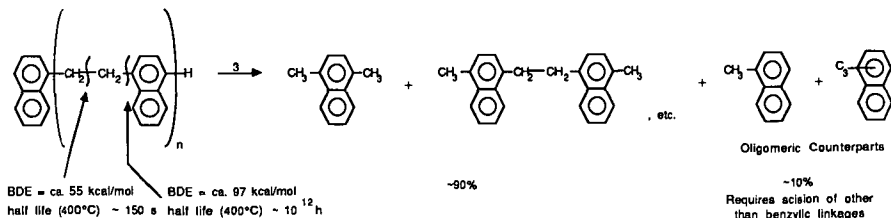
Strong Bond Cleavage by Solvent Mediated Hydrogenolysis. We have used model compound studies (6,8) to show that in hydroaromatic-aromatic PCAH systems, hydrogen-transfer-induced bond scission (hydrogenolysis) of bonds too strong to thermolyze can be significant on liquefaction time scales, even in the absence of  $H_2$  pressure. In addition, we have used hybrid coal/model-compound studies to show (7) that such cleavage tends to be accelerated by the presence of coals, and moreover, to occur by a hydrogen transfer process that does not involve the production of free H-atoms. This "radical hydrogen-transfer" (RHT) occurs in a direct bimolecular process from cyclohexadienyl "carrier" radicals formed from PCAH solvent or coal structures.



The existence of this reaction was for a long time obscured by the fact that it is often in competition with elimination and addition reactions of free H-atoms. Evidence for RHT has now been presented by several groups (14-16). While an addition-elimination sequence can yield the same products as RHT, side reactions ( $H_2$  formation and ring hydrogenation) are associated with elimination addition. For this reason, a shift in the competition between H-transfer by the RHT process and an elimination-addition process can have a substantial impact on the utilization efficiency of solvent or coal hydrogen (6). Thus, we suggest not only that hydrogen-transfer-induced bond scission may be important in coal pyrolysis as well as in liquefaction, but also that the mode of hydrogen transfer may be more critical in pyrolysis, where the available hydrogen is limited to that which can be transferred from the relatively hydrogen-rich portions of the coal structure. The importance of hydrogenolysis mediated by solvent radicals (or coal radicals) moves such radicals from the category of species for which the only goal is to prevent retrograde reactions, to species which can, in addition, be sources of bond cleavage activity.

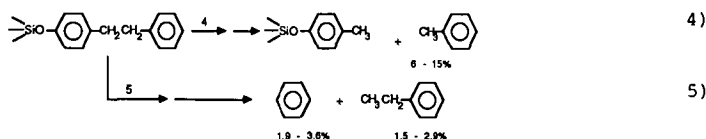
Strong-Bond Scission in Pyrolysis of Coal Models. Direct evidence for induced scission of alkyl-aryl linkages in the nominal absence of solvents can be seen in the pyrolyses of polymeric coal models consisting of aliphatic linkages between PCAH clusters. Solomon and co-workers have pyrolyzed a series of polymers  $(-Ar-CH_2-CH_2-)_n$  at 400 to 430°C and analyzed the tars by field

ionization mass spectrometry (17). This analysis revealed that polymeric coal models purposely synthesized to decompose entirely by thermolysis of the weak central bond, provide, in addition, a small but significant amount of product indicative of cleavage of the much stronger aryl-alkyl linkage.

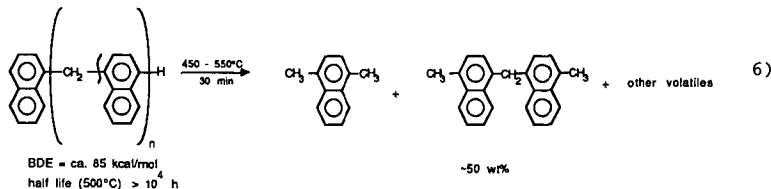


The known strengths of the two bonds (18) are such that at 400°C, the thermolysis half-life of the weaker bond is several hundred seconds, whereas the half-life of the stronger bond would be 10<sup>10</sup> times longer -- wholly unobservable if thermolysis were the only available cleavage route.

These results with weakly bonded polymers are parallel to those of Buchanan (19) and co-workers who have shown that when bibenzyl is immobilized by bonding to a silica surface, induced bond-scissions become substantially more important than they are in the liquid phase. The yield of benzene and ethylbenzene ranges from about 40 to 70% of the yield of toluene. In other words, for every one to two bibenzyl linkages that break spontaneously, there is another, very strong bond whose scission is induced by hydrogen transfer. As discussed by Buchanan, the restraint provided by the bonding makes radical-radical reactions less likely, and unimolecular reactions such as rearrangement and H-atom elimination more likely. The latter reaction can then lead to hydrogenolysis of an adjacent bibenzyl structure.

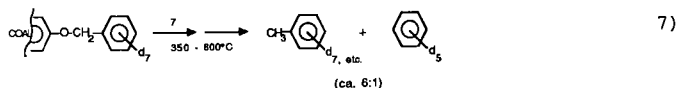


Similarly, earlier work by Van Krevelen (20) on polymers that contained no weak linkages whatsoever had shown that when heated in a nitrogen stream at 3°C/min, these single methylene bridged polymers were roughly half converted into volatile material during the 30 minute passage through the 450 to 550°C temperature range.



For the case of the methylene-bridged naphthalene polymer, where the central linkage has a bond strength of ~ 85 kcal/mol (18), the thermolysis half-life even at 550°C would be >10<sup>3</sup> hours.

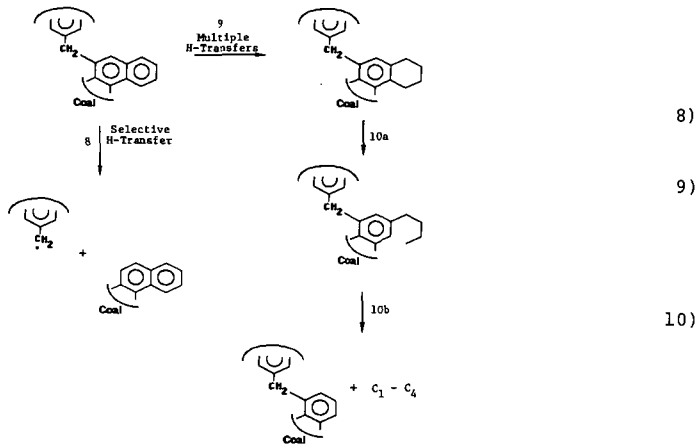
Pyrolysis of O- and C- Alkylated Coals. Various groups have shown that the methylation of coals (17,21), particularly low-rank coals, prior to pyrolysis improves the yields of the volatiles. These yield increases have been attributed to inhibition of retrograde reactions involving phenolic -OH, but they can also reflect an increased contribution from induced bond scission processes. This has been illustrated recently by Stock and co-workers (22) who have examined the product of O- methylated and O- and C- benzylated coals and found not only the expected cleavage (thermolysis) of the weak O-benzyl and C-benzyl bonds, but also the cleavage of the much stronger phenyl-C bond.



#### IMPORTANCE OF INDUCED BOND SCISSION

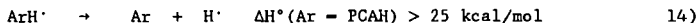
The above results provide a very clear demonstration that induced scission of strong bonds in known structures does take place under pyrolysis conditions. These results suggest, but do not prove, that such cleavages also take place in coals during pyrolysis. However, the pertinent question we have to ultimately consider is whether such cleavage is of any significance to the practice of coal pyrolysis. In the following paragraphs we show that the same competing H-transfer steps we have found to be important under liquefaction conditions can account for striking variations in the yields of oil and gas resulting from modest changes in pyrolysis conditions.

Oil and Gas Yield Variations in Hydropyrolysis. Gorbaty and Maa have reported (27) that the product distribution in a fixed-bed hydropyrolysis is critically dependent upon whether the reaction temperature exceeds the threshold above which there is a pronounced exotherm. The incremental yields obtained by a switch of the pyrolysis gas from N<sub>2</sub> to H<sub>2</sub> go almost exclusively to oil if the temperature remains below this threshold, but go almost exclusively to gas if the threshold temperature is exceeded. These results are shown in Figure 1. As indicated by the authors, the higher temperatures produced in the exotherm evidently result in more ring hydrogenation and ring opening (followed by cleavage of the newly produced side chains), yielding more gas.





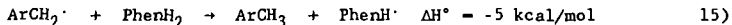
The effectiveness of the aromatic pool in regaining "wastefully" transferred hydrogen is a function of the nature and concentration of the aromatic and the temperature. At a given temperature, the rate of this retrieval of hydrogen increases with increasing aromatic concentration in the solvent (or in the coal if there is no solvent). On the other hand, to the extent that the concentration of aromatic is too low, the non-*ipso* radicals will obtain a second hydrogen (e.g., from another molecule of ArH<sub>2</sub>) to yield uncleaved dihydro product. At higher temperatures, the endothermic reactions



are shifted to the right, and any given Ar becomes less effective as a "reservoir" for H-transfer activity. This means that the non-*ipso* radicals will have a greater opportunity to obtain a second hydrogen to form dihydroaromatics. Such dihydronaphthalene-type species are very reactive and will be rapidly further reduced to tetrahydro products. The dihydro and tetrahydro products are then subject to ring-opening and loss of all or part of the newly formed chains as C<sub>1</sub> to C<sub>4</sub> hydrocarbons.

What helps make the shift in incremental yields from oil to gas so dramatic is the fact that the decreasing effectiveness of the aromatic pool with increasing temperature provides the system with marked feedback potential. When the temperature reaches the point where ineffectiveness of the solvent pool in regaining H-atoms allows sufficient ring hydrogenation such that the heat evolved exceeds the fixed-bed heat transfer capability, the temperature begins to rise faster. This rise further decreases the ability of the aromatic pool to regain wastefully transferred H-atoms, ring hydrogenation is further promoted, the temperature goes up still faster, and so on, in an accelerating manner.

Role of Coal Fragments in Induced Bond Scission. All of the results summarized here support, in one way or another, the hypothesis that aromatic/hydroaromatic reaction media, and H<sub>2</sub> as well, serve not only to scavenge coal radicals, but also to generate hydrogen transfer activity. Making the very probable assumption that the connections in coals consist of some weak covalent linkages, which will undergo thermal scission regardless of the reaction medium, and some linkages so strong they will cleave only when induced to do so by hydrogen transfer, it becomes clear that the radicals generated by scission of the weak links have a much more important role to play than merely being "capped" by hydroaromatic species (or H<sub>2</sub>). To the extent they are non-hydroaromatic radicals (e.g., benzyl), these radicals typically have no hydrogenolysis activity: they cannot transfer a hydrogen to a cleavable substrate because they cannot, in so doing, form an aromatic system. If not capped, such thermally generated radicals may indeed become involved (as the conventional view would have it) in retrograde reactions. The important point however, and the one not included in most pyrolysis pictures, is that when the scavenger is a hydroaromatic, the capping process actually constitutes a chain transfer step that converts a radical with no hydrogenolysis activity into a radical that can induce hydrogenolysis.



The potential role of coal radicals in providing hydrogenolysis activity suggests that the high reactivity of coals in the initial stages of conversion may result from a "burst" of coal radicals that is large compared to the steady state level of ArH<sup>·</sup> supplied by the hydroaromatic media. If this is the case, then the conversion of inactive, non-donor radicals into ArH<sup>·</sup> carrier radicals (by either the solvent or by hydroaromatic coal species) could help explain the initial high reactivities of coals. If the number of initiating radical species is too high to be quickly disposed of via the normal termination pathways of the medium (i.e., radical disproportionation), then there should be a significant increase in activity. In hybrid studies involving mixtures of coals and model compounds,

we observed (7) that the addition of coal substantially increases the model compound hydrogenolysis rate. At 400°C, the rate in the modest liquefaction solvent, tetralin, was increased by a factor of about forty. In the more effective solvents, dihydrophenanthrene and dihydropyrene, the rate was increased by a factor of two to three. Thus, under the liquefaction conditions of these experiments, some species generated by the coal (presumably free radicals) very clearly were a source of bond cleavage activity, not merely something to be scavenged. In the absence of evidence to the contrary, it is reasonable to assume that the same phenomenon occurs under pyrolysis conditions.

Coal Pyrolysis in Reactive Vapors. An awareness of the triple role of aromatic/hydroaromatic media (radical scavenger, agent for conversion of inactive radicals into hydrogenolytically active radicals, and retriever of wastefully transferred hydrogen) raises questions about the relative merits of two different approaches to augmenting hydrogenolysis activity in coal pyrolysis: the use of high pressure hydrogen and the use of hydroaromatic PCAH vapor.

The use of hydrogen pressure to augment volatiles yields during coal pyrolysis is not a new approach. H<sub>2</sub> is, of course, a thermodynamically powerful reducing agent. However, owing to the strength of the H-H bond, H<sub>2</sub> is kinetically ineffective at low temperatures (in the absence of a catalyst). Unfortunately, the low temperature range of coal pyrolysis (300 to 500°C) is precisely the region in which coals become highly reactive and in which they seem particularly susceptible to oxidative retrograde reactions. In fact, it is already well appreciated (26) that the presence of H<sub>2</sub> actually tends to decrease volatiles yields (relative to pyrolysis in a vacuum)<sup>2</sup> at temperatures below about 600°C. Consideration of the kinetics of the reaction by which H-atoms are produced from H<sub>2</sub> emphasizes why this is the case.



$$\log k_{16,400} (1 \text{ m}^{-1} \text{ s}^{-1}) = 1.7$$

For Ar = phenyl, this reaction is 16 kcal/mol endothermic (18) in contrast to the analogous "scavenging" reaction shown above (reaction 15), which is 5 kcal/mol exothermic, and at least 100 times faster at 400°C (at equivalent concentrations of the respective "scavengers").

$$\log k_{15,400} (1 \text{ m}^{-1} \text{ s}^{-1}) = 3.8$$

While the hydrogen carrier radical generated (ArH<sup>•</sup>) is not nearly as active as H<sup>•</sup> on a per molecule basis, it, as discussed above, is much more efficient in transferring hydrogen selectively to places where it is utilized for cleavage, and it cannot abstract another H-atom to uselessly form H<sub>2</sub>. In addition, in the low temperature pyrolysis region, near-molar concentrations of such PCAH and their hydroaromatic derivatives can be generated at pressures in the vicinity of one atmosphere, whereas, maintenance of 1M [H<sub>2</sub>] requires about 800 psi. Finally, the Ar/ArH<sub>2</sub> mixtures are themselves sources of these hydrogenolytically active radicals (by reverse radical-disproportionation (25,26) that can rival in numbers the radicals thermally generated from the coal structures. Thus, it seems likely that heating the coal in the presence of ArH<sub>2</sub>/Ar vapors (or with "pre-loaded" Ar/ArH<sub>2</sub>) could offer some of the conveniences of pyrolysis, and be, in the 350 to 500°C temperature range, a more effective way of inducing hydrogenolysis in the coal structures than is provided by heating in hydrogen pressure. The recent work of Gorbaty and co-workers (27) will presumably shed some light on the practicality of this approach, as well as providing data that will help to unify the chemical pictures of coal liquefaction and gasification.

## CONCLUSION

In summary, experimental evidence now strongly supports the hypothesis that induced cleavage of strong bonds is a significant part of coal pyrolysis as well as liquefaction. Furthermore, conversion results indicate that shifts in the modes of hydrogen transfer affect hydrogen utilization efficiency and product distribution, and that variations in reaction conditions do indeed have an impact on the induced bond scission processes. Therefore we suggest that the most fruitful working hypothesis for coal pyrolysis/gasification research is that such induced bond scissions can be substantial and are subject to manipulation, and assert that attempts at manipulation are more likely to be successful to the extent that we obtain an improved understanding of the chemistry of these cleavage processes.

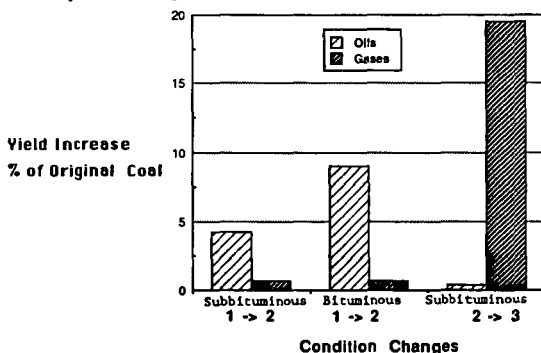
## ACKNOWLEDGEMENT

The authors wish to acknowledge the support of the U.S. Department of Energy under Contract DE-FG22-86PC90908.

## REFERENCES

1. See, for example: Solomon, P. R.; Hamblen, D. G., "Measurements and Theory of Coal Pyrolysis," Report No. DOE/FE/05122-1668, Contract No. DE-AC21-81FE05122, 1984; Howard, J. B., "Fundamentals of Coal Pyrolysis and Hydropyrolysis," in Chemistry of Coal Utilization, Second Supplementary Volume, M. A. Elliot, ed., John Wiley and Sons, New York, 1982, pp. 665-784.
2. Cavalas, G. R.; Cheong, P. H.; Jain, R., Ind. Eng. Chem. Fundam., 1981, 20, 113.
3. Anthony, D. B.; Howard, J. B.; Hottel, H. C.; Meissner, H. P., Fuel, 1976, 55, 121.
4. Jüntgen, H., Fuel, 1984 63, 731.
5. Solomon, P. R.; Serio, M. A., "Evaluation of Coal Pyrolysis Kinetics," presented at NATO Workshop on "Fundamentals of Physical Chemistry of Pulverized Combustion, Les Arcs, France, July 28 - August 1, 1986.
6. McMillen, D. F.; Malhotra, R.; Chang, S.-J.; Nigenda, S. E., Am. Chem. Soc., Div. Fuel Chem. Prep., 1985, 30(4), 297.
7. McMillen, D. F.; Malhotra, R.; Chang, S.-J.; Hum, G. P., Energy and Fuels, 1987, 1, 193.
8. McMillen, D. F.; Malhotra, R.; Chang, S.-J.; Fleming, R. H.; Ogier, W. C.; Nigenda, S. E., "Mechanisms of Hydrogen Transfer and Scission of Strongly Bonded Coal Structures in Donor-Solvent Systems," Fuel, accepted for publication.
9. Finseth, D. H.; Bockrath, B. C.; Cillo, D. L.; Illig, E. G.; Sprecher, R. F.; Retcofsky, H. L.; Lett, R. G., Am. Chem. Soc. Div. Fuel. Chem. Prep., 1983 28(5), 17.
10. Orchin, M.; Columbic, C.; Anderson, J. E.; Storch, H. H.; U.S. Bureau of Mines Bull. No. 505, 1951.
11. Davies, G. O.; Derbyshire, F. J.; Price, R. J., J. Inst. Fuel, 1977, 50, 121.
12. McMillen, D. F., unpublished work.
13. Bockrath, B. C.; Bittner, E.; McGrew, J., J. Am. Chem. Soc., 1984, 106, 135.
14. Bilmers, R. L.; Griffith, L. L.; Stein, S. E., J. Phys. Chem., 1986, 90, 517.
15. Choi, C.-Y.; Stock, L. M., J. Org. Chem., 1984, 40, 2871.
16. Metzger, J. O., Angew. Chem. Int. Ed. Engl., 1986, 25, 80.

17. Solomon, P. R.; Squire, K. R., Am. Chem. Soc. Div. Fuel Chem. Prep., 1985 30(4), 193.
18. a. McMillen, D. F.; Golden, D. M., "Hydrocarbon Bond Dissociation Energies," Ann. Rev. Phys. Chem., 1982, 33, 497.  
b. Benson, S. W., Thermochemical Kinetics, 2nd ed., John Wiley and Sons Inc., New York, 1976.
19. Buchanan, A. C.; Dunstan, T. D. J.; Douglas, E. C.; Poutsma, M. L., J. Am. Chem. Soc., 1986, 108, 7703.
20. Wolfs, P. M. J.; van Krevelen, D. W.; Waterman, H. I., Fuel, 1960, 39, 25.
21. Chu, C. J.; Cannon, S. A.; Hauge, R. H., Margrave, J. L., Fuel, 1986, 65, 1740.
22. Rose, G. R.; Zabransky, R. F.; Stock, L. M.; Huang, C.-B.; Srinivas, V. R.; Tse, K.-T., Fuel, 1984, 64, 1339.
23. Gorbaty, M. L.; Maa, P. S., Am. Chem. Soc., Div. Fuel Chem. Prep., 1986, 31(4), 5.
24. Herndon, W. C., J. Org. Chem., 1981, 46, 2119.
25. King, H.-H.; Stock, L. M., Fuel, 1982, 61, 257.
26. Stein, S. E., "A Fundamental Chemical Kinetics Approach to Coal Conversion," in Advances in Chemistry Series, 192, American Chemical Society, Washington, DC, 1982, p. 97.
27. a. Neskora, D. R.; Schlosberg, R. H., U.S. Patent No. 4,385,981.  
b. Gorbaty, M. L., private communication.



Each of the three sets of bars should be viewed in isolation from the other two. Each represents the distribution of the additional yields obtained as a result changing from one set of conditions to another.

Cond. 1. 372 → 465°C, 35 min, N<sub>2</sub>

Cond. 2. 372 → 465°C, 35 min, H<sub>2</sub>

Cond. 3. 372 → 525°C, 85 min, H<sub>2</sub>

Taken from the data of Gorbaty and Maa, 1986.

Figure 1. Incremental Yields Resulting from Gas and Temperature Changes in Coal Pyrolysis

## Modelling the Thermal Reactions of Benzyl Phenyl Sulfide

by

Martin A. Abraham<sup>1</sup> and Michael T. Klein\*  
Department of Chemical Engineering  
University of Delaware  
Newark, DE 19716

The reactions of benzylphenylsulfide (BPS) neat, in benzene, in tetralin and with added thiophenol were studied. A free-radical mechanism described the neat pyrolysis of BPS to the major products toluene, thiophenol, diphenyldisulfide, and diphenylsulfide. An analytical rate expression deduced from this mechanism was consistent with results from both neat pyrolysis and reaction with additives. The secondary reactions of primary products were detailed.

Our interest in the resolution of reaction fundamentals in supercritical fluid (SCF) solvents has motivated careful study of the thermolysis pathways, kinetics and mechanisms that will generally occur in parallel with any possible solvolysis. Since reactions with a SCF solvent of compounds containing oxygen (Lawson and Klein, 1985; Townsend and Klein, 1985) and nitrogen (Abraham and Klein, 1985; Tiffany, et al., 1984), but not sulfur, have been reported, our interest extended to the reactions of benzylphenylsulfide (BPS). Herein we report on a mathematical model of BPS pyrolysis that is based on our own experiments and also the literature base on which our work is built.

Previous studies suggest that neat pyrolysis of BPS proceeds by a free-radical mechanism (Attar, 1978). The mechanism likely involves fragmentation of the C-S bond to a free-radical pair followed by stabilization through hydrogen abstraction, from either a hydrogen donor source, such as tetralin, or other hydrocarbon molecules in the reaction mixture. Fixari and coworkers (1984) pyrolysed BPS in benzene and in tetralin. For reaction in benzene, they postulated that BPS cleaved to a benzyl-phenylthiyl radical pair, which stabilized primarily by recombination. For reaction in tetralin, hydrogen abstraction was from tetralin, which led to a tetralyl radical intermediate whose disproportionation ultimately led to naphthalene. Huang and Stock (1982) also describe a free-radical mechanism for BPS decomposition. Thus the literature provides a good foundation from which to model the reaction of BPS.

Our investigation into the reactions of BPS addressed its neat pyrolysis first. Special attention was paid to derivative experiments, used in a detailed probe of the mechanism, which included reaction in the hydrogen-donor

---

<sup>1</sup> Current address:  
Department of Chemical Engineering  
University of Tulsa  
Tulsa, OK 74104

\*Correspondence

solvent tetralin, reaction in the inert solvent benzene, reaction with the addition of thiophenol, and the pyrolysis of diphenyldisulfide. This provided a basis with which to summarize the experimental results in terms of plausible reaction pathways and a reaction model.

#### EXPERIMENTAL

The reactants, solvents, and GC standards were all commercially available and used as received. A typical experimental procedure was as follows: the reactants, solvent, and the demonstrably inert (Townsend and Klein, 1985) internal standard biphenyl were loaded into batch "tubing bomb" reactors comprising one Swagelok port connector and two caps of 1/4" nominally sized stainless steel parts. The tubing bombs were sealed and immersed in a constant temperature sandbath. In approximately two min, the reactors reached the nominal reaction temperature and, after the desired time had passed, reactions were quenched by insertion of the reactor into a cold water bath. A representative initial concentration of BPS was 0.5 mol/L.

Spectrophotometric-grade acetone or reagent-grade tetrahydrofuran was used to collect all material from the reactors in one phase. Product identification was accomplished on an HP 5970 series GC/MSD equipped with a 60m DB-5 fused-silica capillary column. Quantitation of individual product yields was by GC using an HP 5880 instrument with the same type of capillary column and a flame ionization detector. Response factors were estimated from analyses of standard mixtures, which allowed quantitative calculation of product yields and, hence, an observed product index (OPI). This was the sum of the mass of identified GC-elutable products divided by the initial mass of reactant charged.

#### RESULTS

The reactions of benzylphenylsulfide (BPS) with a set of coreactants complemented the study of its neat pyrolysis and allowed a deeper probe of operative pathways and mechanisms. Reaction in the hydrogen-donor solvent tetralin highlighted unimolecular fission steps, whereas reaction in benzene allowed determination of the overall reaction order. Experiments with added thiophenol probed a major non-primary pathway, and the secondary reaction of diphenyldisulfide (DPDS) was investigated through its neat pyrolysis. The experimental conditions and major products are summarized in Table 1.

The presentation of the results is organized into sections that describe, respectively, neat pyrolysis and the derivative copyrolysis experiments. Within each section, the identity of all products and the temporal variation of the yields ( $y_i = n_i/n_{\text{BPS}_0}$ ) of major products are presented first. This is followed by examination of product selectivity ( $y_i/x$ ) and the effect of the loading of additive  $i$  ( $S_i = n_{i0}/n_{\text{BPS}_0}$ ). Likely pathways and their kinetics are presented in the discussion.

Neat pyrolysis. Toluene was the major product of the neat pyrolysis of BPS. Other major products were DPDS, diphenylsulfide (DPS), and thiophenol; diphenylmethane and bibenzyl were minor products. The temporal variations of the yields of major products from pyrolysis at 300°C are shown in Figure 1, which indicates, by their initially positive associated slopes, that toluene, DPDS and thiophenol were primary products. OPI was greater than 0.9 at a BPS

conversion  $x = 0.9$ , which occurred after 120 min. The pseudo-first order rate constants and associated Arrhenius parameters for the disappearance of BPS during neat pyrolysis are summarized in Table 2.

Reaction in tetralin. Thermolysis of BPS in tetralin led to toluene and thiophenol as major products along with minor amounts of diphenylmethane and DPDS. The temporal variations of the yields of the major products from thermolysis at 340°C are shown in Figure 2, which indicates, by their initially positive slopes, that both toluene and thiophenol were primary products. OPI remained above 0.9 at a BPS conversion of 0.95, which occurred after 120 min. BPS disappearance in tetralin was described by the pseudo-first order rate constants indicated in Table 2. For reaction at 300°C,  $k_{rel} = k_{TET}/k_{NEAT} = 0.087$ , indicating that BPS reaction in tetralin was much slower than its disappearance during neat pyrolysis.

The effect of tetralin loading on the reaction of BPS was studied over the range  $S_T = n_{TET0}/n_{BPS0}$  from 0.0 to 2.0 at 300°C. Increasing  $S_T$  simultaneously decreased BPS conversion ( $x$ ) and increased selectivity ( $s_i = y_i/x$ ) to the major products toluene and thiophenol. This is illustrated in Figure 3, where  $x$  and  $y_i/x$  are plotted vs.  $S_T$  for a constant reaction time of 50 min. During neat pyrolysis ( $S_T = 0$ ) of BPS,  $x$  was approximately 0.9 after 50 min, whereas it was only 0.15 at  $S_T = 2.0$  after the same reaction time. The selectivity to toluene increased from 0.4 to 1.0 and the selectivity to thiophenol increased from 0.1 to 0.8 as  $S_T$  increased from 0.0 to 2.0.

Reaction in Benzene. Reaction of BPS in benzene at 275°C at varying initial BPS concentrations allowed determination of an apparent overall reaction order. The resulting pseudo-first order rate constants for the disappearance of BPS are plotted vs. initial BPS concentration in Figure 4. The best-fit straight line has a slope of approximately 0.2, indicating an overall reaction order of 1.2 in BPS concentration over the range of conditions examined. The pseudo-first order rate constant corresponding to the neat pyrolysis concentration of 0.6 mol/L in Figure 4 is  $4.47 \times 10^{-3} \text{ min}^{-1}$ , somewhat less than the experimentally determined neat pseudo-first order rate constant of  $0.01 \text{ min}^{-1}$  at the same concentration.

Reaction with Thiophenol. Pyrolysis of BPS at 300°C in the presence of thiophenol with initial molar ratios [ $S_{THP} = n_{THP0}/n_{BPS0}$ ] ranging from 0.0 (neat pyrolysis) to 1.68 yielded toluene, DPDS, and DPS as major products; diphenylmethane and bibenzyl were minor products. Figure 5 summarizes the temporal variation of product yields for  $S_{THP} = 1.68$ . The disappearance of BPS in the presence of thiophenol was characterized by a pseudo-first order rate constant of  $0.0445 \text{ min}^{-1}$ , comparable to that observed from neat pyrolysis.

The effect of added thiophenol on BPS decomposition is illustrated in Figure 6, a plot of BPS conversion and major product selectivities vs.  $S_{THP}$  for a constant reaction time of 20 min at 300°C. As  $S_{THP}$  increased from 0 to 1.68,  $x$  decreased from approximately 0.85 to 0.7, whereas toluene and DPDS selectivity ( $y_{TOL}/x_{BPS}$ ;  $y_{DPDS}/x_{BPS}$ ) increased from 0.3 to 0.7 and 0.6 to 1.3, respectively. Evidently thiophenol functioned as a hydrogen donor to the benzyl radical, and the thus-formed phenylthiyl radical underwent termination by coupling.

Neat pyrolysis of Diphenyldisulfide. Neat pyrolysis of DPDS at 300°C yielded DPS as a primary product; thiophenol was a minor product. OPI was 0.9 at 60 min, which corresponded to a DPDS conversion and DPS yield of 0.7. Thus the selectivity of the reaction of DPDS to DPS was essentially 1.0, which implies the formation of elemental sulfur. The disappearance of DPDS was characterized by a pseudo-first order rate constant of  $0.0196 \text{ min}^{-1}$ .

#### DISCUSSION

The literature and present results for neat pyrolysis and reaction in tetralin combine to provide the basis for development of the mathematical model.

BPS Thermolysis Mechanism. The decomposition of BPS is reasonably interpreted as a set of free radical steps like those described by Attar (1978), Miller and Stein (1979), and Huang and Stock (1982). Illustrated in Figure 7a, a consistent sequence of steps is initiated through fission at the relatively weak (bond dissociation energy = 53 kcal/mol (Fixari et al., 1984)) C-S bond. BPS consumption also occurs through hydrogen abstraction by the initiation-generated benzyl or phenylthiyl radicals, which leads to toluene or thiophenol and a BPS radical. Abstraction of hydrogen from thiophenol by a benzyl radical will produce toluene and a phenylthiyl radical. Termination by radical recombination can involve: two phenylthiyl radicals, yielding DPDS; two benzyl radicals, producing bibenzyl; or other radicals (BPS radicals, for example), yielding unobservable, higher-molecular-weight oligomers. An additional elementary step is required to account for the minor amounts of diphenylmethane observed and also the secondary conversion of DPDS to DPS. Note that the latter might not actually occur in a single elementary step.

Pseudo-steady state analysis of the elementary steps of Figure 7 allows derivation of an analytical rate expression. Under the condition of a steady state, the rate of initiation must equal the rate of termination of radicals; we also consider the concentration of each radical  $\beta_1$ ,  $\beta_2$ , and  $\mu$  to be in a pseudo-steady state. Thus, with the overall BPS reaction rate as in Eq. 1,

$$r = [\text{BPS}](k_1 + k_2\beta_1 + k_3\beta_2) \quad (1)$$

the balances on  $\beta_1$  and  $\beta_2$ , which yield Eq. 2 and 3 for  $\beta_1$  and  $\beta_2$ , respectively,

$$\beta_1 = k_1[\text{BPS}]/(k_2[\text{BPS}] + k_5[\text{THP}]) \quad (2)$$

$$\beta_2 = \frac{1}{2} \left[ -\frac{k_3[\text{BPS}]}{2k_4} + \sqrt{\left(\frac{k_3[\text{BPS}]}{2k_4}\right)^2 + \frac{2}{k_4}(k_5\beta_1[\text{THP}] + k_1[\text{BPS}])} \right] \quad (3)$$

allow formulation of the overall rate of decomposition as in Eq. 4.

$$r = k_1[\text{BPS}] \left\{ 1 + \frac{k_2[\text{BPS}]}{k_2[\text{BPS}] + k_5[\text{THP}]} + \frac{k_3^2[\text{BPS}]}{4k_1k_4} \left[ \sqrt{1 + \frac{8k_1k_4}{k_5^2[\text{BPS}]} \left( \frac{k_5[\text{THP}]}{k_2[\text{BPS}] + k_5[\text{THP}]} + 1 \right)} - 1 \right] \right\} \quad (4)$$

For very low loadings of thiophenol, or at low conversion during neat pyrolysis, the rate expression of Eq. 4 reduces to

$$r = 2k_1[BPS] - \frac{(k_3[BPS])^2}{4k_4} \left( \sqrt{1 - \frac{8k_1k_4}{k_3^2[BPS]}} - 1 \right) \quad (5)$$

Thus the overall BPS reaction rate is a combination of a first-order term and higher-order terms and is therefore consistent with the experimentally determined reaction order of 1.2.

The dependence of  $r$  (Eq. 4) on the addition of thiophenol to the reaction mixture provides further scrutiny of the mechanism of Figure 7. This is the derivative of the rate with respect to thiophenol concentration, shown as Eq. 6.

$$\frac{dr}{d[THP]} = -\frac{k_1 k_2 k_5 [BPS]^2}{(k_2 [BPS] + k_5 [THP])^2} \left\{ 1 - \frac{1}{\sqrt{1 + \frac{8k_1 k_4}{k_3^2 [BPS]} \left( 1 + \frac{k_5 [THP]}{k_2 [BPS] + k_5 [THP]} \right)}} \right\} \quad (6)$$

Since the square root term in Eq. 6 is greater than unity, the term in the braces must be positive. Thus the rate of reaction decreases with increases in thiophenol loading. This is consistent with the observed decrease in conversion with the increase in thiophenol loading illustrated in Figure 6.

The observed effect of thiophenol loading on product selectivities also probes the candidate mechanism. According to Figure 7, the rate of toluene formation is

$$d[TOL]/dt = k_2\beta_1[BPS] + k_5\beta_1[THP] \quad (7)$$

which, after substitution for  $\beta_1$  from Eq. 2 reduces to

$$d[TOL]/dt = k_1[BPS] \quad (8)$$

It is convenient to use the instantaneous selectivity  $s_1 = dy_{TOL}/dx$  as a vehicle with which to analyze the overall selectivity  $s_2 = y_{TOL}/x$ . Since  $r = [BPS]_0 dx/dt$  and  $d[TOL]/dt = [BPS]_0 dy_{TOL}/dt$ ,  $s_1$  is given as Eq. 9.

$$s_1 = d[TOL]/r = k_1[BPS]/r \quad (9)$$

Differentiation with respect to thiophenol concentration, holding [BPS] constant as in the present experiments, provides Eq. 10 as the sensitivity of the instantaneous selectivity to the addition of thiophenol.

$$ds_1/d[THP] = -k_1[BPS]r^{-2}(dr/d[THP]) \quad (10)$$

Thus, since  $dr/d[THP]$  is always negative, as shown in Eq. 6,  $s_1$  will always increase with increases in [THP]. Hence the increase in  $s_2$  observed experimentally is consistent with the mechanism of Figure 7.

Likewise, the elementary step leading to DPDS suggests Eq. 11 for its formation rate.

$$d[\text{DPDS}]/dt = k_4 \beta_2^2 \quad (11)$$

This combines with the pseudo-steady state concentration of  $\beta_2$  from Eq. 3 to allow formulation of Eq. 12

$$\frac{d[\text{DPDS}]}{dt} = \frac{k_4}{2} \left[ -\frac{k_3 [\text{BPS}]}{2k_4} + \sqrt{\left(\frac{k_3 [\text{BPS}]}{2k_4}\right)^2 + \frac{2k_1 [\text{BPS}]}{k_4} \left(\frac{k_5 [\text{THP}]}{k_2 [\text{BPS}] + k_5 [\text{THP}] + 1}\right)} \right] \quad (12)$$

for the overall rate of formation DPDS. This, in turn, allows the determination of  $s_1$  for DPDS and, hence,  $ds_1/d[\text{THP}]$  for DPDS as Eq. 13.

$$\frac{d\left(\frac{d[\text{DPDS}]}{dt}\right)}{d[\text{THP}]} = + \frac{k_1 k_2 k_5 [\text{BPS}]^2}{(k_2 [\text{BPS}] + k_5 [\text{THP}])^2} \left\{ 1 - \frac{1}{\sqrt{1 + \frac{8k_1 k_4}{k_3^2 [\text{BPS}]} \left(1 + \frac{k_5 [\text{THP}]}{k_2 [\text{BPS}] + k_5 [\text{THP}]} \right)}} \right\} \quad (13)$$

Eq. 13 predicts that the selectivity to DPDS will increase as the concentration of thiophenol in the reaction mixture increases. This was observed experimentally, as shown in the plot of  $s_2$  for DPDS vs. thiophenol loading of Figure 6.

Thermolysis of BPS in tetralin is by the neat pyrolysis steps and additional steps involving tetralin and its derived radicals. These are illustrated in Figure 7b, steady-state analysis of which allows formulation of the overall BPS reaction rate as Eq. 14:

$$r = k_1 [\text{BPS}] \left\{ 1 + \frac{k_2 [\text{BPS}]}{k_2 [\text{BPS}] + k_5 [\text{THP}] + k_6 [\text{TET}]} \right\} + \frac{k_3 (k_3 [\text{BPS}] + k_7 [\text{TET}])}{4 k_1 k_4} \left\{ \sqrt{1 + \frac{8k_1 k_4 [\text{BPS}]}{(k_2 [\text{BPS}] + k_7 [\text{TET}])^2} \left(\frac{k_5 [\text{THP}]}{k_2 [\text{BPS}] + k_5 [\text{THP}] + k_6 [\text{TET}]} + 1\right)} - 1 \right\} \quad (14)$$

In the limit of high tetralin loading, Eq. 14 reduces to  $r = k_1 [\text{BPS}]$ , less than one-half the rate predicted for neat pyrolysis. This is consistent with the experimentally determined rate constants listed in Table 2. Under these conditions, the rates of toluene and thiophenol formation are given by Eq. 15,

$$d[\text{TOL}]/dt = d[\text{THP}]/dt = k_1 [\text{BPS}] \quad (15)$$

which shows that added tetralin will increase the selectivity to both toluene and thiophenol.

## CONCLUSIONS

1. Neat pyrolysis of benzylphenylsulfide was through a free-radical mechanism to toluene, thiophenol, and diphenyldisulfide. Pseudo-steady state analysis of consistent elementary steps allowed formulation of the rate expression as:

$$r = k_1 [\text{BPS}] \left\{ 1 + \frac{k_2 [\text{BPS}]}{k_2 [\text{BPS}] + k_5 [\text{THP}]} + \frac{k_3^2 [\text{BPS}]}{4 k_1 k_4} \left( \sqrt{1 + \frac{8 k_1 k_4}{k_3^2 [\text{BPS}]} \left( \frac{k_5 [\text{THP}]}{k_2 [\text{BPS}] + k_5 [\text{THP}]} + 1 \right)} - 1 \right) \right\} \quad (4)$$

Results of experiments with a set of co-reactants were consistent with the rate expression and aided in the elucidation of the mechanism.

2. The overall reaction order for pyrolytic decomposition of BPS was 1.2. This is consistent with the theoretical rate expression derived from the postulated mechanism.

## ACKNOWLEDGEMENTS

We gratefully acknowledge the support of this work by the Petroleum Research Foundation and Standard Oil.

## NOMENCLATURE

$k_i$	rate constant
$n_i$	mole number of $i$
OPI	Observed Product Index, $\sum \text{weight}_i / \text{weight}_{\text{BPS}_0}$
$r$	reaction rate, $\text{mol L}^{-1} \text{min}^{-1}$
$S_i$	coreactant loading, $n_{i0} / n_{\text{BPS}_0}$
$s_1$	instantaneous selectivity of $i$ , $dy_i / dx$
$s_2$	integral selectivity of $i$ , $y_i / x$
$x$	conversion, $1 - n_{\text{BPS}} / n_{\text{BPS}_0}$
$y_i$	molar yield of $i$ , $n_i / n_{\text{BPS}_0}$
$[ ]$	concentration, $\text{mol L}^{-1}$

### Chemical Species

BPS	Benzylphenylsulfide, $\text{PhCH}_2\text{SPh}$
DPDS	Diphenyldisulfide, $\text{PhSSPh}$
DPS	Diphenylsulfide, $\text{PhSPh}$
THP	Thiophenol, $\text{PhSH}$
TOL	Toluene, $\text{PhCH}_3$

### Greek Symbols

$\beta_1$	benzyl radical
$\beta_2$	phenylthiyl radical
$\mu$	BPS radical

### Subscripts

$o$	initial condition
-----	-------------------

#### LITERATURE CITED

Abraham, M.A.; Klein, M.T. Ind. Eng. Chem. Product Research and Development 1985, 24, 300.

Attar, A. Fuel 1978, 57, 201-212.

Fixari, B.; Abi-Khers, V.; LePerche, P. Nouveau Journal De Chimie 1984, 8(3).

Huang, C.B.; Stock, L.M. ACS Division of Fuel Chemistry Preprints 1982, 27 (3-4), 28-36.

Lawson, J.R.; Klein, M.T. Ind. Eng. Chem., Fundam. 1985, 24, 203-8.

Miller, R.E.; Stein, S.E. ACS Division of Fuel Chemistry Preprints 1979, 24(3), 271-77.

Tiffany, D.M.; Houser, T.J.; McCarville, M.E.; Houghton, M.E. ACS Division of Fuel Chemistry Preprints 1984, 29(5), 56-62.

Townsend, S.H.; Klein, M.T. Fuel 1985, 64, 635-8.

Table 1: Experimental conditions for the reactions of Benzyl Phenyl Sulfide.

Additive	Temperature (°C)	Major Products
Neat	275-386	Toluene, Thiophenol Diphenyldisulfide, Diphenylsulfide
Tetralin	300-386	Toluene, Thiophenol
Benzene	275	Toluene, Thiophenol Diphenyldisulfide, Diphenylsulfide
Thiophenol	300	Toluene, Diphenyl- disulfide, Diphenyl- sulfide

Table 2: Pseudo-first-order rate constants summarizing the reactions of Benzyl Phenyl Sulfide.

Temperature (°C)	Neat Pyrolysis	In Tetralin
275	0.0182±0.0039	-
300	0.0334±0.0019	0.0029±0.0006
340	0.175±0.045	0.0269±0.0008
386	0.530±0.046	0.3467±0.0284
$\log_{10}A(\text{min}^{-1})$	7.25	13.4
$E^*(\text{kcal/mol})$	22.6	41.7

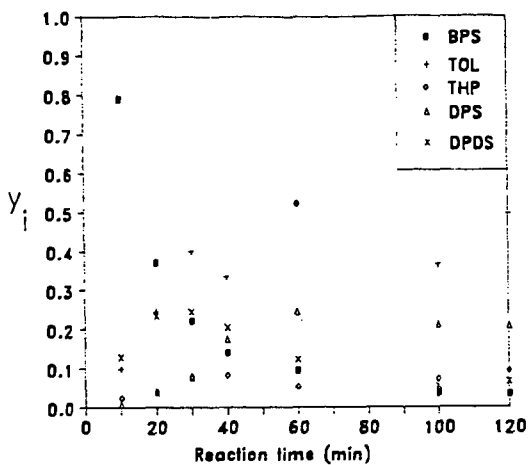


Figure 1: Temporal variation of the yields of the products of neat BPS pyrolysis at 300°C.

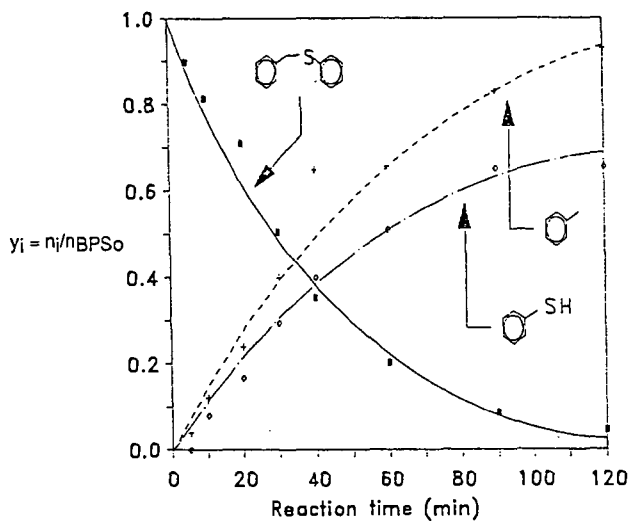


Figure 2: Temporal variation of the yields of the products of BPS thermolysis in tetralin at 340°C.

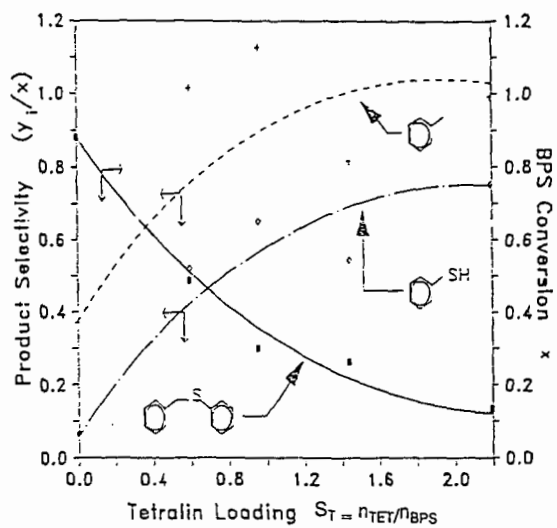


Figure 3: Dependence of product selectivity and BPS conversion on tetralin concentration during reaction at 300°C.

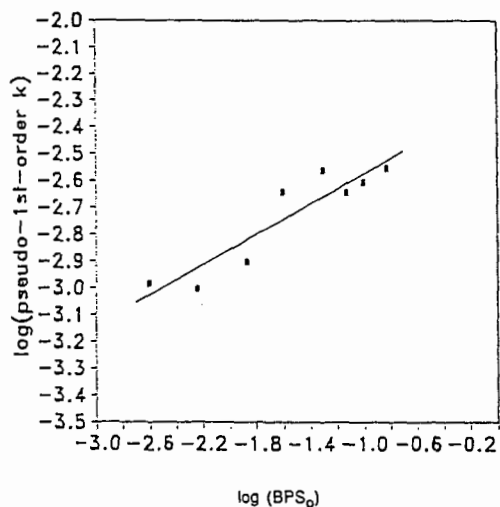


Figure 4: Overall order of reaction of BPS in benzene.

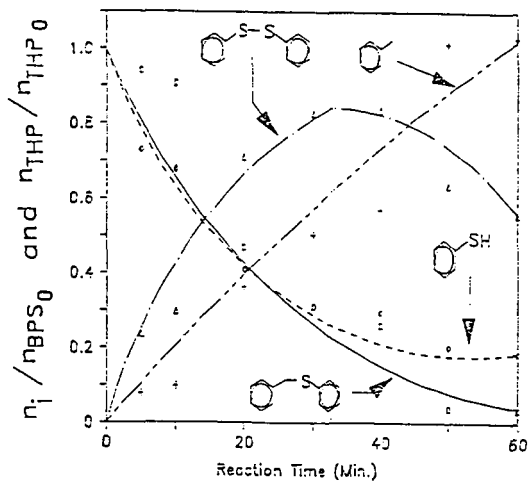


Figure 5: BPS pyrolysis at 300°C with added thiophenol:  $S_{THP} = n_{THP}/n_{BPS} = 1.68$ .

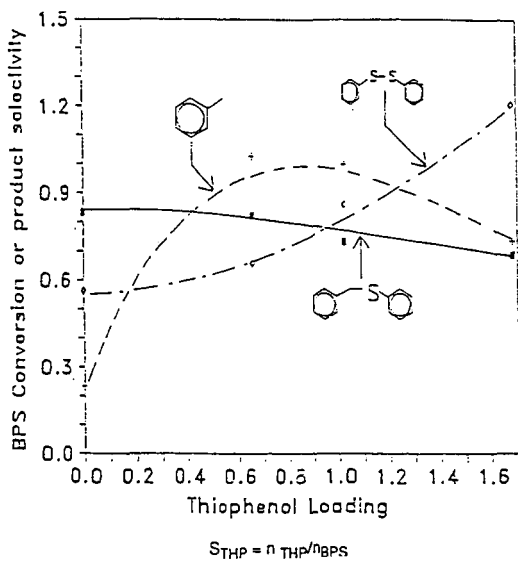


Figure 6: Dependence of product selectivity and BPS conversion on thiophenol concentration during reaction at 300°C.

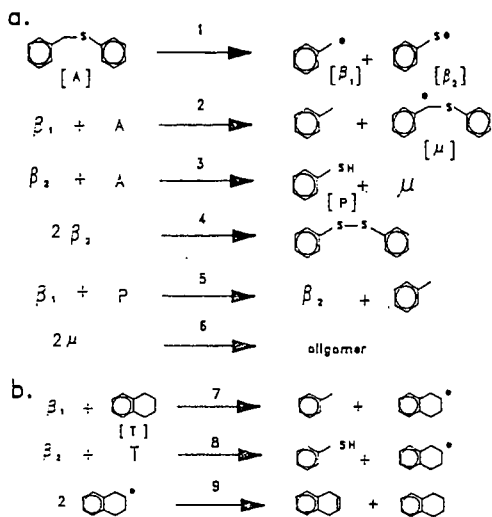


Figure 7: Free-radical steps for EPS reaction: (a) Neat pyrolysis; (b) Additional steps for reaction with tetralin.

A NOVEL APPLICATION OF  $^{31}\text{P}$  NMR SPECTROSCOPY TO THE ANALYSIS  
OF ORGANIC GROUPS CONTAINING -OH, -NH AND -SH FUNCTIONALITIES  
IN COAL EXTRACTS AND CONDENSATES

A. E. Wroblewski, R. Markuszewski, and J. G. Verkade  
Fossil Energy Program, Ames Laboratory  
and

Department of Chemistry, Iowa State University, Ames, Iowa 50011

Abstract

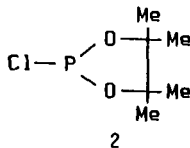
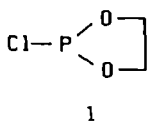
Over one hundred model organic compounds including phenols, aliphatic alcohols, aromatic acids, aliphatic acids, amines, and thiols have been derivatized with two members of a phospholane series of phosphorus-containing reagents, namely,  $\text{ClPOCH}_2\text{CH}_2\text{O}$  and  $\text{ClPOCMe}_2\text{CMe}_2\text{O}$ . Measurement of proton-decoupled  $^{31}\text{P}$  chemical shifts of these derivatives reveals that, in general, the resonances fall into well-separated regions for derivatized classes of these organic compounds. Both phosphorus reagents were also tested on pyridine extracts of Illinois No. 6 coal, revealing the presence of various phenols, carboxylic acids, and aliphatic alcohols. Similar derivatization of a low-temperature pyrolysis condensate from Illinois No. 6 coal showed no detectable concentrations of carboxylic acids, a relatively small amount of aliphatic alcohols, but considerable quantities of a variety of phenols. The current scope and limitations of this NMR technique and its applicability to the quantitation of -OH, -SH and -NH functionalities in organic solutions of coal-derived materials are discussed.

Introduction

Analysis of coal-derived materials, such as low-temperature pyrolysis condensates, is usually carried out by GC/MS methods. However, these techniques are relatively non-routine and time consuming. As an alternative as well as complementary approach, IR and NMR spectroscopic procedures have been developed in recent years. Although direct analysis of complex mixtures obtained in coal processing can sometimes be performed,<sup>1</sup> derivatization of certain classes of compounds with suitable reagents is advantageous in NMR spectroscopy if the reagent introduces an NMR-reactive label that gives a resonance signal specific for the component being analyzed.

Previous determinations of OH functionalities in coal-derived materials have been performed by silylation<sup>2-6</sup> or acetylation<sup>6,7</sup> followed by IR<sup>5</sup>, FT-IR<sup>2,7</sup> and/or  $^1\text{H}$   $^{2,3,6}$ ,  $^{29}\text{Si}$   $^4$ , and  $^{13}\text{C}$  NMR<sup>2,6</sup> measurements. In other studies, derivatization of various phenols with hexafluoroacetone allowed observation of  $^{19}\text{F}$  NMR signals associated with the adducts.<sup>6,8,9</sup> The  $^{31}\text{P}$  nucleus is also suitable for NMR monitoring. The P(V) reagents diethylchlorophosphate and chloro(dimethyl)thiophosphinate have been used for the derivatization of variety of phenols; however, the resonances of the respective aromatic esters spanned regions of only about 1 ppm.<sup>10</sup> In contrast, three P(III) organophosphorus reagents were examined previously in this laboratory, of which 2-chloro-1,3,2-dioxaphospholane appeared to be very promising in terms of widening the chemical shift range to achieve better peak separation.<sup>11</sup>

In this report, we present preliminary results on the scope and limitations of 2-chloro-1,3,2-dioxaphospholane (**1**)<sup>12</sup> and its 4,4,5,5-tetramethyl analogue (**2**)<sup>13</sup> as reagents for the derivatization and analysis by  $^{31}\text{P}$  NMR spectroscopy of a variety of phenols, aliphatic alcohols, carboxylic acids,



amines, and thiols. In addition, the applicability of both reagents to the identification of components bearing -OH, -NH, and -SH functionalities in coal extracts and pyrolysis condensates is assessed. The condensates were obtained from a low-temperature preheating step intended to modify a chemical leaching process for desulfurization of coal.<sup>14</sup>

### Experimental

An NMR tube (10 mm) was charged under N<sub>2</sub> with chloroform-d (2.0 mL), chlorophospholane (1, 0.20 mL or 2, 0.25 mL),<sup>2</sup> and triethylamine (0.31 mL). For qualitative measurements, the standard solutions were reacted at room temperature with model compounds (a drop of liquid or a few crystals of solid). <sup>31</sup>P NMR spectra were recorded after successive additions of different model compounds until the reagent was almost exhausted. For application to coal-derived materials, approximately 100-200 mg of the coal extracts or pyrolysis condensates were added to the standard solutions, and <sup>31</sup>P NMR spectra were recorded after 15 minutes.

The extracts and condensates were prepared from an Illinois No. 6 coal. For preparation of the extract, about 1 g of coal was refluxed for 2 hr. with dry pyridine under N<sub>2</sub>. The condensate was obtained by pyrolyzing another sample of the same Illinois No. 6 coal at 455° for 45 min. in a protective atmosphere of N<sub>2</sub> and collecting the volatiles condensing in an air-cooled column packed with glass beads. For a 25-g charge of coal, the yield of condensate was about 1-2 g.

### Results and Discussion

Regions associated with the <sup>31</sup>P NMR resonances for representative model phenols, aliphatic alcohols, carboxylic acids, amines, and thiols derivatized with 1 and 2 are shown in Figures 1 and 2, respectively.

Derivatization of phenols with 1 at room temperature afforded the respective 2-aryloxy-1,3,2-dioxaphospholanes instantaneously. Most of these compounds gave <sup>31</sup>P NMR resonances in a rather narrow region (128.5 to 129.1 ppm). Only derivatives of di-ortho substituted phenols showed signals at lower field (131.0 - 131.5 ppm), with a low-field limit of 136.42 ppm for 2,6-di-*t*-butyl-4-methylphenoxy-1,3,2-dioxaphospholane. With reagent 2, better separation of the <sup>31</sup>P NMR signals of derivatized phenols (138.0 - 139.7 ppm) and di-ortho substituted phenols (142.9 - 143.7 ppm) was achieved. In these cases, the reaction was completed at room temperature in less than five minutes, except for 2,6-di-*t*-butyl-4-methylphenol which did not react at all, presumably because of its bulky nature.

Carboxylic acids rapidly reacted with 1 and 2 to give derivatives displaying <sup>31</sup>P NMR signals between 127.4 and 129.5 ppm, and between 134.8 and 136.2 ppm, respectively. Although the sets of resonances for phenols and

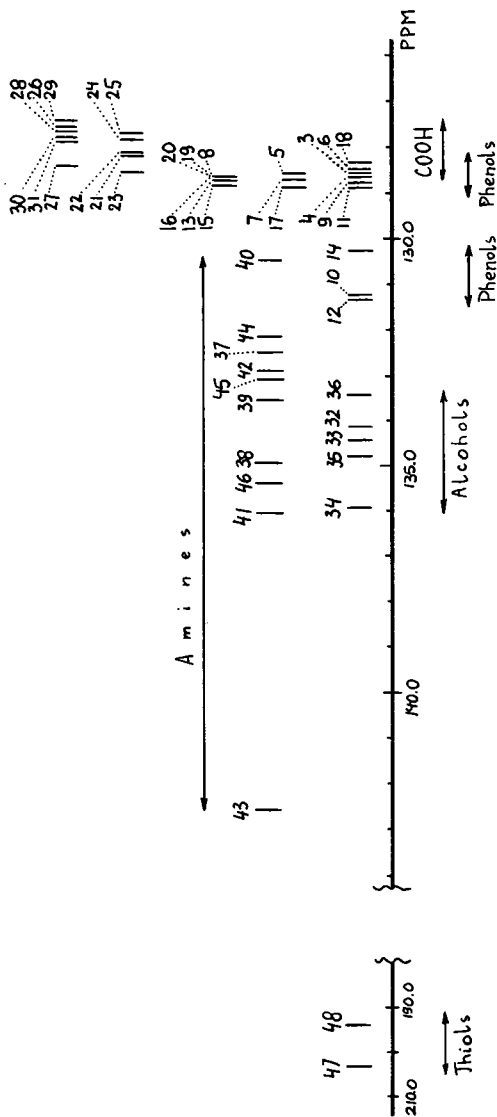


Figure 1.  $^{31}\text{P}$  NMR chemical shifts (in ppm relative to 85%  $\text{H}_3\text{PO}_4$ ) for selected model compounds derivatized with 2-chloro-1,3,2-dioxaphospholane (1) [secondary standard:  $\delta(3\text{ip})$  175.90 ppm].

PHENOLS: 3, phenol, 128.59; 4, o-cresol, 128.70; 5, m-cresol, 128.60; 6, p-cresol, 128.53; 7, 2,3-xyleneol, 128.74; 8, 2,4-xyleneol, 128.64; 9, 2,5-xyleneol, 128.81; 10, 2,6-xyleneol, 131.30; 11, 2,3,5-trimethylphenol, 128.90; 12, 2,4,6-trimethylphenol, 131.42; 13, 3,4,5-trimethylphenol, 128.72; 14, catechol, 130.30; 15, resorcinol, 128.83; 16, p-methoxyphenol, 128.62; 17, 2-methylresorcinol, 128.95; 18, p-methoxyphenol, 128.37; 19,  $\alpha$ -naphthol, 128.63; 20,  $\beta$ -naphthol, 128.62.

AROMATIC ACIDS: 21, benzoic, 128.24; 22, p-toluic, 128.19; 23, m-phthalic, 129.54; 24, 2,5-dihydroxybenzoic, 127.89; 25, 2,4,6-trimethoxybenzoic, 127.71. ALIPHATIC ACIDS: 26, oleic, 127.56; 27, mandelic, 128.47; 28, succinic, 127.63; 29, 3,3-dimethylglutaric, 127.47; 30, indole-3-acetic, 127.77; 31, trans-cinnamic, 127.93.

ALIPHATIC ALCOHOLS: 32, isoamyl, 134.10; 33, benzyl, 134.45; 34, menthol, 135.93; 35, benzhydrol, 134.70; 36, triphenylcarbinol, 133.41. AMINES: 37, aniline, 132.55; 38, o-toluidine, 134.92; 39, anthranilic acid, 133.56; 40, diphenylamine, 130.46; 41, proline, 136.10; 42, 4-methylpiperidine, 137.80; 43, 2,6-dimethylpiperidine, 142.60; 44, 4-methylpiperazine, 137.17; 45, carbazole, 133.10; 46, indole-3-acetic acid, 135.37. THIOLS: 47, 1,3-propanedithiol, 203.12; 48, benzenethiol, 194.28.

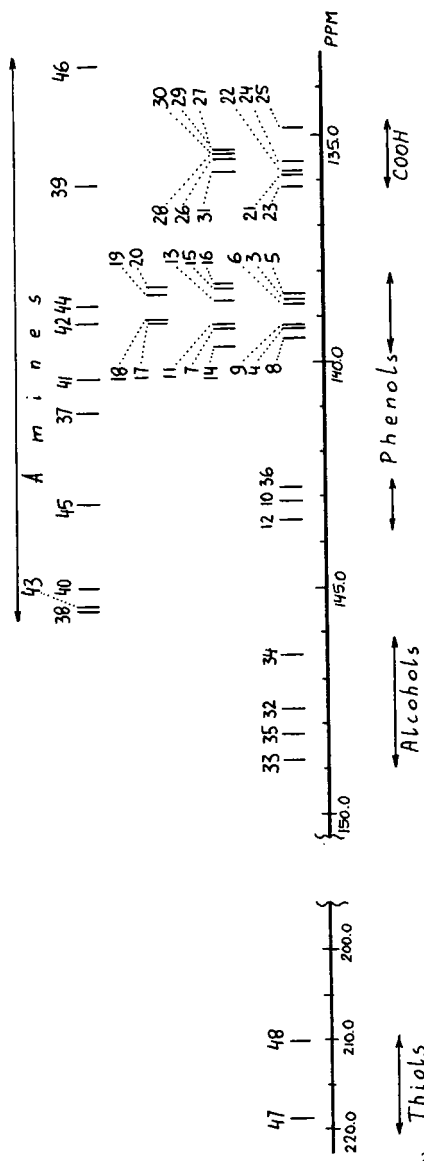


Figure 2. 31P NMR chemical shifts (in ppm relative to 85% H<sub>3</sub>PO<sub>4</sub>) for selected model compounds derivatized with 2-chloro-4,4,5,5-tetramethyl-1,3,2-dioxaphospholane (2) [secondary standard δ(31P) 175.90 ppm].

PHENOLS: 3, phenol, 138.70; 4, o-cresol, 139.29; 5, m-cresol, 138.60, 6, p-cresol, 138.83; 7, 2,3-xyleneol, 139.29; 8, 2,4-xyleneol, 139.52; 9, 2,5-xyleneol, 139.21; 10, 2,6-xyleneol, 143.04; 11, 2,3,5-trimethylphenol, 139.21; 12, 2,4,6-trimethylphenol, 143.55; 13, 3,4,5-trimethylphenol, 138.68; 14, catechol, 139.71; 15, resorcinol, 138.44; 16, m-methoxyphenol, 138.33; 17, 2-methylresorcinol, 139.14; 18, p-methoxyphenol, 139.08; 19, α-naphthol, 138.54; 20, β-naphthol, 138.36.

AROMATIC ACIDS: 21, benzoic, 135.89; 22, p-toluic, 135.81; 23, m-phthalic, 136.17; 24, 2,5-dihydroxybenzoic, 135.62; 25, 2,4,6-trimethoxybenzoic, 134.91. ALIPHATIC ACIDS: 26, oleic, 135.51; 27, mandelic, 135.41; 28, succinic, 135.49; 29, 3,3-dimethylglutaric, 135.43; 30, indole-3-acetic, 135.48; 31, trans-cinnamic, 135.80; ALIPHATIC ALCOHOLS: 32, isoamyl, 147.76; 33, benzyl, 148.80; 34, menthol, 146.53; 35, benzhydrol, 148.24; 36, triphenylcarbinol, 142.82. AMINES: 37, aniline, 141.19; 38, o-toluidine, 145.56; 39, anthranilic acid, 136.14; 40, diphenylamine, 145.00; 41, proline, 140.41; 42, 4-methylpiperidine, 139.15; 43, 2,6-dimethylpiperidine, 145.48; 44, 4-methylpiperazine, 138.75; 45, carbazole, 143.14; 46, indole-3-acetic acid, 133.46. THIOLS: 47, 1,3-propanedithiol, 217.85; 48, benzenethiol, 210.31 ppm.

carboxylic acid derivatized with 1 were partially superimposed, good separation of these regions was observed when 2 was used as the derivatizing reagent.

Aliphatic hydroxy functionalities can also be analyzed by  $^{31}\text{P}$  NMR spectroscopy after derivatization with the reagents 1 and 2. Alkoxyphosphites derived from 1 presented  $^{31}\text{P}$  NMR signals between 133.4 and 136.0 ppm, while those obtained from 2 revealed absorptions from 146.4 to 148.8 ppm, with exception of derivatives of tertiary alcohols (triphenylcarbinol and t-butanol) which resonated far upfield (both at 142.8 ppm). In both cases the regions of absorptions for derivatized aliphatic alcohols are well separated from those of phenols and carboxylic acids.

$^{31}\text{P}$  NMR resonances of amines derivatized with reagents 1 and 2 are widely spread, overlapping regions represented by aliphatic alcohols, phenols and carboxylic acids. On the other hand,  $^{31}\text{P}$  NMR signals of compounds having the P-N bond are significantly broader than those from other derivatives, thus making their assignment to amines easy.

The few thiols examined showed that the  $^{31}\text{P}$  NMR signals for their reaction products with 1 and 2 (190 to 210 ppm and 210 to 220 ppm, respectively) are downfield from the regions observed for phenols and aliphatic alcohols. Thus, the technique shows good promise for identification of SH-bearing groups.

Derivatization of a low-temperature pyrolysis condensate from Illinois No. 6 coal with 1 and 2 revealed the almost exclusive presence of a variety of phenols (Figures 3 and 4, respectively). In addition, residual quantities of aliphatic hydroxyl groups were detected at 135 - 135.5 ppm and 147 - 148 ppm, respectively. No carboxylic acids were found, however. An identification of phenols was carried out by the addition of selected authentic compounds to the derivatized condensate containing an excess of 2. This procedure allowed us to tentatively assign most of the prominent signals to specific substituted phenols (Figure 4). The presence of such a variety of phenolic compounds is consistent with the well-documented role that phenols play during low-temperature pyrolysis of coal.<sup>15,16</sup>

A pyridine extract of Illinois No. 6 coal was derivatized with both reagents to give deep-brown opaque solutions. Examination of these solutions by  $^{31}\text{P}$  NMR spectroscopy showed broad absorptions (Figures 5 and 6), which revealed the presence of mostly phenols (at 138-140 ppm), together with a small amount of di-ortho substituted phenols (at about 143 ppm). In addition, significant amounts of carboxylic acids were found in the extract at 135-136 ppm. Identification of particular phenolic and/or acidic components was precluded by the breadth of signals. Furthermore, the extract derivatized with 1 displayed apparently significant amounts of aliphatic OH functionalities (at about 135 ppm), while the extract derivatized with 2 showed only a relatively small quantity of this functionality. This contradictory result is currently under further investigation.

### Conclusions

Reagents of the type 1 and 2 provide improved  $^{31}\text{P}$  chemical shift dispersion for compounds derived from carboxylic acids, phenols, alcohols, amines, and thiols. Therefore, they offer considerable promise for the

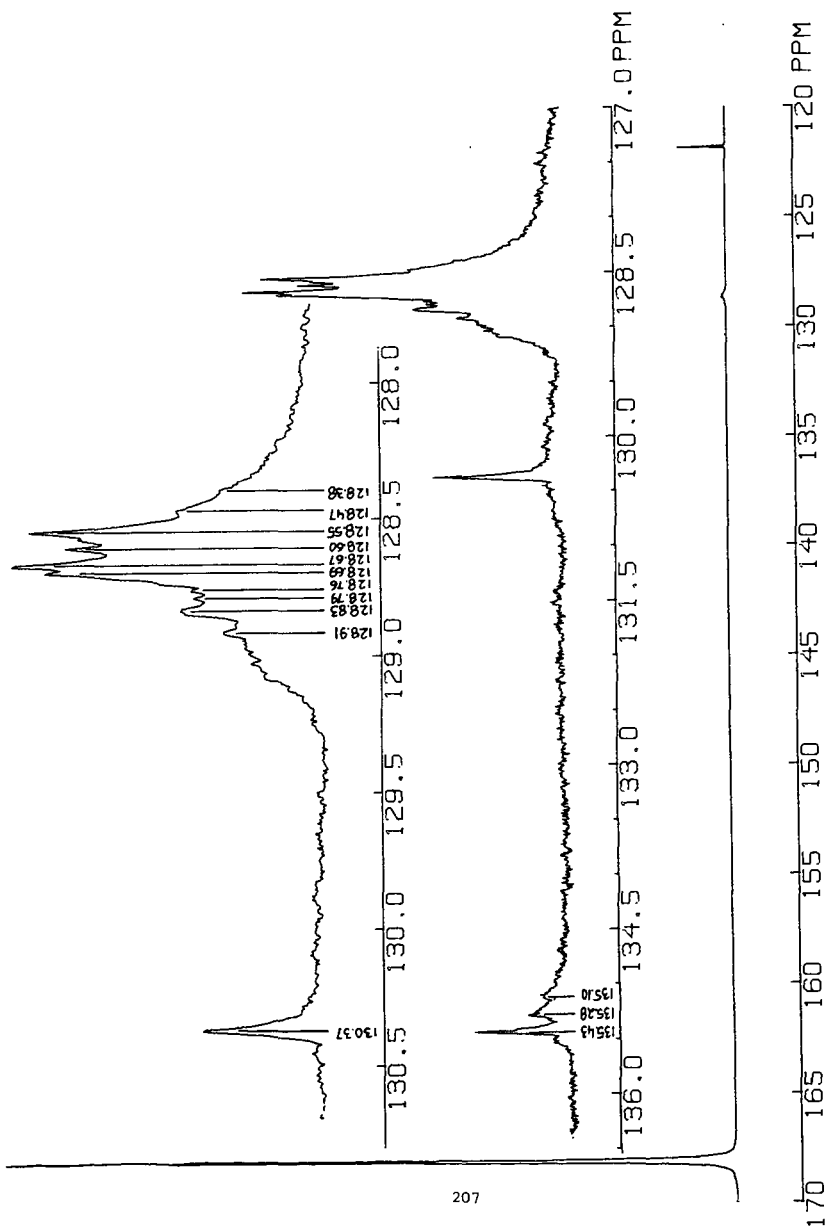


Figure 3.  $^{31}\text{P}$  NMR spectrum of low-temperature pyrolysis condensate of Illinois No. 6 coal derivatized with **1**.

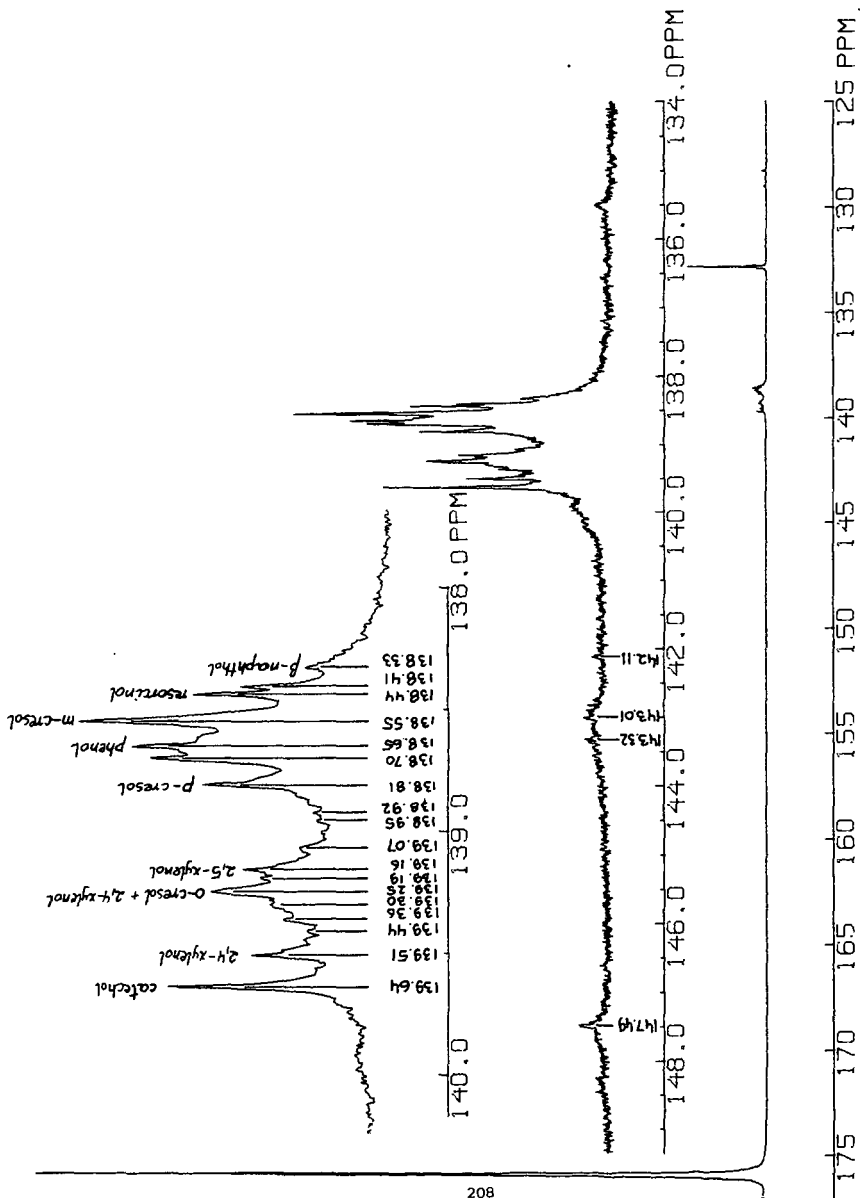


Figure 4.  $^{31}\text{P}$  NMR spectrum of low-temperature pyrolysis condensate of Illinois No. 6 coal derivatized with 2.

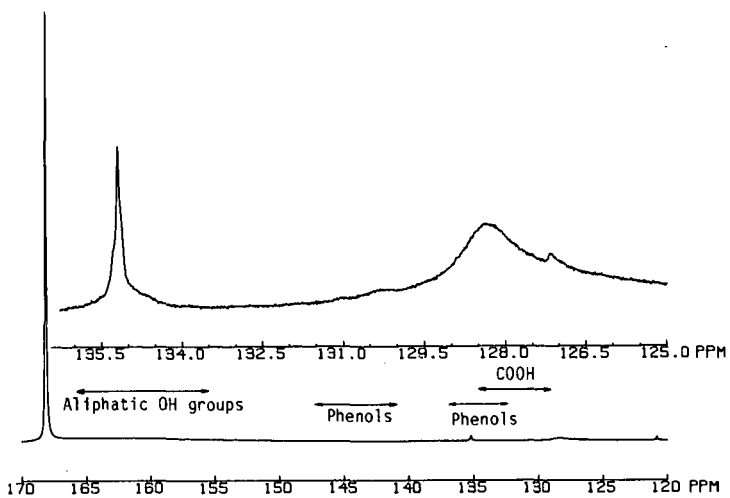


Figure 5.  $^{31}\text{P}$  NMR spectrum of a pyridine extract of Illinois No. 6 coal derivatized with 1.

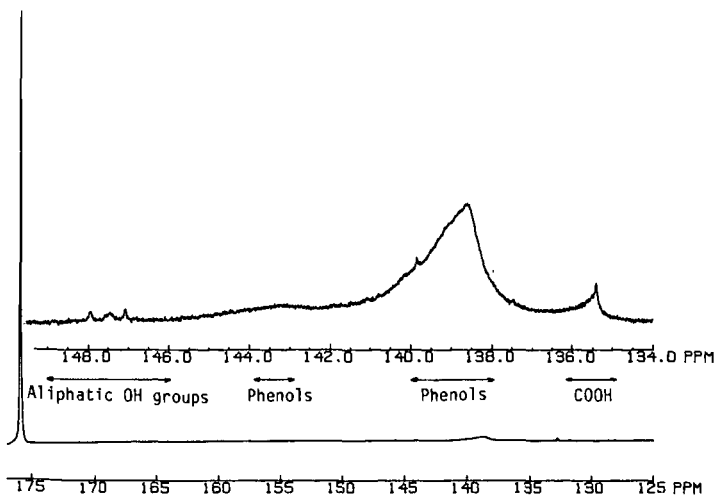


Figure 6.  $^{31}\text{P}$  NMR spectrum of a pyridine extract of Illinois No. 6 coal derivatized with 2.

identification (and possibly quantification) of coal-derived organic moieties bonded to -OH, -NH, and -SH functionalities. Such a capability will be extremely useful in characterizing coal extracts, pyrolysis condensates, and liquefaction products.

#### Acknowledgements

Ames Laboratory is operated for the U. S. Department of Energy by Iowa State University under Contract No. W-7405-ENG-82. This work was supported, in part, by the Assistant Secretary for Fossil Energy through the Pittsburgh Energy Technology Center. Special thanks are due to Dr. N. D. Shah for providing the low-temperature pyrolysis condensate.

#### References

1. Kanitskaya, L. V., Kushnarev, D. F., Polonov, V. M., and Kalabin, G.A., Khim. Tverd. Topl., 19, 76-82 (1985); Engl., pp. 70-76.
2. Snape, C. E. and Bartle, K. D., Fuel, 58, 898 (1979).
3. Schweighardt, F. K., Retcofsky, H. L., Friedman, S., and Hough M., Anal. Chem., 50, 368 (1978).
4. Coleman, W. M. and Boyd, A. R., Anal. Chem., 54, 133 (1982).
5. Friedman, S., Kaufman, M. L., Steiner, W. A., and Wender I., Fuel, 39, 33 (1960).
6. Snape, C. E., Smith, C. A., Bartle, K. D., and Matthews, R. S., Anal. Chem., 54, 20 (1982).
7. Snyder, R. W., Painter, P. C., Havens, J. R. and Koenig, J. L., Appl. Spectrosc. 37, 497 (1983).
8. Matthews, R. S., Stadelhofer, J. W., and Bartle, K. D., Erdol, Kohle, Erdgas, Petrochem., 34, 173 (1981).
9. Bartle, K. D., Matthews, R. S., and Stadelhofer, J. W., Appl. Spectrosc. 34, 615 (1980).
10. Pomfret, A., Bartle, K. D., Barret, S., Taylor, N., and Stadelhofer, J. W., Erdol, Kohle, Erdgas, Petrochem., 37, 515 (1984).
11. Schiff, D. E., Verkade, J. G., Metzler, R. M., Squires, T. G., and Venier, C. G., Applied Spectrosc., 40, 348 (1986).
12. Lucas, H. J., Mitchell, F. W., and Scully C. N., J. Am. Chem. Soc., 72, 2491 (1950).
13. Zwierzak, A., Can. J. Chem., 45, 2501 (1967).
14. Markuszewski, R., Mroch, D. R., and Norton, G. A., in Fossil Fuels Utilization: Environmental Concerns, R. Markuszewski and B. D. Blaustein, eds., Am. Chem. Soc., Washington, D. C. 1986, pp. 42-50.
15. Karr, C., in Chemistry of Coal Utilization, Suppl. Vol., H. H. Lowry, ed., J. Wiley, New York, 1963, pp. 539-579.
16. Gavalas, G. R., Coal Pyrolysis, Elsevier, Amsterdam, 1982.

Time-Resolved Pyrolysis Mass Spectrometry of Coal: A New Tool for  
Mechanistic and Kinetic Studies

Tanmoy Chakravarty, Henk L.C. Meuzelaar, Willem Windig and George R. Hill

University of Utah, Biomaterials Profiling Center  
391 South Chipeta Way, Suite F, Research Park  
Salt Lake City, Utah 84108

Rashid M. Khan

Morgantown Energy Technology Center  
Morgantown, West Virginia 26505

## INTRODUCTION

Most coal devolatilization studies so far have focussed on the determination of reaction rates for reactions occurring under widely different conditions encountered in liquefaction, gasification, coking or combustion processes. Published rates on more or less comparable coals may differ by several orders of magnitude, especially when obtained at high temperatures ( $>1000$  K) and/or high heating rates ( $10^2$ - $10^5$  K/s) (1,2).

At the present state-of-the-art in coal devolatilization research, more emphasis should perhaps be placed on elucidating the mechanisms of the chemical reactions underlying the observed phenomena. When studying thermal conversion reactions in coal it seems correct to concentrate first on the so-called "primary" reactions before attempting to elucidate the many possible secondary reaction pathways. This is especially true since most secondary reaction pathways are strongly influenced by reactor design and experimental conditions.

The devolatilization behavior of coal will be determined primarily by the chemical composition of coal and secondly by the experimental conditions. Under properly designed vacuum micropyrolysis experiments working with sufficiently small particles ( $<50$   $\mu$  diameter), it is possible to avoid mass and heat transport limitations (3) and minimize the secondary reactions. Using premium coal samples from Argonne National Laboratory (4) the chemical composition can be well defined and possibly characterized by major factors such as rank and depositional environment (5). Recent advances in pyrolysis mass spectrometry (Py-MS), viz, time-resolved Py-MS (TR Py-MS), along with multivariate analysis techniques enable extraction of underlying chemical components (6) from a single experiment; thus reducing the uncertainty due to varying reactions conditions in different experiments. This paper demonstrates the feasibility of obtaining valuable mechanistic and kinetic data using microgram amounts of carefully selected coal samples under properly designed reaction conditions using TR Py-MS techniques in combination with advanced multivariate data analysis methods.

## EXPERIMENTAL

A sample of hvAb Pittsburgh #8 coal was picked up in large chunks from the mine mouth and subsequently ground and sieved under nitrogen. Ultimate and proximate analysis data are shown in Table I. Sample preparation was discussed earlier (7) in detail.

### (Time-Resolved Pyrolysis Mass Spectrometry)

Time-resolved Py-MS analyses were done under the following conditions: Curie-point temperature  $610^\circ\text{C}$ , temperature-rise time 5.4 s, total heating time 10 s, electron energy 12 eV, mass range scanned 50 to 200 amu, scanning speed 1000 amu/s, number of scans 41, total scan time 8 s. Each spectrum scanned was stored separately in the IBM 9000 computer.

### (Multivariate Data Analysis)

In order to give all the variables an equal contribution, and for reasons explained by Malinowski (8), factor analysis was done on the "correlation around the origin" matrix. For this study, the number of factors used was selected by determining the leveling off of the slope (8) and the ratio of the eigenvalue (9). Deconvolution of the components was performed by using a combination of "pure mass" (8,10) and "variance diagram" (VARDIA) (6) techniques.

### (Kinetic Analyses)

Kinetic analysis was based on the total ion current plot. The assumption was made that each maximum in the bimodal curve reflects a single rate process and that a first order rate equation describes the process. The parameters computed based on the maximum rate of generation at the peak of the curve are listed in Table I. The distributed activated energy model (11) was used as an alternative approach.

## RESULTS AND DISCUSSION

The time-resolved total ion current (TIC) profile of the Pittsburgh #8 coal sample is shown in Figure 1b. The TIC profile has a distinctly bimodal character with a pronounced low temperature maximum near 370°C and a larger, high temperature maximum near 560°C. These temperatures, estimated from the temperature/time profile of the blank Curie-point pyrolysis filament (shown in Figure 1a) are believed to be accurate within 5%. The time-integrated spectrum of the coal sample, shown in Figure 2, shows that the most abundant homologous ion series in the pyrolysis mass spectra of fresh whole coals are the "phenols". Other major components dominating the spectra are the "benzenes", "naphthalenes" and the short chain aliphatic hydrocarbons. This matches with the results from this laboratory obtained on 102 Rocky Mountain coals (5).

Using the multivariate data analysis procedures, mentioned before, the evolution profiles of the components (separate groups of correlated mass peaks) were obtained. These profiles, labeled A, B, C and D are shown in Figure 1c. The corresponding numerically extracted spectra showing the composition of each component along with the total variance percentage are shown in Figure 3a, b, c and d.

The low temperature component A appears to represent a vacuum distillable oil consisting largely of aromatic hydrocarbon series ("benzenes", "naphthalenes" and "biphenyls/acenaphthenes"). Bench scale vacuum extraction studies of a hvBb Hiawatha coal showed the naphthene rich distillable fraction to represent approx. 4% of the fresh coal (12). It is now rather widely accepted that coal deposits go through an "oil formation window" during their coalification history in a similar manner observed for oil shale deposits. Maximum oil generation is likely to occur in coals of high volatile bituminous rank. Interestingly, in our experience this component is not readily observed under typical thermal analysis conditions.

Components B, C, and D together make up the main pyrolysis event in Figure 1b. Component B appears at a somewhat lower temperature than components C and D. The near symmetrical shape of the intensity profiles of components B and C indicates a depolymerization (such as found in thermoplastic materials) degradation behavior leading to rapid, complete pyrolysis without major charring tendencies. Component D, however, behaves more like a crosslinking substance (such as found in thermoplastic materials) with a wider temperature profile and a slow, high temperature tail indicating incomplete pyrolysis, presumably accompanied by char formation.

Which structural moieties, if any, are represented by components B, C and D? Identification of component D is relatively straightforward. As shown in Figure 3d, this component is dominated by a strong series of alkyl substituted phenols and resembles the Py-MS patterns of pure vitrinites (13) and fossil wood (14) samples.

Highly similar patterns have been observed in numerically extracted component spectra of various coal data sets obtained by Py-MS (15). Consequently, component D appears to represent the abundant vitrinite macerals present in the Pittsburgh #8 coal sample.

Component B is the early component in the "depolymerization" region (see later) and is characterized by branched or alicyclic hydrocarbons. This component is also characterized by a prominent ion series at  $m/z$  60, 74, 88, 102, etc. (most prominent in the corresponding loading spectra, not shown here), as marked by stars in Figure 3b and thought to represent short chain fatty acids. Patterns similar to Figure 3b can be observed in Messel shale (16) as well as in sporinite concentrates (13) and may represent liptinitic structural moieties present in several different coal macerals.

The numerically extracted spectrum of component C (Figure 3c) reveals an entirely different chemical structure consisting nearly exclusively of aliphatic hydrocarbon moieties. On the basis of previously reported Py-MS studies of model compounds and maceral concentrates (13), this component is believed to consist primarily of straight chain alkanes, alkenes and alkadienes. Under the low voltage electron ionization conditions used in this experiment, short chain alkanes ( $<C_{15}$ ) produce mainly the alkene and alkadiene molecular ion series as well as various fragment ion series, which are visible in Figure 3c. Mixtures of straight chain aliphatic hydrocarbons such as seen in Figure 3c are typical of the pyrolyzates of polyethylene-like structures such as found under vacuum micropyrolysis conditions in liptinitic macerals derived from fossil plant cuticles (17) and or algal materials (16).

It should be mentioned, however, that by selecting a limited mass range ( $m/z$  50-200) many important small molecules (e.g.,  $CH_4$ ,  $NH_3$ ,  $H_2O$ ,  $HCN$ ,  $CO$ ,  $CH_2O$ ,  $CH_3OH$ ,  $H_2S$ ,  $HCl$ ,  $CO_2$  and various  $C_2$  compounds) are ignored in addition to many large organic molecules. This limits the characterization of the char forming process, as well as making it hard to compare our data with the data of other workers on the kinetics of evolution of small molecules (18, 19).

In spite of these limitations, the data obtained on the kinetic parameters seem to match very well with our understanding of the events marked by the two distinct humps in Figure 1b. The activation energy of  $10 \text{ Kcal mol}^{-1}$  is reasonable to expect for the thermophysical kinetics related to "desorption" of the mobile phase. The latter value of  $62 \text{ Kcal mol}^{-1}$ , which also matches with the value calculated using the distributed activation energy model, is expected for thermochemical kinetics for breaking of ethylene bridges between aromatic rings and agrees well with reported values for this step (2).

The observation of three different types of thermal behavior, as judged from the shape of the deconvoluted components, namely "desorption" (vacuum distillable component A), "depolymerization" (thermoplastic components B and C), and "thermal degradation" (thermosetting component D) points to the need for a kinetic model with at least three different reaction order terms. The desorption process is likely to have a reaction order between 0 and 1. The thermosetting (char formation) terms, on the contrary, would be expected to exhibit reaction orders substantially greater than 1. Only the two thermoplastic components (B and C) should follow first order unimolecular decomposition pathways under our vacuum micropyrolysis conditions. We are working on the development of a devolatilization model based on these TR Py-MS observations. In principle, this methodology can be applied to the "pure" maceral constituents of coal. Once the kinetic models for each maceral type are well established, a useful devolatilization model for the "mixture" coal might be within reach. In conclusion, computer-assisted TR Py-MS techniques enable deconvolution of chemical components, thereby allowing more insight into the chemistry of coal devolatilization.

## ACKNOWLEDGEMENTS

Funding for this work was supported by the Department of Energy (Grant No. DE-FG22-84PC70798) and the National Science Foundation (Contract CDR-8322618). Furthermore, the authors wish to thank Dr. Clint Williford for supplying the parameters for the Distributed Activation Energy Model.

## REFERENCES

- Howard, J. B., Peters, W. A., Serio, M. A., EPRI Report No. AP-1803, Palo Alto, California (April 1981)
- Solomon, P. R., Serio, M. A., Carangelo, R. M. and Markham, J. R., *Fuel* **65**, 182 (1986)
- Bliek, A., van Poelje, W. M., van Swaaij, W. P. M., van Beckum, F. P. H., *AICHE Journal*, **31**, No. 10, 1666 (1985)
- Vorres, K. S., Janikowski, S. K., in Karl S. Vorres (editor) *ACS Preprint*, **32**, No. 1, 492 (1987)
- Meuzelaar, H. L. C., Harper, A. M., Hill, G. R. and Given, P. H., *Fuel* **63**, 793 (1987)
- Windig, W., Jakab, E., Richards, J. M., Meuzelaar, H. L. C., *Anal. Chem.*, **59**, 317 (1987)
- Chakravarty, T., Meuzelaar, H. L. C., Technical report to METC, Department of Energy, April 1986
- Malinowski, E. R., Howery, D. G., *Factor Analysis in Chemistry*, John Wiley & Sons, 1980, New York
- Wirsz, D. F., Blades, M. W., *Anal. Chem.*, **58**, 51 (1986)
- Knorr, F. J., Futrell, J. H., *Anal. Chem.*, **51**, 1236 (1979)
- Anthony, D. B., Howard, J. B., *AICHE Journal*, **22**, 4, 625 (1976)
- Unpublished results.
- Meuzelaar, H. L. C., Harper, A. M., Pugmire, R. J., Karas, J., *Int. J. of Coal Geo.*, **4**, 143 (1984)
- Metcalf, G. S., Windig, W., Hill, G. R., Meuzelaar, H. L. C., *Coal Geology*, in press (1987)
- Yongseung, Yun., Jakab, E., McClennen, W., Hill, G. R., Meuzelaar, H. L. C., *ACS Preprints*, **32**, No. 1, (1987)
- Meuzelaar, H. L. C., Windig, W., Futrell, J. H., Harper, A. M., Larter, S. R., *ASTM STP 902*, Thomas Aczel, Ed., ASTM, Philadelphia, (1986)
- Nip, M., Tegelaar, E. W., Brinkhuis, H., de Leeuw, J. W., Schenck, P. A., Holloway, P. J., *Adv. in Org. Geochem.*, in press (1987)
- Suuberg, E. M., Peters, W. A., Howard, J. B., *Ind. Eng. Chem., Process Design and Develop.*, **17**, 37 (1978)
- Campbell, J. J., Stephens, D. R., *ACS Preprints* **21**, No. 7, 94 (1976)

TABLE I

### ANALYSIS OF COAL

	C	H	N	S	O	H/C	BTU/lb
Ultimate Analysis (DAF)	83.75	5.46	1.56	2.15	7.08	0.78	13,976
Proximate (as rec'd)	Moisture		Ash		Volatile Matter		
	0.57		7.27		37.86		

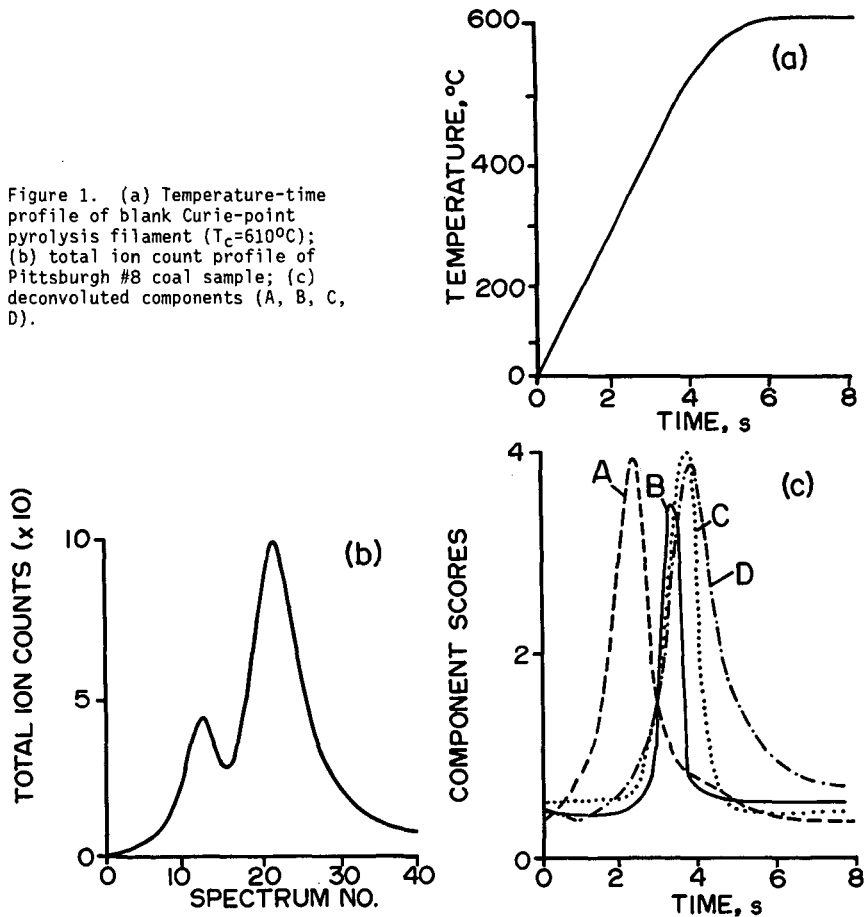
TABLE II  
KINETIC PARAMETERS CALCULATED FROM TIME-RESOLVED PY-MS DATA

	Thermal Extraction Step	Bulk Pyrolysis Step
Energy of Activation, Kcal mol <sup>-1</sup>	10	62(60)*
Frequency Factor, s <sup>-1</sup>	10 <sup>5</sup>	10 <sup>12</sup> (10 <sup>13</sup> **)

\* reference (2)

\*\* Distributed Activation Energy Model

Figure 1. (a) Temperature-time profile of blank Curie-point pyrolysis filament ( $T_c=610^\circ\text{C}$ ); (b) total ion count profile of Pittsburgh #8 coal sample; (c) deconvoluted components (A, B, C, D).



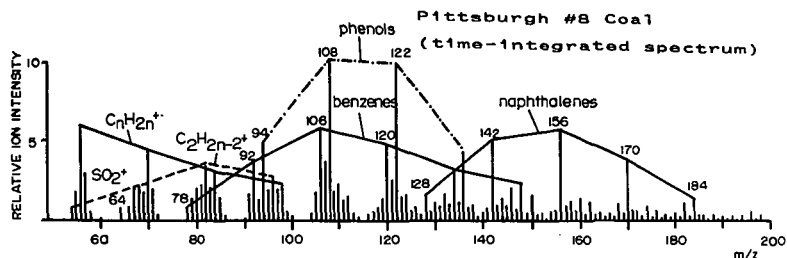


Figure 2. Time-integrated spectrum obtained by summing all 41 spectra recorded during time-resolved pyrolysis MS run. Note dominant series of homologous molecular ions characteristic of rank (hvAB) as well as of depositional environment and weathering status. Compare with deconvoluted spectra in Figure 3.

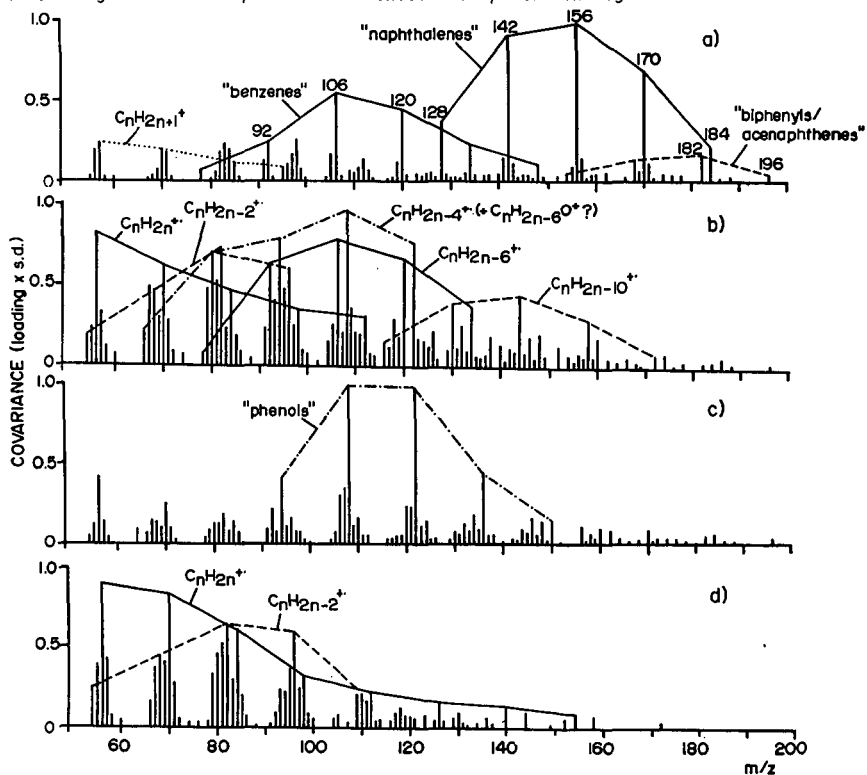


Figure 3. Numerically extracted ("deconvoluted") spectra of the four components shown in Figure 1. Note differences in % variance represented (summed variance of the four components is 99% of the total variance in all 41 spectra).

EPR STUDY OF THE CATALYTIC EFFECTS OF  
MINERALS ON FREE RADICAL FORMATION DURING COAL PYROLYSIS

M.S. Ali and W.R.M. Graham

Department of Physics, Texas Christian University  
Fort Worth, Texas 76129

A systematic *in situ* study of free radicals in Pittsburgh No. 8, acid treated coal (ATC) as a function of temperature and residence time has been carried out using the electron paramagnetic resonance (EPR) technique at temperatures up to 900 K. The catalytic effects of pyrite, pyrrhotite, calcite, and clays on free radical formation during pyrolysis have been examined.

INTRODUCTION

Various investigators have reported that the inherent mineral matter in coal may have a positive effect during conversion processes (1-3). Pyrite and pyrrhotite are of particular interest since pyrite, which is the major iron-sulfur compound in coal, is known to affect various stages in coal processing, and pyrrhotite, which is formed from pyrites under liquefaction conditions, has been found in one study (4) to influence conversion efficiency, although other work is in disagreement with this conclusion (5).

Since the formation of free radicals by the rupture of coal bonds during pyrolysis is believed to be an important step in liquefaction, the EPR technique has been used to advantage in studies on pyrolyzed and heat-treated coals (6,7). Recently Srinivasan and Seehra (8,9) have reported results of studies on the effects of pyrite and pyrrhotite on free radical formation in two West Virginia coals which were heated to ~900 K. Observing that the maximum increase in the number of free radicals occurred at ~800 K for coal samples containing 8% added pyrite, with a somewhat smaller increase for pyrrhotite, they concluded that both the conversion of pyrite to pyrrhotite and pyrrhotite itself contributed to the enhancement in the number of free radicals. An overall increase in the number of free radicals which was smaller on heating in H<sub>2</sub> than in vacuum, was interpreted as indicating that free radicals were stabilized by hydrogen.

An important point to note about the studies so far (8,9) on the effects of pyrite and pyrrhotite on free radical formation, is that the EPR measurements were carried out on coal samples which had been sealed in evacuated or gas-filled sample tubes, heated in a furnace, and then cooled. This procedure may preclude the observation of information on transient effects, which may be lost on cooling down the sample before EPR measurements are taken. A significant objective of the present work therefore, was to examine mineral effects on radical formation *in situ* during pyrolysis at temperatures up to 900 K. A step in this direction was recently reported by Seehra and coworkers (10) who carried out *in situ* measurements on samples of raw coal, and were able to de-

tect several distinct stages in pyrolysis based on the variation in spin concentration as the temperature increased during pyrolysis.

#### EXPERIMENTAL PROCEDURE

The coal samples used in this work were derived from a ground sample (C19825 in reference 14) from the Pittsburgh No. 8 seam, a high volatile bituminous coal, which has been the subject of several previous EPR investigations in this laboratory (11-13) and has been otherwise extensively characterized (14). Mineral samples used include pyrite from Custer, South Dakota, pyrrhotite from Falconbridge, Ontario, and calcite. Standard clay samples of well crystallized kaolinite (KCa-1), illite (IMT-1), and montmorillonite (SCa-2) were obtained from the Clay Minerals Society.

Small samples for EPR studies were prepared by thoroughly grinding mineral/coal mixtures so that the average particle size was much smaller than the microwave skin depth (15). The coal and mineral were dispersed in KBr in the ratio 1:100 (16), and then ground further in a ball grinder using plexiglass vials and balls to avoid metal contamination. Samples were placed in vacuum and usually used immediately following grinding; however, when necessary, they were stored for 24 h under nitrogen, with no observable deterioration in the EPR spectrum.

The low temperature ash fraction (14.5%) from the Pittsburgh No. 8 coal has been analyzed to contain 16% pyrite, 25% calcite, 8% quartz, with the remaining 54% composed of kaolinite, illite, expandable clays, and other minerals. For experiments designed to study the evolution of free radicals in the absence of the inherent mineral matter, acid treated samples were used. These were prepared by boiling raw coal with 5M HCl for 30 minutes, thoroughly washing with acetone and ethanol, and then drying at 375 K for 8 h. Subsequent preparation proceeded as already described for raw coal.

Prior to carrying out the EPR measurements, each coal sample was placed in a 4 mm o.d. quartz sample tube which was evacuated through a side arm. The sample tube was inserted into a double-walled quartz dewar inside the microwave cavity. Nitrogen gas heated by passage over a series of two chromel-alumel heater elements flowed through the dewar. By suitable adjustment of the gas temperature and flow rate, the sample temperature, as measured by a chromel-alumel thermocouple, could be raised to 900 K with a stability of  $\pm 1$  K. The Varian TE<sub>102</sub> mode cavity was maintained at room temperature by means of refrigerated water circulating inside a jacket which surrounded, and was in good thermal contact with the cavity. The signal intensity from a sample of DPPH fixed to the cavity wall was unchanged by heating the sample inside the dewar, confirming that the sensitivity of the cavity was not affected.

EPR measurements were made at  $\sim 9$  GHz using a Varian V-4500 spectrometer equipped with 100 kHz field modulation. The arrangement for pyrolysis experiments has already been described; low temperature experiments on the acid following demineralization were done using a Varian variable temperature

accessory. Field measurements were made using a Harvey-Wells NMR gaussmeter and a Hewlett-Packard frequency counter. The spectrometer is interfaced to an IBM XT computer which is used for data acquisition, calibration, storage, and analysis.

#### RESULTS AND DISCUSSION

Figure 1 shows plots of the absolute temperature (T) versus the product of the temperature and the intensity of the EPR absorption obtained by numerical double integration of the observed line profile (IT). The results illustrated are for a sample of raw Pittsburgh No. 8 coal and for two other samples, coal + 8% pyrite and coal + 8% pyrrhotite, heated for 20 minutes at ~40 K intervals. In the case of raw coal there is no significant change in free radical concentration until ~600 K, after which it rises, but at a slower rate than the curves for the samples with mineral added. Both of the latter samples show evidence of an intermediate step in which a small increase in concentration is followed by a decrease, before the onset of the steep rise at ~600 K. The preliminary step is similar to that observed by Seehra *et al.* (10) for *in situ* measurements on three raw coals, but was not observed in their earlier study (8,9) on the effects of the addition of pyrite and pyrrhotite in which measurements were made after heating outside the cavity. The number of free radicals increases faster for added pyrrhotite than for pyrite until it reaches a peak at 800 K and then drops rapidly thereafter. The pyrolysis of the raw coal and coal + 8% pyrite continues to yield additional free radicals up to the cutoff in the data at 900 K. This continued enhancement of the free radical yield in coal + 8% pyrite samples contrasts with the earlier observations for samples pyrolyzed outside the cavity and recorded cold (8,9), where all three samples showed a decline in free radical concentration back to prepyrolysis levels, and suggests the importance of *in situ* observations in monitoring the dynamic process. The observation that at temperatures up to 800 K the coal + 8% pyrrhotite sample shows higher concentrations of free radicals than pyrite, which then continues to enhance free radical formation as the yield from pyrrhotite declines, suggests that the catalytic activity of the pyrrhotite has been depleted, while in the coal + 8% pyrite sample the pyrite continues to convert to pyrrhotite which then enhances the free radical yield. This tends to support the view that the conversion to pyrrhotite as well as the mineral itself are positive influences.

A significant question is the possible influence of the inherent mineral matter on radical yield. In an attempt to investigate this possibility samples of acid treated coal were studied. Figs. 2(a) and (b) show the EPR spectrum of the raw coal at room temperature (296 K) and after heating at 814 K, respectively. The room temperature spectrum shows evidence of  $\text{Fe}^{3+}$  at  $g \approx 4.4$  which is probably contained in clays, and a broad weak signal underlying the free radical signal at  $g \approx 2.0$ , which may be from metallic iron. Pyrite, with  $\text{Fe}^{2+}$ , has no EPR spectrum; however, after heating, conversion of pyrite to pyrrhotite has occurred, and a strong ferromagnetic resonance signal is

observed at center field. The spectrum shown in Fig. 2(c) of ATC-1 at room temperature shows that the  $Fe^{3+}$ -bearing mineral has been removed, and Fig. 2 (d) recorded at 869 K shows no evidence of converted pyrrhotite. Finally, when 8% pyrite is added to ATC-1, heating to 871 K again reveals the presence of pyrrhotite as shown in Fig. 2 (e). The spectrum shown in Fig. 2 (f) of a glass of the HCl which was used in the demineralization, shows evidence of the iron extracted from the coal.

Figure 3 shows the IT versus T curves obtained for two samples of acid treated coal (ATC-1 and ATC-2) which were heated *in situ* for ~85 min at ~40 K intervals, compared to the curve for the same ground sample of raw coal before acid treatment which was heated for ~20 min at each interval. The consistently higher concentration of free radicals generated in the pyrolysis of the raw coal compared to the ATC supports the contention that the inherent mineral component contributes to the radical yield.

Prior to examining the influence on free radical yield of adding specific minerals to the ATC, a series of experiments was carried out to determine the effect of residence time. Figs. 4(a) - (e) show the time evolution of radical concentration for ATC with added pyrite, pyrrhotite, calcite, clays (4% kaolinite, 2% illite, 2% montmorillonite), and a mixture of calcite and pyrite. In each case the results were obtained by pre-heating the dewar in the cavity to ~830 K, inserting the sample tube, and beginning to record observations after 5 minutes residence. It is seen that the maximum in free radical concentration occurs for widely different residence times for the various coal/mineral combinations. In particular, the radical concentration for ATC-1 + 8% pyrrhotite reaches a maximum after only 10 min, while at least 50 min are required for ATC-1 + 8% pyrite. This again points to the importance of converted pyrrhotite. A mixture of 4% calcite + 4% pyrite added to ATC appears to be even more effective. Radical concentration increases rapidly in the first 5 minutes, and after 30 minutes has reached a maximum. By contrast, the addition of clays, pyrite, or calcite separately, appears to produce no dramatic increases.

Plots of the the relative concentration of free radicals as a function of temperature for ATC and ATC with the five minerals mentioned earlier are shown in Fig. 5. At temperatures up to ~825 K the number of free radicals produced is generally best for a mixture of calcite and pyrite. Pyrrhotite also enhances free radical yield, but only up to ~800 K. Pyrite appears to be much less effective when added to the ATC than it was when added to the raw coal. Pittsburgh No. 8 coal does, of course, contain calcite, and these results at least raise that this inherent calcite and the pyrite together play a role in the observed increase in free radical concentration shown in Fig. 1.

#### CONCLUSIONS

Several conclusions may be drawn from the results reported here. The increase in radical concentration observed on the addition of pyrrhotite to ATC in contrast to the relative ineffectiveness of pyrite supports the view

that the conversion of pyrite to pyrrhotite and pyrrhotite itself are responsible. Of interest, is the apparent positive influence of calcite on free radical yield. In studies on the pyrolysis of Pittsburgh No. 8 coal in helium and hydrogen at temperatures up to 1300 K Franklin *et al.* (17,18) found strong effects by calcium minerals. In particular, they concluded that  $\text{CaCO}_3$  and its decomposition product during pyrolysis  $\text{CaO}$ , are especially active in cracking oxygen functional groups and aromatics. We note however, that the free radical yield shows substantial enhancement only when in the presence of pyrite.

#### ACKNOWLEDGMENTS

This work was supported by the TCU Research Fund and in part by The Welch Fund.

#### REFERENCES

1. P.H. Given, D.C. Cronauer, W. Spackman, H.L. Lovell, A. Davis, and B. Biswas, *Fuel* 54, 34 (1975).
2. D.K. Mukherjee and P. B. Chowdhury, *Fuel* 55, 4 (1976).
3. B. Granoff and P.A. Montano, in *Chemistry and Physics of Coal Utilization 1980*, B.R. Cooper and L. Petrakis, ed. (AIP, New York, 1981) pp. 291-308.
4. P.A. Montano and B. Granoff, *Fuel* 59, 214 (1980).
5. N.J. Mazzocco, E.B. Klunder, and D. Krastman, "Study of catalytic effect of mineral matter level on coal reactivity", Pittsburgh Energy Technology Center Rep. DOE/FETC TR-81/1 (1981).
6. H.L. Retcofsky, M.R. Hough, M.M. Maguire, and R.B. Clarkson, in *Coal Structure*, ACS Adv. Chem. Ser. 192, 37 (1981).
7. L. Petrakis and D.W. Grandy, *Free Radicals in Coals and Synthetic Fuels* (Elsevier, New York, 1983).
8. G. Srinivasan and M.S. Seehra, *Fuel* 61, 1249 (1982).
9. G. Srinivasan and M.S. Seehra, *Fuel* 62, 792 (1983).
10. M.S. Seehra, B. Ghosh and S.E. Mullins, *Fuel* 65, 1315 (1986).
11. V.M. Malhotra and W.R.M. Graham, *Fuel* 64, 270 (1985).
12. V.M. Malhotra and W.R.M. Graham, *J. Appl. Phys.* 57, 1270 (1985).
13. V.M. Malhotra and W.R.M. Graham, *Fuel* 64, 579 (1985).
14. J.K. Kuhn, F. Fiene, and R. Harvey, "Geochemical Evaluation and Characterization of a Pittsburgh No. 8 Coal and a Rosebud Seam Coal), Morgantown Energy Technology Center Rep. DOE/METC CR-78/8 (1978).
15. L.S. Singer, *Proc. 5th Carbon Conf.* 2, 37 (1963).
16. H.L. Retcofsky, M.R. Hough, M.M. Maguire, and R.B. Clarkson, *Appl. Spectrosc.* 36, 187 (1982).
17. H.D. Franklin, W.A. Peters, F. Cariello, and J.B. Howard, *Ind. Eng. Chem.* 20, 670 (1981).
18. H.D. Franklin, W.A. Peters, and J.B. Howard, *Fuel* 61, 155 (1982).

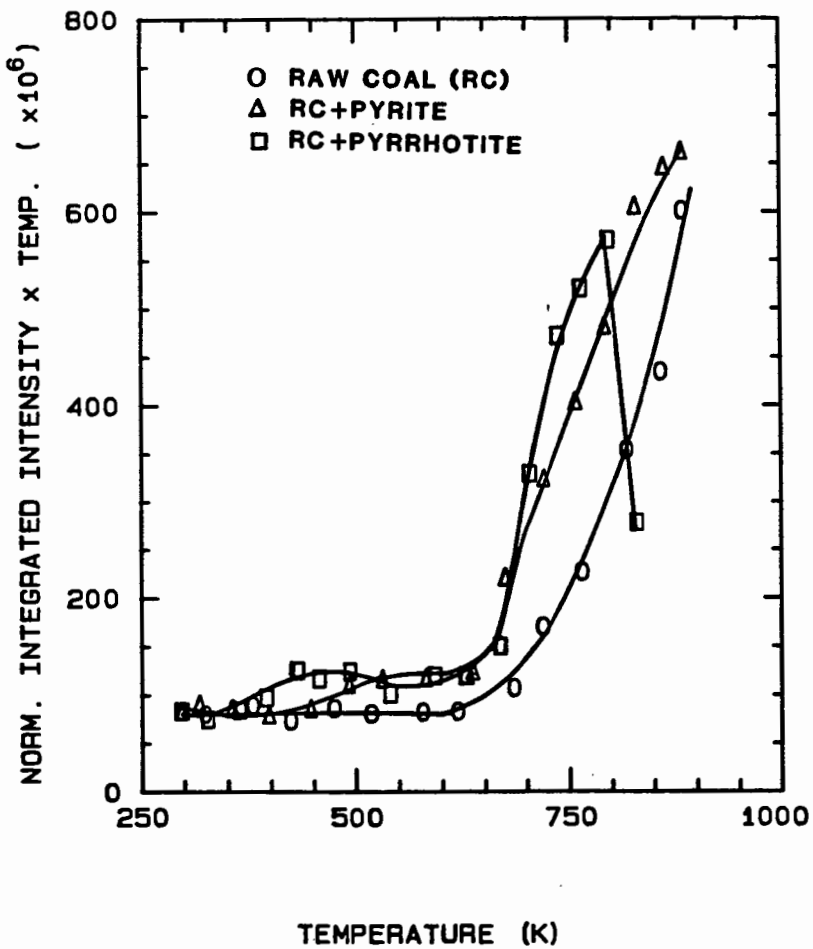


Fig. 1. Plot of IT versus T for raw coal, raw coal + 8% pyrite, and raw coal + 8% pyrrhotite.

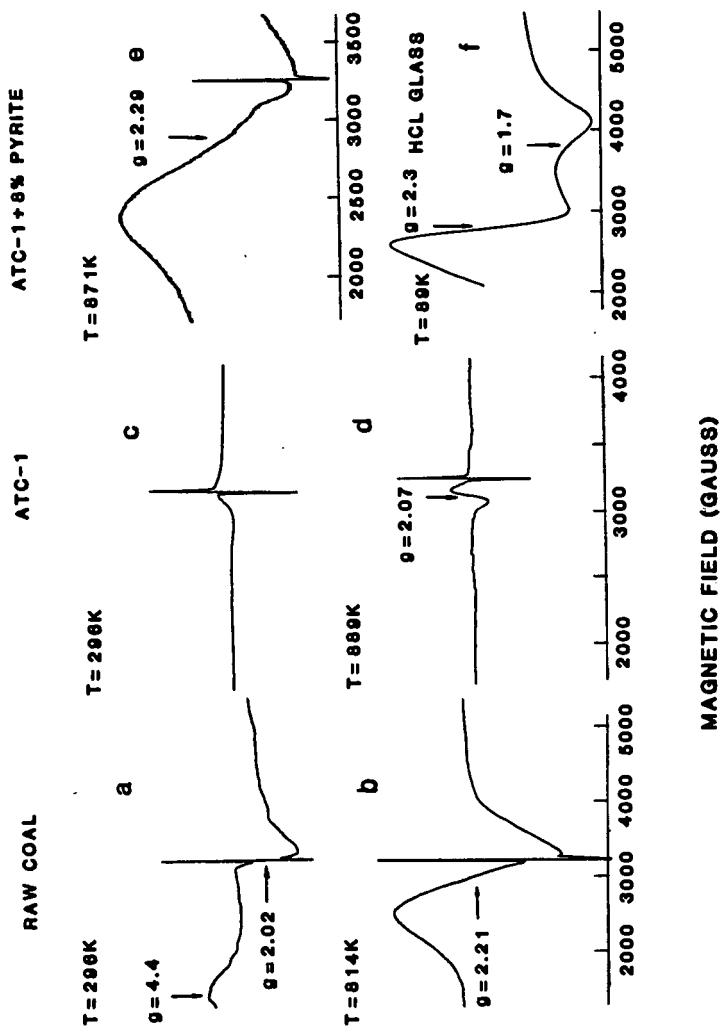


Fig. 2. EPR spectra of raw coal at (a) 296 K and (b) 814 K; ATC-1 at (c) 296K and (d) 869 K; (e) ATC-1 + 8% pyrite at 871 K; and (f) a glass at 89 K of the HCl extract from demineralization.

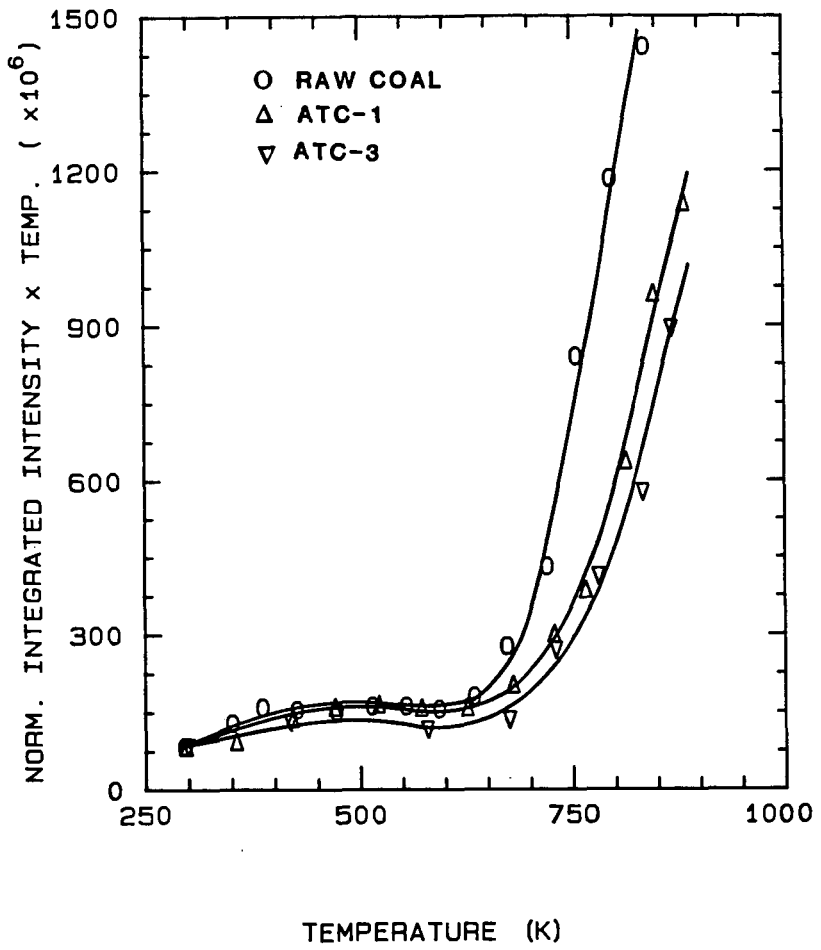


Fig. 3. Plot of IT vs. T for ATC-1, ATC-3, and raw coal.

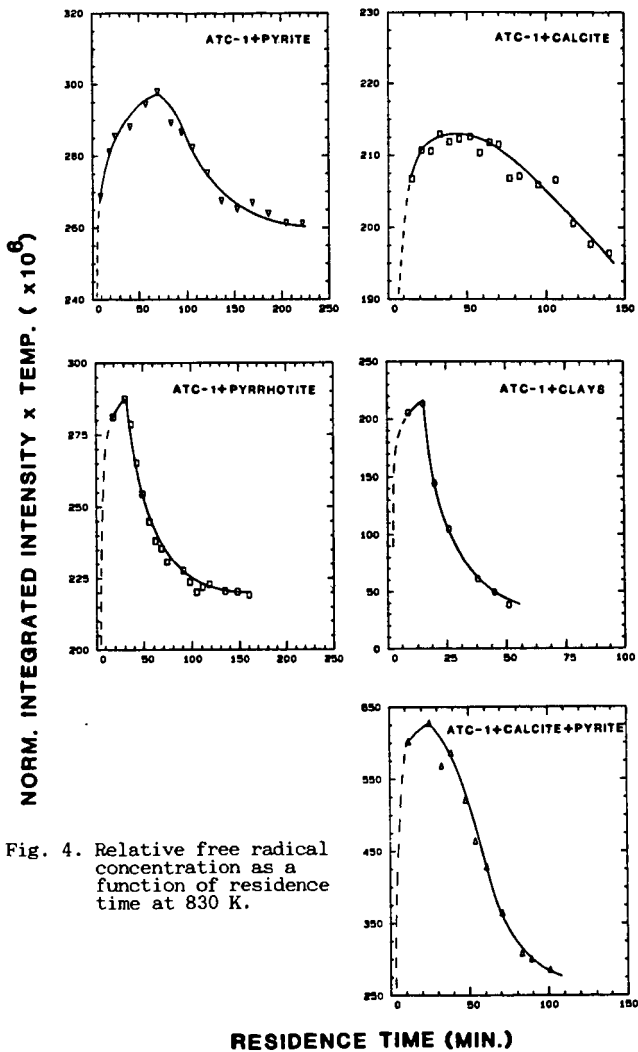


Fig. 4. Relative free radical concentration as a function of residence time at 830 K.

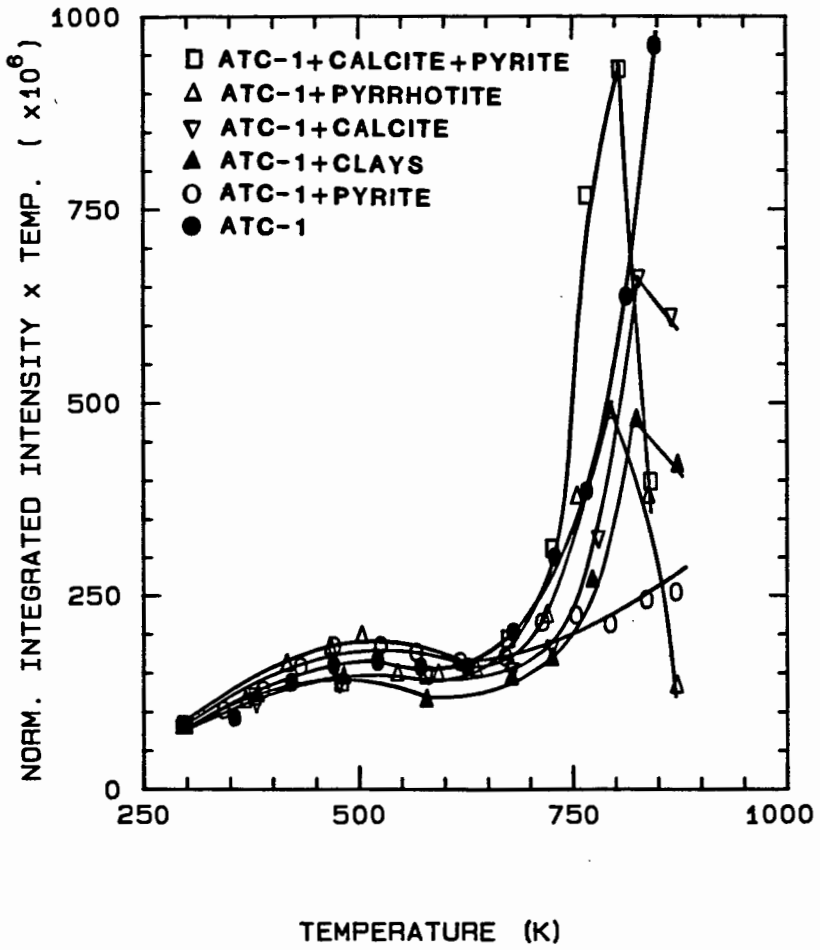


Fig. 5. Plot of IT vs. T for ATC-1 and ATC-1 + 8% various minerals.

## COPPER CATALYZED LOW-TEMPERATURE PYROLYSIS AS A MEANS FOR UPGRADING LOW-RANK SOLID FUELS

S. Stournas, M. Papachristos and G. B. Kyriakopoulos

Chemical Engineering Department, National Technical University  
42 Patission Street, 106 82 Athens, Greece

### ABSTRACT

Low-rank solid fuels (lignite and peat) are characterized by a high oxygen content on a DAF basis, a large proportion of which belongs to carboxyl and hydroxyl groups. These groups being thermally labile, the oxygen content of low-rank coals can be substantially decreased (and their heat content per unit mass correspondingly increased) by subjecting them to simple pyrolytic treatment.

It has been found that the behavior of certain types of lignite and peat is similar to that of simple carboxylic acids, in that the thermal decarboxylation process can be catalyzed by specific metal ions. Thus when lignite and peat, in the presence of small amounts of copper, are pyrolyzed at low temperatures (160°-200° C), they readily undergo decarboxylation and dehydration and their higher heating values on a DAF basis show increases of the order of 30%. When uncatalyzed, these same reactions require temperatures in excess of 300° C.

### INTRODUCTION

Among the known fossil fuel reserves those of the low-rank coals (i.e. lignite and peat) remain underutilized, despite their significant potential as a readily recoverable energy resource. The main problem associated with these solid fuels is their low heat content per unit mass, which in turn is due to the high moisture and ash content but also to the relatively low heating value of the DAF coal itself.

It has been a well known fact for many years<sup>1</sup> that, on moving from high rank to low rank coals, the ratio of oxygen content to carbon content increases substantially; it is not unusual for a lignite coal to contain around 30% oxygen on a DAF basis, whereas peat approaches 40%.

It is evident that the upgrading of lignite and peat to forms that come close to hard coal in properties and performance may involve:

- a. Moisture removal through the various drying processes<sup>2</sup>
- b. Ash removal through processes such as leaching<sup>3</sup> and flotation<sup>4</sup>
- c. Oxygen removal from the DAF coal

The first two approaches deal with the separation of the fuel component (DAF coal) from extraneous materials (moisture and ash), whereas the third approach is concerned with the chemistry of the fuel component itself.

The higher oxygen content of low-rank coals is coupled with marked differences in the relative contents of the various oxygen functionalities. This is particularly pronounced in the case of the carboxyl group, which is one of the main oxygen functionalities occurring in lignite and peat but is almost totally absent in coals

of bituminous and higher ranks.<sup>5,6</sup> An efficient means of decarboxylation, therefore, could lead to a significant improvement of the overall properties, and particularly the heat content of lignite and peat.

The decarboxylation of low-rank coals can be achieved by heating the coal at a high enough temperature. Thus, simple heating of lignite to about 330° C leads to decarboxylation and an increase of about 21% in the gross calorific value of the coal.<sup>7</sup> Similar results were obtained by heating low-grade solid fuels at about 400° C either in the presence of base<sup>8</sup> or in the presence of acid,<sup>9</sup> whereas processes involving even higher temperatures have also been reported.<sup>10, 11</sup>

It is apparent that, for thermal decarboxylation of low-rank coals to take place to any significant extent, temperatures in excess of 300° C are required. However, it has been known for a long time that copper will catalyze the decarboxylation of carboxylic acids,<sup>12, 13</sup> and the mechanism of this reaction has been studied in detail.<sup>14, 15</sup> The purpose of the present study was to assess the possibility of utilizing copper as a catalyst for the decarboxylation of lignite and peat at low temperatures, thus making the process energetically more efficient.

#### EXPERIMENTAL

Three types of coal were used in this study, Megalopolis lignite, Ptolemais' lignite, and Philippi peat; their characteristics are given in Table I. The experimental procedure was similar to that described in a preliminary report on the heat-treatment behavior of two of the above coals<sup>16</sup> and is summarized below.

Samples of about 10 g of each coal (40 to 200 mesh) were slurried with 20 mL of a dilute aqueous solution of cupric sulfate; the copper content was equal to 1% or 3% of the DAF coal of the sample. An amount of sodium carbonate equivalent to the copper sulfate was dissolved in distilled water and was added to the previous slurry with stirring. The coal was then filtered off under mild suction and washed with distilled water. This method achieved an intimate mixture of the coal under study with copper in the form of cupric carbonate. The treated coal was then transferred to a porcelain crucible and placed in an oven at the desired temperature (140° - 400° C) for a period of 30 minutes. This length of time was found adequate for low temperature pyrolysis after a series of experiments with varying heating durations. For comparison purposes, blank samples of coal (i.e. containing no copper) were subjected to exactly the same procedure, except that the initial slurry was made with distilled water.

#### RESULTS AND DISCUSSION

The measured higher heating values of the various samples, before and after heat treatment, are shown in Tables II, III, and IV. It can be seen that thermal treatment invariably increases the heat content of Megalopolis lignite and Philippi peat; the magnitude of the increase, however, depends both on the temperature of the treatment and on the presence of copper as the decarboxylation catalyst. This behavior can be more easily visualized if one refers to figures 1 and 2, which illustrate the increase in higher heating value as a function of temperature and copper content.

TABLE I  
COAL CHARACTERISTICS

	<u>Megalopolis</u> <u>Lignite</u>	<u>Philippi</u> <u>Peat</u>	<u>Ptolemais</u> <u>Lignite</u>
<u>As Received Basis</u>			
Moisture (%)	45.0	16.1	56.3
Volatile Matter (%)	24.4	45.8	18.0
Fixed Carbon	12.5	16.7	12.1
Ash (%)	18.1	21.4	13.7
HHV (MJ/Kg)	9.02	12.72	7.05
<u>DAF Basis</u>			
C %	60.4	56.7	63.2
H %	5.9	5.5	5.2
S %	2.9	1.1	1.6
N %	1.8	1.8	1.6
O % (by difference)	29.0	34.9	28.4
HHV (MJ/Kg)	24.42	20.36	23.43

TABLE II  
CHANGE IN CALORIFIC VALUE (DAF BASIS) AS A FUNCTION OF TREATMENT  
TEMPERATURE AND COPPER CONTENT  
MEGALOPOLIS LIGNITE

<u>Treatment Temperature</u> (°C)	<u>Higher Heating Value</u> (MJ/Kg)		
	<u>No Cu</u>	<u>1% Cu</u>	<u>3% Cu</u>
No Heat Treatment	24.42	24.25	24.28
140	24.45	24.64	24.70
160	26.06	30.43	30.08
200	26.74	30.98	31.24
250	27.67	31.62	31.82
300	33.34	34.07	33.16

TABLE III  
CHANGE IN CALORIFIC VALUE (DAF BASIS) AS A FUNCTION OF TREATMENT  
TEMPERATURE AND COPPER CONTENT  
PHILIPPI PEAT

<u>Treatment Temperature</u> (°C)	<u>Higher Heating Value</u> (MJ/Kg)		
	<u>No Cu</u>	<u>1% Cu</u>	<u>3% Cu</u>
No Heat Treatment	20.36	20.25	20.38
140	20.38	20.39	20.56
160	20.44	20.57	21.83
200	20.55	23.87	25.63
250	21.38	24.36	26.12
300	25.84	28.05	28.79

In the case of Megalopolis lignite (Figure 1) it is evident that the presence of copper is of minor significance up to about 140° C. the temperature being too low even for the catalyzed decarboxylation to take place. Starting at around 160° C. however, the catalytic effect of copper becomes significant and an increase of the order of 20% is observed in the higher heating value of the heat-treated lignite. Increasing the concentration of copper from 1%

to 3% appears to have essentially no effect on its catalytic activity. When the heat-treatment temperature reaches 300° C. the role of copper becomes much less significant, inasmuch as the rate of decarboxylation is quite fast even in the absence of catalyst.

In the case of Philippi peat (Figure 2) the experimental results display a similar pattern, except that the onset of significant catalytic activity of the added copper does not occur until the heat-treatment temperature has reached about 200° C. It is also worth noting that in this particular case the catalytic effect of copper is more pronounced at the higher metal concentration (3%).

TABLE IV  
CHANGE IN CALORIFIC VALUE (DAF BASIS) AS A FUNCTION OF TREATMENT  
TEMPERATURE AND COPPER CONTENT  
PTOLEMAIS LIGNITE

<u>Treatment Temperature (°C)</u>	<u>Higher Heating Value (MJ/Kg)</u>		
	<u>No Cu</u>	<u>1% Cu</u>	<u>3% Cu</u>
No Heat Treatment	23.51	23.22	23.43
160	23.56	23.90	24.06
200	25.26	25.54	26.36
250	25.66	26.34	26.58
280	-	-	25.64
300	26.35	27.34	23.73
320	26.88	28.35	22.95
340	-	-	22.50
370	29.66	29.27	22.59
400	-	-	22.66

As can be seen in Table IV and Figure 3, the behavior of Ptolemais lignite is quite different than that of the other two coals under the experimental conditions that were employed. In the presence of 1% copper, the increase in higher heating value of the pyrolysis residue is only slightly higher than the one occurring in the absence of catalyst. In the presence of 3% copper the results are even more remarkable, in that the higher heating value of the residue starts decreasing at around 250° C and falls below that of the unheated sample at temperatures above 300° C. It thus appears that, in the case of Ptolemais lignite, the presence of copper can lead to the evolution of combustible gases in addition to carbon dioxide and water. The exact nature of this reaction is currently under investigation in our laboratory.

Due to the loss of volatiles (mostly carbon dioxide and water), the mass of the fuel that is recovered after heat treatment is lower than the original one; this loss of mass increases with increasing temperature. The recovery of total heat content, however, is almost quantitative (over 98% in most cases) up to a treatment temperature of 200° C. At higher temperatures the observed heat loss is more pronounced, due to evolution of combustible gases such as carbon monoxide. In the case of Ptolemais lignite the loss of both mass and heat content is much more significant in the presence of 3% copper. Figure 4 is an illustration of typical heat recovery patterns, i.e. the total heat content of the pyrolyzed coal as a percentage of the amount that was contained in the sample before thermal treatment.

The process described in this paper appears to offer the possibility of additional improvements in the quality of the treated coals, including:

a. Lowering of the ash content of the treated coals, probably due to the leaching of the water-soluble components during the slurring operation.

b. Lowering of the sulfur content.

c. Decrease of the hydrophilicity of the coal, thus making it potentially more amenable to ash-removing processes such as flotation and gravity separation.

The magnitude and mode of occurrence of the above effects are currently under study.

### CONCLUSIONS

In two of the three samples of low-rank coals that were studied in the course of this work, the addition of small amounts of copper appears to catalyze decarboxylation of the coals in a manner reminiscent of the copper catalyzed decarboxylation of carboxylic acids. As a result, low temperature (160°-250° C) heat treatment in these cases leads to an increase of about 25-30% in the higher heating value of the DAF coal.

The third coal, Ptolemais lignite, offers a different picture. Decarboxylation in the presence of copper is more sluggish, and it appears that other reactions are also being catalyzed, leading to the evolution of combustible gases at comparatively low temperatures.

### REFERENCES

1. Van Krevelen, D.W., 1950. Fuel, 29: 269
2. Rozgonyi, T.G. and Szigeti, L.Z., 1985. Fuel Processing Technol., 10: 1
3. Wang, Z.Y., Ohtsuka, Y. and Tomita, A., 1986. Fuel Processing Technol., 13: 279
4. Mitchell, D.R. and Charmbury, H.B., 1963. Chapter 8 in Lowry, H.H., (Ed.), "Chemistry of Coal Utilization", Suppl. Volume. J. Wiley, New York
5. Whitehurst, D.D., Mitchell, T.O. and Farcasiu, M., 1980. Coal Liquefaction. Academic Press, New York, p. 18
6. Doolan, K.R. and Mackie, J.C., 1985. Fuel, 64: 400
7. Elliott, D.C., 1980. Fuel, 59: 805
8. Sharma, D.K., 1983. NSTA Technol. J., 8(2): 93
9. Van Raam, L. and Ruyter, H.P., 1981. Eur. Patent 26011. Chem. Abstracts, 95: 45957
10. Mitsubishi Heavy Industries, 1981. Jap. Patent 157494. Chem. Abstracts, 96: 126107
11. Koppelman, E., 1977. U.S. Patent 4,052,168
12. Dougherty, G., 1928. J. Am. Chem. Soc., 50: 571
13. Fieser, L.F. and Fieser, M., 1967. Reagents for Organic Synthesis. J. Wiley, New York, pp. 157, 158, 163
14. Schambach, R., 1980. Ph.D. Thesis, Univ. of Pittsburgh
15. Cohen, T., Berninger, R.W. and Wood, J.T., 1978. J. Org. Chem. 43: 837
16. Stournas, S., Papachristos, M., and Kyriakopoulos, G.B., 1987. Fuel Processing Technol., in press

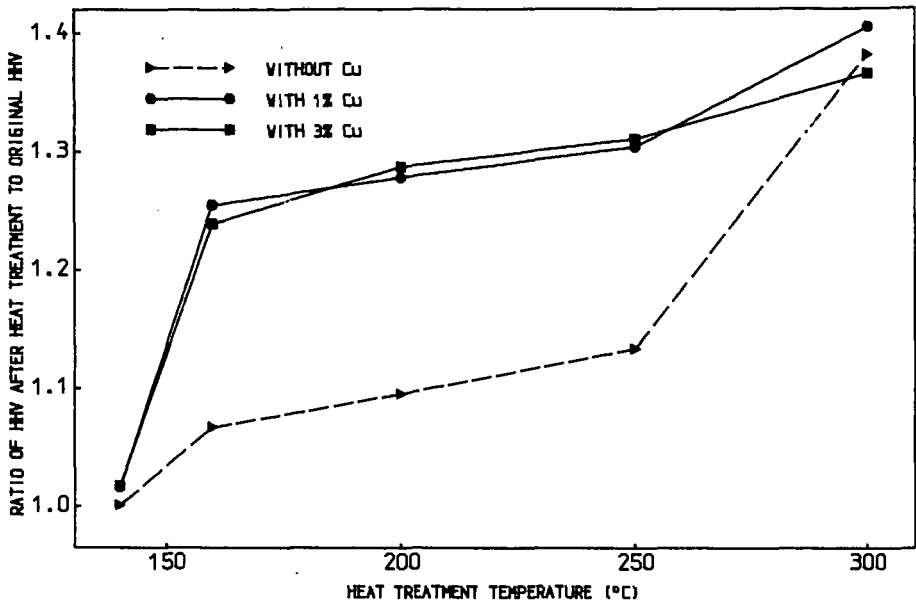


FIGURE 1. LOW TEMPERATURE PYROLYSIS OF MEGALOPOLIS LIGNITE

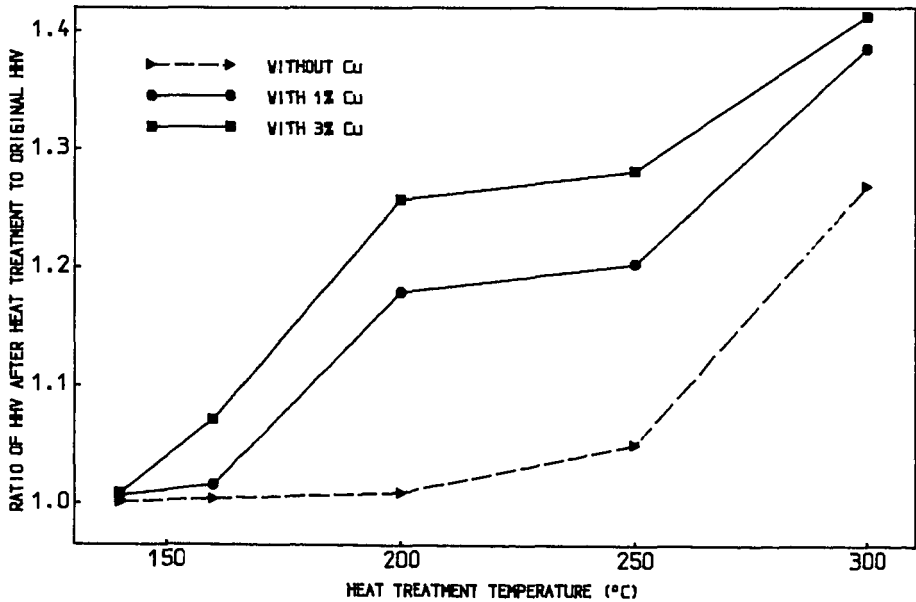


FIGURE 2. LOW TEMPERATURE PYROLYSIS OF PHILIPPI PEAT

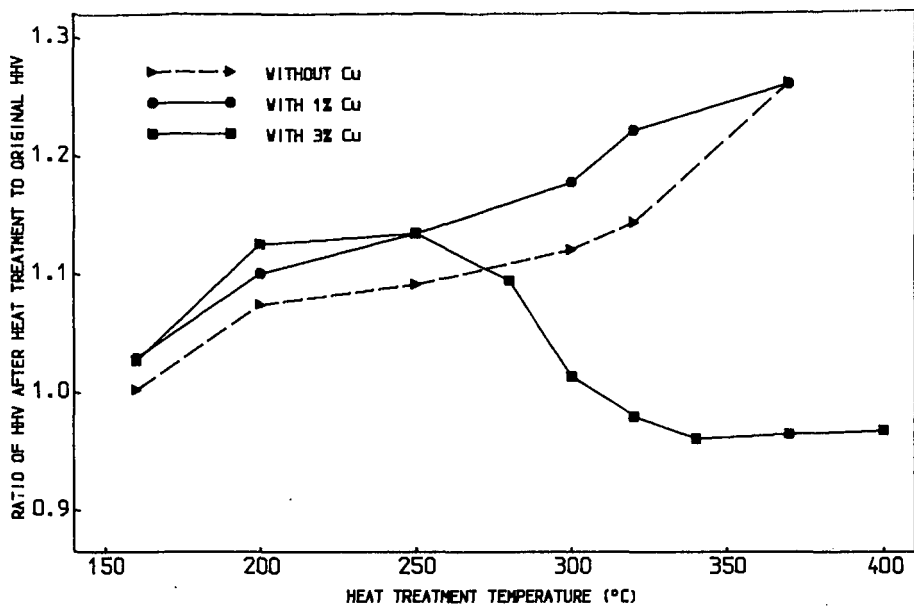


FIGURE 3. LOW TEMPERATURE PYROLYSIS OF PTOLEMAIS LIGNITE

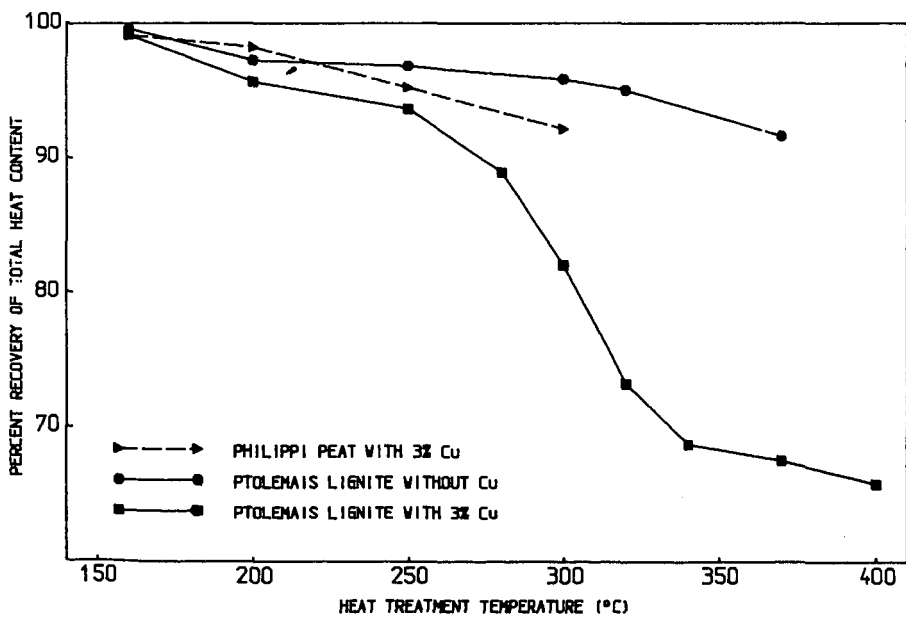


FIGURE 4. RECOVERY OF TOTAL HEAT CONTENT IN THE PYROLYSIS RESIDUE

## PYROLYSIS OF WILSONVILLE COAL LIQUEFACTION RESIDUES

By W. A. Leet and D. C. Cronauer  
Amoco Oil Company  
P. O. Box 400  
Naperville, Illinois 60566

Wilsonville coal liquefaction residues including vacuum tower bottoms (VTB), critical solvent deashing (CSD) product resids, and CSD ash concentrates were pyrolyzed via isothermal thermogravimetric analysis. Pyrolysis yields of gas, liquid, and coke were found to be insensitive to temperature over the range of 800-1200°F. The yields of pyrolysis products generated from the CSD resids indicate that the CSD resids represent the more thermally reactive and volatile portions of the VTB. The tendency of such resids to form coke upon pyrolysis correlates with phenolic hydroxyl content. Unusually low gas plus liquid yields for the relatively hydrogen rich ash concentrates correlates with high heteroatom and mineral matter contents. Differences observed in pyrolysis yields for samples from Wilsonville runs made with and without recycle of unconverted coal and mineral matter further characterize the role of such recycle.

### INTRODUCTION

In the development of coal liquefaction processes, the pyrolysis (notably delayed and fluid coking) of coal liquefaction residues (resids) has been incorporated into liquefaction process design to supplement liquid yields. The following report presents an update on the viability of low temperature pyrolysis for the processing of coal liquefaction resids. Specifically, the report examines short contact time pyrolysis yields from various liquefaction resids generated at the Advanced Two-Stage Coal Liquefaction R&D Facility at Wilsonville.

### EXPERIMENTAL

Liquefaction resid samples were obtained from the coal liquefaction facility at Wilsonville, AL. (1) The Wilsonville pilot plant was operating in a two-stage mode with direct coupling of the thermal liquefaction and catalytic (hydrotreater) reactors as shown in the schematic, Figure 1. After flashing and vapor recovery, the residual vacuum bottoms (VTB) cut was fed to a critical solvent deashing (CSD) unit (currently designated the ROSE-SR process by Kerr McGee Corp.) to reject an ash concentrate and recover an ash free-resid. The VTB product, CSD resid, and CSD ash concentrate from three Runs were studied. In Run 250D, the liquefaction feed solvent consisted of recycle distillates plus CSD resid. In Runs 250H and 251E, the recycle of VTB resid, including unconverted coal and mineral matter, was added to the feed solvent. In Run 251E, catalyst was also loaded into the thermal liquefaction reactor.

All three runs were made with Illinois No. 6 coal at essentially the same reaction conditions. The relevant characterization data are presented in Table I for the runs of interest.

Thermogravimetric (TGA) was used to screen pyrolysis coke, liquid, and gas yields as a function of temperature. Traditionally operated under an inert atmosphere at a preprogrammed heating rate of 5-50°C/min., an isothermal TGA procedure was developed to mimic the more rapid heating rates characteristics of short contact time pyrolysis processes. Provision was made to collect and weigh the liquids as well as recovered "coke" (residual mineral matter, unconverted coal, and coke). Gas yields were calculated by difference. Although representative process variable effects and product quality data could not be obtained due to the small sample sizes involved, such screening provided a relative measure of pyrolysis yields among samples as a function of temperature.

## RESULTS

Preliminary screening of the coke yield of the Wilsonville samples was carried out by standard and isothermal TGA runs. Initial screening of Run 250H VTB indicated that coke yields were insensitive to heating rate, sample size, and purge nitrogen flow rate. Pyrolysis yields for Run 250D and Run 250H VTB products are plotted in Figure 2 as a function of pyrolysis temperature. The insensitivity of the yields to pyrolysis temperature over the range (800-1200°F) investigated suggests that the VTB cuts are highly aromatic and not readily thermally cracked under pyrolysis conditions. Such high aromaticity is due to the condensed structure of the original coal feedstock and the liquefaction and concomitant retrogressive reactions to which it is subjected in the liquefaction process. The decrease in liquid yields with VTB recycle, which is seen in comparing products of Run 250D with those of Run 250H and 251E, is attributed to additional solubilization and reaction of recycled VTB organic matter in the liquefaction reactors. This leads to the formation of more highly condensed resids.

For the key Wilsonville runs on bituminous coal, average pyrolysis liquid yields are plotted versus feed H/C ratio in Figure 3. The liquid yields, despite diminished vapor phase cracking of the volatiles evolved in the TGA experiments, are comparable to average Exxon simulated fluid coking yields for samples of resids from the H-Coal and SRC-I processes. Such results support a physical picture in which fluid coking of Wilsonville resids lead primarily to vaporization of remaining volatiles with little concomitant liquids upgrading. Liquid yields obtained from pyrolysis of the CSD resids represent the more volatile fractions of the thermally reactive portion of the CSD feeds. Moreover, considering the high H/C ratio, the CSD ash concentrates yield unusually low quantities of liquid product upon pyrolysis. The organic matter rejected in the ash concentrate represents highly condensed and nonvolatile aromatic structures which are heteroatom rich and exhibit strong interactions (adsorption and/or chemical bonding) with the ash mineral matrix.

To examine the coking tendencies of the Wilsonville Streams, selected CSD feed and product resids were fractionated by sequential Soxhlet extraction with n-pentane, toluene, and tetrahydrofuran (THF) to oil (pentane soluble),

asphaltene (pentane insoluble, toluene soluble), preasphaltene (toluene insoluble, THF soluble), and lumped ash/unconverted coal/coke (THF-insoluble) fractions. Although arbitrary in measure, such a fractionation scheme permits a finer resolution of the chemistry involved in terms traditionally applied to coal-derived products. The fractions in turn were pyrolyzed at 1100°F to examine the propensity of each to form coke. The results are summarized in Table II for VTB and CSD resids.

Comparison of the results of Table II shows that all three VTB cuts are similar in character. Coke yields from CSD feed oils, asphaltenes, pre-asphaltenes, and THF-insoluble residues average about 4, 47, 67, and 89 wt%, respectively, seemingly independent of the actual feed contents of each fraction. Given Soxhlet extraction data of a Wilsonville CSD feed, linear weighting of the above ratios by concentration results in a prediction of actual coke make accurate to  $\pm 3\%$ . Deviations from the cited averages and resultant yield predictions coincide with shifts in phenolic hydroxyl activity measured by FTIR. Decreasing coke make in the pyrolysis of 250D, 250H, and 251E VTB organic fractions (oils, asphaltenes, and preasphaltenes) parallels decreasing phenolics content of the whole resid (Figure 4). Quick calculations show that this simple ratio approach also predicts well the coke make of the CSD ash concentrates, underpredicting coke yield by only 1%. As with the VTB cuts, the deviations can be correlated with phenolic hydroxyl content via FTIR.

Attempts to correlate the CSD product resid fractions of Table II proved less successful. The material which is recovered as product resid represents the more volatile and thermally reactive components of the VTB cuts. As the nature of such material varies with liquefaction severity and subsequent CSD unit operation, the tendency of the various CSD resid fractions (oils, asphaltenes, etc.) to form coke appears to vary greatly with coal feedstock and process configuration. The CSD resid oil fraction makes up the bulk of the VTB oil fraction recovered by extraction and solidification. The CSD resid asphaltene and preasphaltene fractions form less coke than their VTB product counterparts; thus they appear to represent the more volatile fractions and cracked products of the parent VTB resid fractions. Among the three CSD resids studied, like results are obtained for coke yields from the Soxhlet fractions for Runs 250D and 251E. Again, the increased coke make of Run 250H asphaltene and preasphaltene fractions relative to the corresponding fractions of 250D and 251E CSD resids coincides with an increase in the phenolic hydroxyl content of the whole resids.

## CONCLUSIONS

Despite an increase of liquid yields due to the development of two-stage liquefaction processes, Wilsonville liquefaction resids are similar to those obtained from older liquefaction processes in that they give similar yields when subjected to thermal pyrolysis. The resids are highly aromatic and hence resistant to thermal cracking, leading to a pyrolysis in which liquid recovery is effected by limited cracking and extensive vaporization of lighter oil and asphaltenic fractions. Heteroatom content and retrogressive reactions<sup>(5)</sup> partially masked by poorly understood organic-inorganic interactions with the mineral matter play a dominant role in determining the nature of the liquefaction resids.

#### ACKNOWLEDGEMENT

The analytical support of R. W. Tumbula and the suggestions of B. A. Fleming are acknowledged.

#### REFERENCES

1. Lamb, C. W., Nalithan R. V., and Johnson T. W., "Process Development Studies of Two-Stage Liquefaction at Wilsonville," Am. Chem. Soc. Div. Fuel Chem. Preprints, 31(4), 240, 1986.
2. "Fluid Coking of Coal Liquefaction Residues," Interim Technical Progress Report for First Residue, DOE FE-2422-10, June, 1977.
3. "Fluid Coking of Coal Liquefaction Residues," Interim Technical Progress Report for the Second and Third Residues, DCE FE-2422-21, October, 1978.
4. "Fluid Coking of Coal Liquefaction Residues," Final Technical Progress Report for Fourth Residue," DOE FE-2422-28, January, 1979.
5. Hoover, D. S., "Investigation of Deleterious Coking Mechanisms," Final Report, EPRI AP-4451, February, 1986.

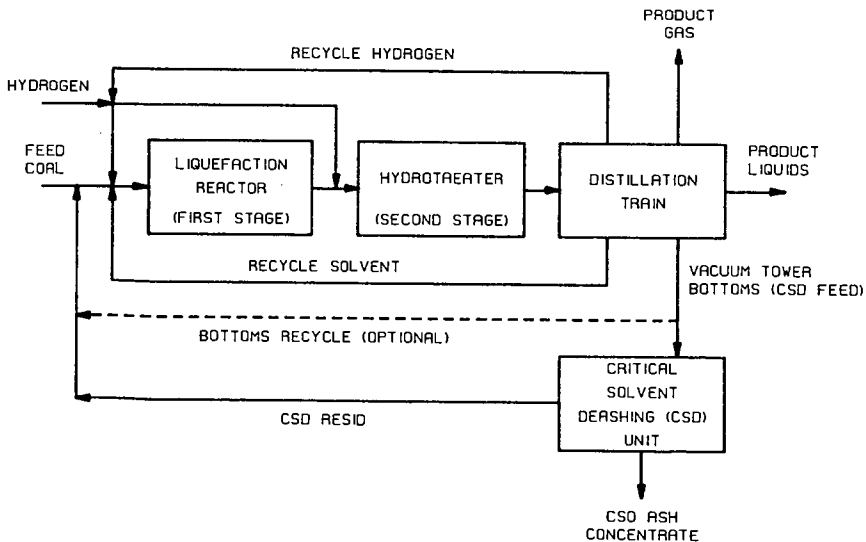


Figure 1. Wilsonville flowsheet.

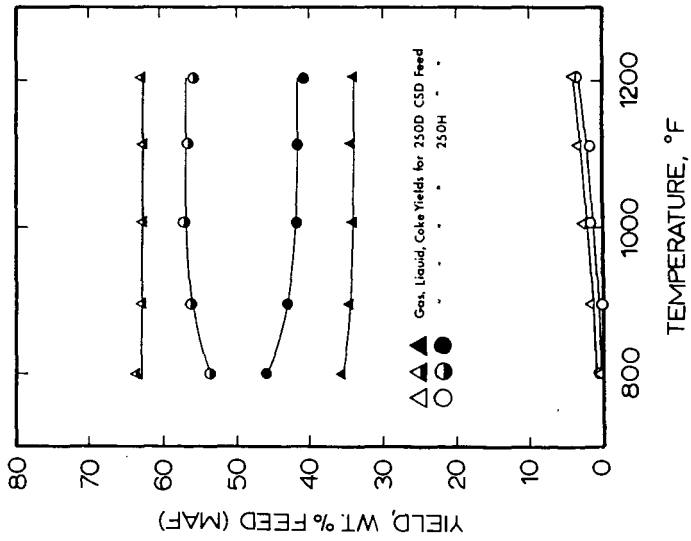


Figure 2. TGA pyrolysis yields for Wilsonville Run 250D and 250H VTB's.

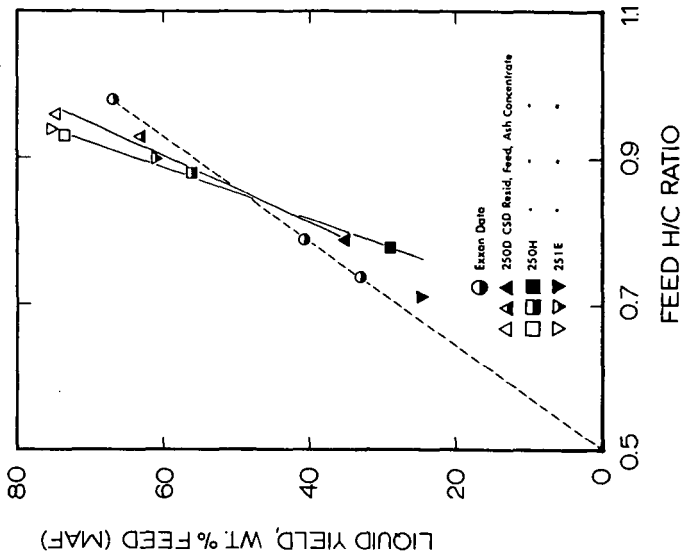


Figure 3. Average liquid yield vs. feed H/C ratio for pyrolysis of Wilsonville resids.

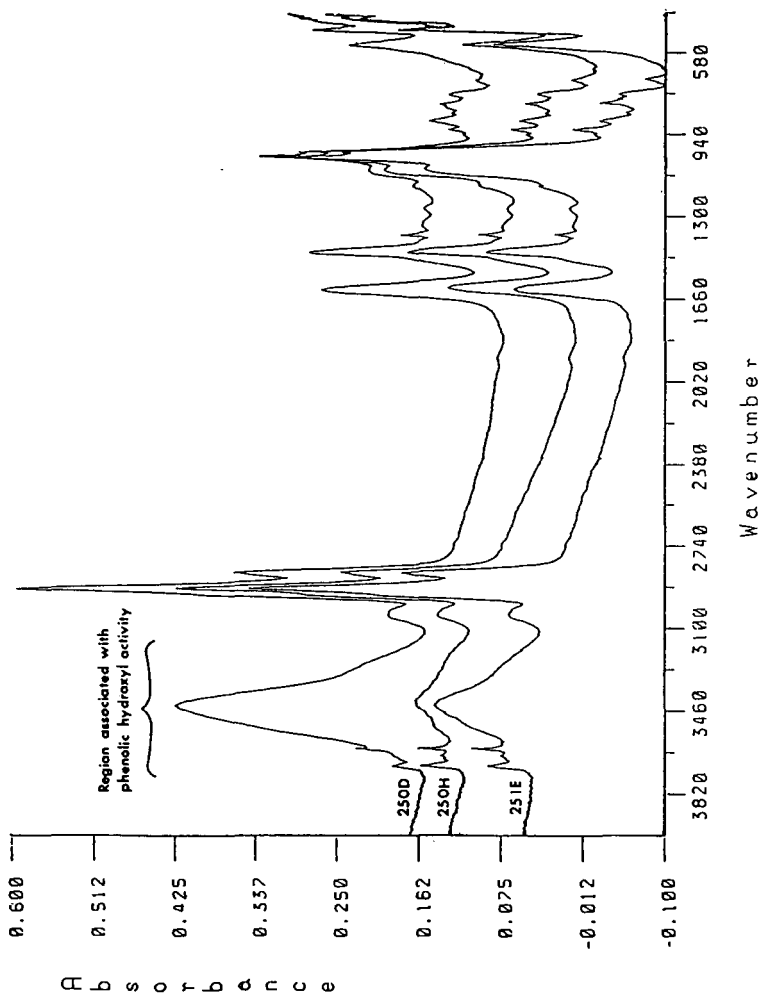


Figure 4. FTIR spectra of VB's.

TABLE I

ANALYTICAL CHARACTERIZATION OF WILSONVILLE COAL LIQUEFACTION RESIDS  
FOR KEY RUNS ON ILLINOIS NO. 6 BITUMINOUS COAL

	Run Number and Date											
	250D (020586)				250H (031786)				251E (060586)			
	VTB	CSD Resid	CSD Concentrate	VTB	CSD Resid	CSD Concentrate	VTB	CSD Resid	CSD Concentrate	VTB	CSD Resid	CSD Concentrate
<u>Proximate Analysis</u>												
Moisture, wt%	0.09	0.05	0.31	0.10	0.05	0.39	0.08	0.20	0.40			
Volatiles, wt%	67.8	84.4	28.7	58.1	86.5	18.6	56.9	82.9	22.6			
Fixed Carbon, wt% (by diff.)	22.3	14.8	35.2	24.9	13.5	35.3	20.0	16.7	30.9			
Ash, wt%	9.8	0.8	35.8	16.9	0.0	45.7	23.6	0.24	46.2			
<u>Ultimate Analysis</u> <sup>(1)</sup>												
C, wt%	81.2	90.2	56.3	74.2	90.3	46.3	69.5	88.9	46.4			
H, wt%	6.29	7.25	3.72	5.43	7.04	3.03	5.20	6.95	2.75			
N, wt%	1.26	1.10	1.07	1.24	1.45	1.21	1.13	1.16	1.01			
S, wt%	0.98	0.27	2.86	1.58	0.34	4.10	1.85	0.31	3.58			
O, wt%	2.09	1.54	4.65	3.66	1.80	5.78	3.29	2.63	5.27			
Atomic H/C	0.93	0.96	0.79	0.88	0.93	0.78	0.90	0.94	0.69			
<u>Soxhlet Extraction</u>												
Oils, wt%	46.4	22.2	3.1	29.3	39.8	0.8	33.2	39.8	1.5			
Asphaltenes, wt%	24.0	49.7	18.7	21.4	27.2	3.0	17.7	34.3	4.1			
Preasphaltene, wt%	8.8	27.0	8.5	13.1	33.0	12.9	9.4	25.5	12.2			
Ash + Coke + Unconverted Coal, wt%	20.8	1.2	69.7	36.2	0.0	83.3	39.7	0.3	82.2			

(1) Uncorrected for mineral matter.

TABLE II

PYROLYSIS YIELDS OF WILSONVILLE RESID FRACTIONS AT 1100°F

<u>Wilsonville Run No.</u>	<u>Extracted Fraction</u>	<u>Feed Composition, Wt%</u>	<u>Pyrolysis Coke Yield, Wt% Feed Sample</u>
<u>I. VTB FRACTIONS</u>			
250D	Oils	46.4	7
	Asphaltenes	24.0	52
	Preasphaltenes	8.8	74
	Ash + Unconverted Coal + Coke	20.8	88
250H	Oils	29.3	4.5
	Asphaltenes	21.4	49
	Preasphaltenes	13.1	68
	Ash + Unconverted Coal + Coke	36.2	91
251E	Oils	33.2	1.9
	Asphaltenes	17.7	46
	Preasphaltenes	9.4	58
	Ash + Unconverted Coal + Coke	39.7	89
<u>II. CSD PRODUCT RESID FRACTIONS</u>			
250D	Oils	22.2	8
	Asphaltenes	49.7	26
	Preasphaltenes	27.0	40
	Ash + Unconverted Coal + Coke	1.2	76
250H	Oils	39.8	4.5 ± 0.7
	Asphaltenes	27.2	49 ± 2.3
	Preasphaltenes	33.0	58 ± 3.5
	Ash + Unconverted Coal + Coke	0.0	--
251E	Oils	39.8	3.7
	Asphaltenes	34.4	37
	Preasphaltenes	25.5	51
	Ash + Unconverted Coal + Coke	0.3	86